Summer Semester 2014

Nano-structure of bone after the application of bio-resorbable implants

ausgeführt zum Zwecke der Erlangung des akademischen Grades eines Diplom Ingenieurs

unter der Leitung von

Univ. Prof. Mag. Dr. rer nat Helga LICHTENEGGER

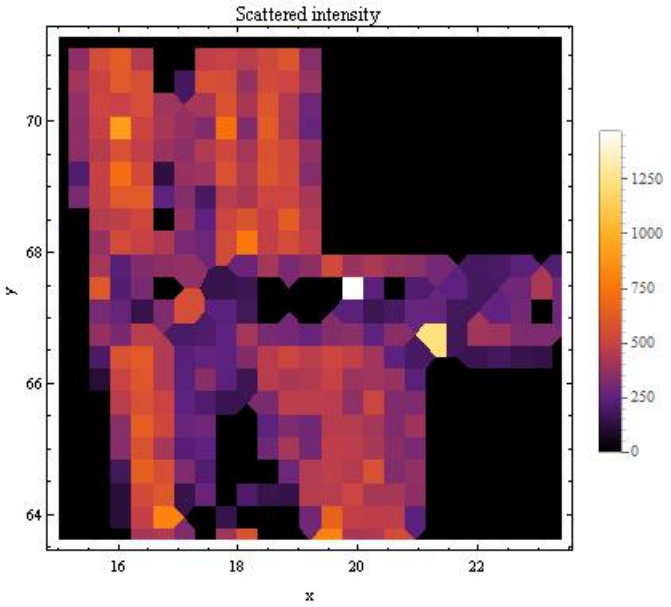

---

eingereicht an der Technischen Universität Wien Fakultät für Maschinenwesen und Betriebswissenschaften

von

Agathe OGIER 1227742

Universität für Bodenkultur Wien - Technische Universität Wien

Abstract

Bioresorbable implants are a class of implants that are resorbed by the body of a patient over the time of healing. Especially magnesium based alloys are a promising class of implants as no further operation is necessary but, unlike polymer systems they exhibit sufficient mechanical properties to effectively support the bone structure mechanically in case of a fracture. A class of patients that can hugely benefit from this behavior are children as they still exhibit significant skeletal growth and would hence need a second operation in the case of a non-degradable implant. The investigations are embedded into the BRIC (BioResorable Implants for Children) project that is a currently running project initiative of the Laura Bassi Laboratory under the project lead of MedUni Graz. This thesis deals with the nanostructural response of the bone structure on the implant over a certain span of time as studied by the method of small angle x-ray scattering (SAXS). The nanostructural changes of six rat femur bones with different Magnesium implant dwelling times from one to 18 month has been characterized on the basis of the orientation and morphology of the mineral platelets that make up the mineral reinforcement of the collagen matrix of the bone. A 2D mapping has been carried out to gain knowledge on local transitions in response to the implant with a resolution of about 350 µm. From the scattering patterns averaged information on the degree and direction of preferential orientation as well as the shape, thickness of the mineral platelets has been extracted. In this master thesis it is shown that:

- the direction of the platelets changes with the distance to the implant.
- the thickness of the mineral increases over time
- a different degradation behaviour of the pin is visible of in different types of bone.

Zusammenfassung

Bioresorptive Implantate sind Implantate, die vom PatientInnenkörper in der Heilungszeit resorbiert werden. Besondere Magnesiumlegierungen sind eine zukunftsträchtige Implantateklasse, weil keine weitere Operation nötig ist. Sie besitzen jedoch im Gegensatz zu Polymersystemen ausreichende mechanische Eigenschaften, um die Knochenstruktur im Falle eines Bruches mechanisch auf effektive Weise zu unterstützen. Eine PatientInnengruppe die stark von diesen Eigenschaften profitiert sind Kinder, da sie noch signifikantes Skelettwachstum aufweisen und daher im Falle eines nicht abbaubaren Implantats eine zweite Operation benötigen würden. Die Forschungen sind Teil des BRIC (BioResorbable Implants for Children) Projekts, welches eine Projektinitiative des "Laura Bassi Laboratory" ist, das gegenwärtig unter der Projektleitung des Med Uni Graz durchgeführt wird. Diese Masterarbeit behandelt die nanostrukturelle Reaktion des Knochenstruktur auf das Implantat über eine bestimmte Zeitspanne. Als Methode wurde die Röntgenkleinwinkelstreuung- Small Angle X-ray Scattering (SAXS) verwendet. Von 6 Ratten wurden die nanostrukturellen Veränderungen der Femurknochen mit Magnesiumimplantaten untersucht. Die Implantationszeiten erstreckten sich von 1 bis 18 Monate. Als Grundlage der Untersuchung dienten die Ausrichtung und Morphologie der Mineralplättchen, welche die mineralische Verstärkung der Kollagenmatrix des Knochens bilden. Mit Hilfe eines 2D Mapping wurden Informationen über lokale Veränderungen gesammelt, welche in Reakion auf das Implantat stattfanden. Die Auflösung des Mapping war c.a. 350 µm. Aus den Streuungsignalen wurden gemittelte Informationen über die Mineralplättchen gewonnen: Grad und Orientierung einer bevorzugte Ausrichtung, sowie Form und Dicke der Plättchen werden untersucht. In dieser Masterarbeit wurde gezeigt dass:

- sich die Richtung des Partikels mit der Distanz zum Implantat verändert,
- die Dicke des Minerals im laufe der Zeit zunimmt,
- ein unterschiedliches Abbauverhalten des Implantates in den unterschiedlichen Knochentypen sichtbar wird.

Acknowledgements

I would like to thanks first the Professor Helga Lichtenegger for the support she gave me, the patience she had for my " just one more question", and the clear and valuable advice she gave me. A great thanks also to Tilman Grünewald for his patience, availability and enthusiasm. I would like to thanks also Johanna Akbarzadeh and the Professor Herwig Peterlik, for the measurement that they allowed us to do at their laboratory. I would also like to thank Martin Meischel and Stefanie Tschegg, for the information they gave me on the project. I also thank the Professor Annelie Weinberg for the histological image. A great thanks to Harald Rennhofer, for his smile and for his help with Latex, and with the SAXS measures. I also would like to thank the whole institute for Physics and material science for their warm welcome. A huge thanks also for the numerous correction that Maximin made for this thesis. I am also grateful to the rats who were sacrificed for this project.

Contents

Introduction

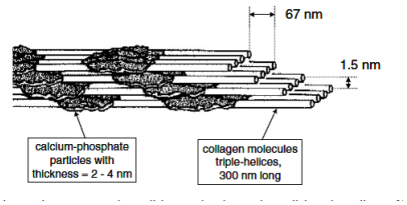

Figure 1: The crystals of hydroxyapatite in the collagen fibers [1]

Bone as a biomaterial

The main representation that we have from bones is a white and resistant material. But bone is much more than just an inert recollection of minerals. It has more functions than only bearing our body's weight and allowing us to move, as it acts as calcium storage, blood cells production in the bone marrow. Thanks to those structures, the bone is light and resistant, adaptable and optimized for the load it has to endure. This biocomposite material allying high strength and fracture resistance has been often analyzed und studied to inspire

Aim of the study

When a kid breaks his arm, usually, two solutions are available, either, his arm is put in an orthopedic cast, or, if the wound is more serious, he has to be operated to have metallic implants that realign and maintain the bone in a more efficient way. The alloy chosen to make the implants is biocompatible and also resists to corrosion. But this has the consequence of needing a second operation when the fracture is repaired, in order to take the implants back, so it does not disturb bone growth by constraining it. A second surgery leads to more trauma, more scars, a need for rehabilitation, which in the end, has not only an impact on the health of the child, but has also a cost. Current research aims at avoiding this second operation, by having an implant that would dissolve itself when the bone is healed. The aim of the study is to see how bone nanostructure react to such implants and their degradation and which ways are the way to follow to improve its reaction.

The use of the SAXS method

SAXS stands for Small Angle X-ray Scattering. This is a non destructive method, which in contrast to conventional X-ray absorption imaging, use the scattering of the X-ray to give information on the structure. With a wave length in the range of the angstrom, information on crystals structure and on the nanometer scale can be gained. The SAXS method was used in this study to investigate the potential influences of Mg alloy and its residues after resorption on bone growth.

Figure 2: The partners in the BRIC project

Part I

Theory

Chapter 1

Bone

Bones are those kind of material that scientists are eager to understand. Its properties are efficient, allying mechanical resistance, light weight design, regeneration process and adaptation to stresses. The role of bones is not only to support the movement of the body; they also have a role in the blood cell production, and in the calcium regulation. For this master thesis, the focus is made on the structure of bone. The properties of bone depends on many factors as, the species that produces it, the age of the individual, the type of bone that is taken, e.g. long bones or skull, and also, it may depend of the health of the specimen. Structures on seven levels are usually described [2, 3], from the biggest structure to the smallest (see figure 1.1):

- Whole bone decimeter and centimeter scale,
- Spongy versus compact bone, centimeter to millimeter scale,
- Cylindrical motifs, osteons and laminae, millimeter scale to micrometer scale,
- Fibril array patterns micrometer scale,
- Fibril array micrometer to nanometer scale,
- Mineralized collagen fibril nanometer to angstrom scale,
- Molecular components of the bone sub nanometer scale.

1.1 Bones hierarchical structure

1.1.1 Macrostructure, the whole bone

The bone in itself is a very interesting structure, the general geometry of which allows movement, muscle attachment, articulation and mobility. Its general form is also linked to its function. Long bone provide a good resistance to bending and buckling as tibia, whereas short bones as the vertebra are found to be optimized to resist to compression.

1.1.2 Mesostructure, spongy bone versus cortical bone

When a bone is represented in cross section, as for the femur, strong structural differences can be distinguished between generally the outside part and the inside part (see figure 1.2). The outer part,

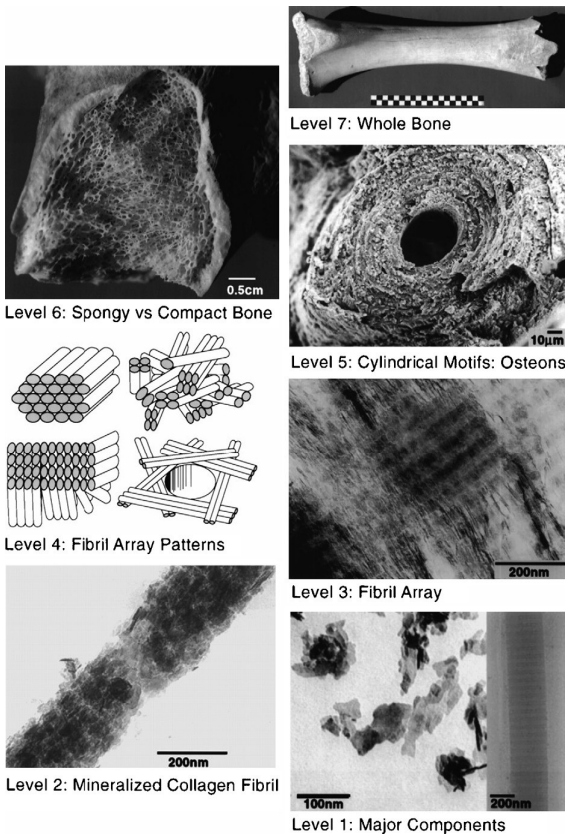

Figure 1.1: The hierarchical levels of structure found in secondary osteonal bone, as demonstrated by Weiner and Wagner [2]

more dense, and strongly oriented is the cortical or compact bone. This outer shell thickness can go from a few millimeters to a few centimeters. The inner part, less dense, with a higher porosity is the trabecular bone or cancellous bone with a meshing from approximately 100 to 300 µm (see figure1.3). Those structure have different mechanical properties and it is hard to obtain an overall value for the Young modulus as it strongly depends of where the sample is taken, value can range from 0.3 MPa to 3000 MPa [1]. Those structures are differentiable already with a naked eye, and the differences are also visible on a lower level. The porosity of cortical bone is low, around 6%, mainly due to the presence of blood vessels. The blood vessels are usually surrounded by material placed concentrically, the osteons, the next level in the hierarchical structure of the bone. The holes formed by the meshing of the trabecular bone are called trabeculae. These trabeculae are responsible for the high mean porosity in the cancellous bone, approximately 80%. Their orientation depends on the load in the bone. The trabeculae are filled with bone marrow, thus with nutrient for the bone cells.

Figure 1.2: Spongy bone and cortical bone [4]

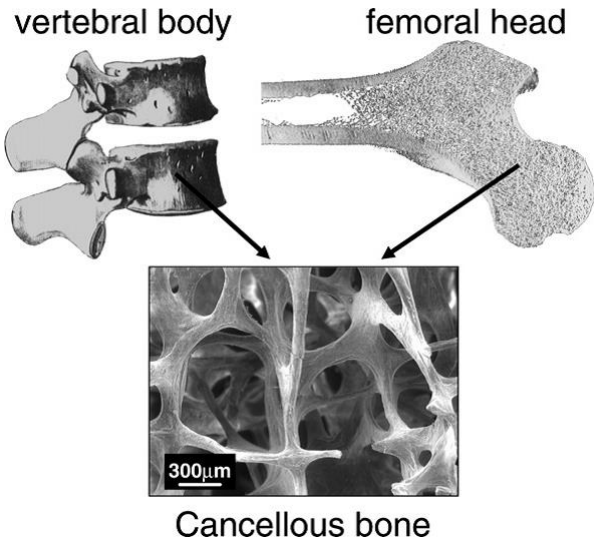

Figure 1.3: Cancellous bone [1]

1.1.3 Microstructure, osteons with Haversian system and substructure, the lamellae

On a lower level, mainly in the cortical bone, concentric structures can be observed, centered on canals. Those are osteons around Haversian canals, essential to supply the cells, allowing blood circulation in the cortical bone (see figure 1.4). The size of those structures is approximately 10 µm to 500 µm. Those canals are formed by lamellae. The lamellae are long structures which enable the bone to have a better resilience and thus resist better to fracture. The size of lamella is comprised between 3 µm to 7 µm.

1.1.4 Nanostructure, collagen fibers and fibrils, bone crystals formation

At a nanometer scale, from 100 nm to 1 µm the bone is organized in collagen fibers, themselves composed of collagen fibrils, with mineral deposition. These fibers are made of collagen fibrils, the next level of the hierarchical structure of the bone. The collagen fibrils, are made from the periodic arrangements of collagen molecules mainly from the type I collagen, (28 types are known nowadays) and constitute 85-90% of the bone [1]. Those molecules, are approximately 300 nm long, and have a diameter from 1.23 nm have themselves a sub structure, three proteins named procollagen, which

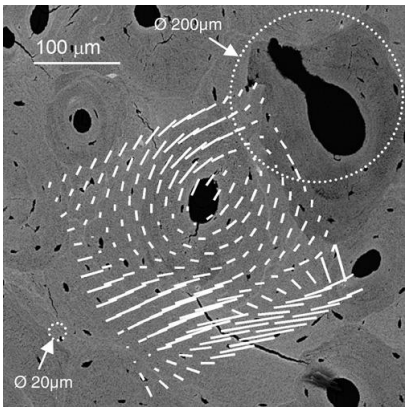

Figure 1.4: Osteons centered on blood vessels (black holes) [1]

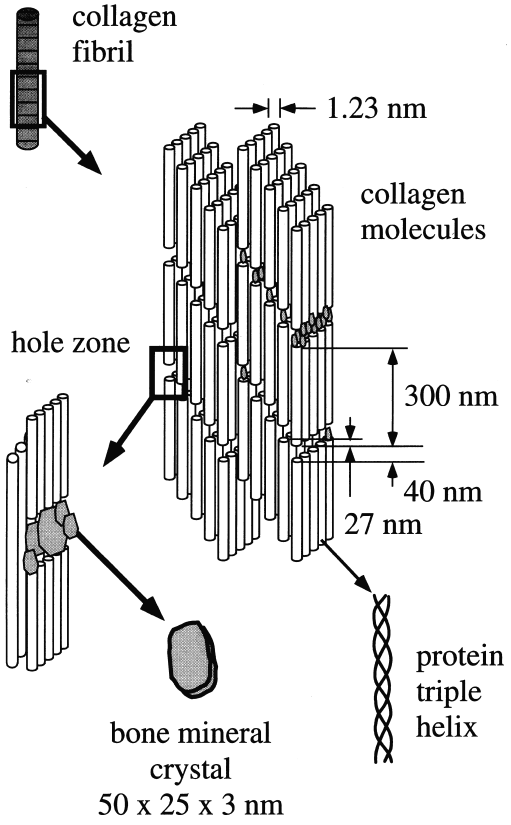

Figure 1.5: The structure of collagen fibrils [3]

form an helix. This helix assembles itself with other helix to form a tertiary structure having a 67 nm periodicity with a gap zone of 40 nm and a overlapping zone of 27 nm [3] (see figure 1.5).

The collagen fibrils are interspersed by tiny crystals of hydroxyapatite $Ca_5(PO_4)_3OH$, which are nucleated in the collagen gap zone. The amount of impurities in the crystals is small, but neither negligible and it is not exactly known why, but it is thought to play a role in bone reformation [5]. Indeed, thanks to those impurities, the crystal is less stable, and the bone is a material which is perpetually renewed and then, needs to be easily removed, thus if the crystal is not too stable, it will be more easily removed, which is an advantage. This crystals are small platelets, for human, arranged mainly parallel to the collagen molecules with a periodicity approximately of 67 nm. Their length and width are approximately 50 X 25 nm and the crystal thickness range from 1.5 to 4.5 nm (depending usually on the age of the crystals). This is the parameter that we are going to observe with the SAXS experiments as they give us information to the growth of bone. The crystals is thought to nucleate in the gap zone, then to grow needle like, then platelet like and only there to thicken. Those mechanisms are not perfectly known, and the means of exploration of this structure influence the answer. In order to have a better idea of the mechanisms, the scientists are trying to regrow the nanostructure of bone synthetically. [5]

At last, in the bone, some no collagenous proteins are present, their role being thought as template and director for bone growth.

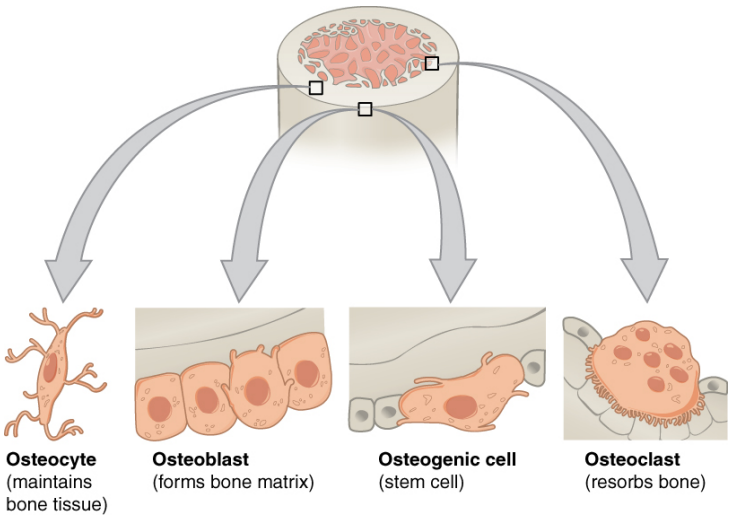

Figure 1.6: The different bone cells and their role [6]

1.2 Bone growth

The mechanism of bone growth is also an important matter for our study. Indeed, when the implant is inserted into the bone, as it is aimed to be on broken bone, bone is going to have to grow at this place. We have to be able to know how the bone is normally growing to say if the growth is normal, stimulated or retarded. There are many hypotheses on how the bone is growing and they are going to be explained in the following pages. The bone formation is usually made in two steps, called primary and secondary osteogenesis.

The primary ossification is rapid and needs a precursor, usually cartilage; this ossification happens during the prenatal life, during the skeleton formation, and also when the bone is injured and that the two pieces of bone are not joined, but only an orthopedic cast is put around the broken limb. During this bone formation, the bone is relatively unorganized and forms what is called a woven bone, where the collagen fibers are not mineralized from the inside but only on the exterior of the fibrils. The degree of mineralization is lower than in the bone formed by the second osteogenesis.

The second form of osteogenesis is slower, and happens after the primary ossification. During this bone formation, the structures explained above are modeled, the bone is more efficient if repaired quickly a first time then slowly deeply rebuild. Nevertheless, this second ossification needs more time than the primary one, and it can be understood as an evolution selection to have this two stepped answer to bone fracture. The bone is constantly being remodeled in order to have a better adaptation to the loads and it is estimated that 10% of an adult skeleton are renewed each year. [7] The cells responsible for those remodeling are the osteocytes, osteoblastes and osteoclastes. Osteoclastes are the cells responsible for the bone resorption, osteoblats for the bone formation and osteocytes are thought to play a role in directing the bone remodeling, they derived from osteoblasts. It is interesting to know that the bone degradation time by osteoclasts lasts approximately 2 or 3 weeks and the bone formation is much slowly, approximately 3 months (see figure 1.6).

1.3 Means of investigation on bones

To study the bone, many techniques are used, enabling access to different information. Those techniques are summarize in the following table 1.1

Technique	Information gained
X-ray imaging	General density of the bone, shape, macro parameters
Optical microscope	Texture, structure, local information
Scanning electronic microscope	Texture, structure, local information
Transmission electronic microscope	Electron density, local information
Ultrasound studies	Mechanical properties, Young modulus, Poisson ratio
Nanoindentation	Local hardness, Young modulus
Mechanical testing	Young modulus, fracture behavior, Poisson ratio
Small Angle X-ray Scattering	**Shape, thickness and orientation of the mineral platelets, bulk information**
Wide Angle X-ray Scattering	Crystal in the bone, bulk information

Table 1.1: Techniques of exploration of the bone

Chapter 2

Implants

2.1 General considerations

First point to notice is that an ideal implant is ideal for a certain use. If a hip prosthesis has to be placed on a patient, the characteristics of the implanted new hip are totally different from an implant for a child who broke his arm. For the first case, it is expected from the implant to be as resistant to time as possible, to be a substitute to the bone and cartilage that has been removed. On the opposite, an ideal implant for a broken bone would be an implant that would replace bone as long as the bone is broken and would promote its growth. It should be strong enough to keep bone pieces in place the time that the bone heals and then should disappear without any other operation and without releasing any harmful substances in the body. The time during which it should be solid, should be approximately 12 weeks. Moreover, it should also not over constrained the bone nor bother its growth. The body should not have a defensive reaction to it, but should consider it as a part of itself. The following table 2.1 summarizes the characteristics expected for biomedical applications.

Property	Desirables
Biocompatibility	Non-inflammatory, non-toxic, non-carcinogenic, non-pyrogenic, blood compatible, non-allergic
Sterilizability	Not destroyed by typical sterilizing techniques like auto-claving, dry heat, ethylene oxide, radiation
Physical characteristics	Strength, elasticity, durability
Manufacturability	Machinable, extrudable, moldable

Table 2.1: Material specifications for biomedical applications [8]

2.2 State of the art on orthopedic implants

Before introducing the different biomaterials used in orthopedic surgery, it seems important to define what is the biocompatibility of an implant. According to the IUAPC, the biocompatibility is the ability to be in contact with a living system without producing an adverse effect. Indeed it could be differentiated many levels of biocompatibility, from having a full reject of the implant, or an indifference to its presence, to promote the growth of cells around the implant. The research in the implants field has kept on trying to improve the answer of the bone.

Figure 2.1: Intramedullar rod and plates [9]

In the early 1900's an alloy called "vanadium steel" was developed to the specific use of human implants. Plates and rods of this alloy were made to stabilize fractures. Then, facing problems of biocompatibility and implants failure, doctors tried to improve the alloys used and also the design used. Indeed, they were at the time using the available materials, as steel or iron and noted how quickly those implants dissolve, and also how the bone was badly reacting to their presence. The noble metals such as gold or silver were too weak to be used to maintain the bone.[9]

Intramedullary rods were invented during the World War II by Gerhard Küntscher (see figure 2.1), and enabled the soldiers to have a much shorter time of immobilization a few weeks instead of a few months as they were sharing the loads with the bone and not only taking all the weight. Those implants where made from stainless steel and were the first to have a wide use. Then alloy from stainless steel was improved with molybdenum, the 316 stainless steel had a better resistance to corrosion. A small drop in the percentage of carbon in the alloy increased again the resistance of 316L stainless steel in the 1950's.

The other alloys that changed the landscape in orthopedic implants are the titanium alloys introduced around 1947 and the cobalt-chromium alloys more recently. The biocompatibility of both alloys are higher and their mechanical properties better than previously used materials.. Those two alloys are now widely used, and in the following table 2.2, are shown, the application of the different metallic alloys in the biomedical field. The main problem with metallic implants is of course the corrosion, but is also due to the difference of mechanical properties between the bone and the implant. Having a higher elastic modulus than the bone can cause in the end its osteolysis.

Not only metallic alloys are used in the orthopedic field, but also ceramic and polymers and even autograph of bone of the patient. For the aim of repairing broken bones, only the ceramic are discussed as it can bear load more than polymers. The problem with ceramic is their fragility and their lack of resistance to the shock. Research is also done in ceramic with phosphate substitute, calcium ceramic or even with mother of pearl because of the mechanical properties that are not too different from those of the bone. The following table 2.3 summarizes, the current ceramic used in the biomedical field.

The bone grafting techniques are used when, the risk of failure of the implant or of the healing process is high, or is very complex. Bone pieces can be taken on the patient himself, autograph, or come from cadaver, allograph, or being placed on scaffold made from hydroxyapatite or from calcium. The procedure is expensive and reserved for critical cases.

Metal	Application
Cobalt–chromium alloys	Artificial heart valves, dental prosthesis, orthopedic fixation plates, artificial joint components, vascular stents
Stainless steel	Dental prostheses, orthopedic fixation plates, vascular stents
Titanium alloys	Artificial heart valves, dental implants, artificial joint components, orthopedic screws, pacemaker cases, vascular stents
Gold or platinum	Dental fillings, electrodes for cochlear implants
Silver–tin–copper	alloys Dental amalgams

Table 2.2: Commonly used metals in biomedical applications [8]

Ceramic	Application
Aluminium oxides	orthopedic joint replacement, orthopedic load-bearing implants, implant coatings, dental implants
Zirconium oxides	orthopedic joint replacement, dental implants
Calcium phosphates	orthopedic and dental implant coatings, dental implant materials, bone graft substitute materials
Bioactive glasses	orthopedic and dental implant coatings, dental implants, facial reconstruction components, bone graft substitute materials, bone cements

Table 2.3: Commonly used ceramic in biomedical applications [10, 8]

2.3 Magnesium implant

2.3.1 History of magnesium implants

In the section above, we only described what was currently done in the orthopedic field, but the subject of this thesis was to study a new type of implant, the biodegradable magnesium implant. Already in 1878, magnesium was used to ligature blood vessels and its degradable behavior was noticed.[11] Indeed, what is very interesting with the magnesium implants is that when implanted, it is degradable, thus can disappear. Another positive point of the magnesium implant is that it does not release toxic metallic ions or particles through wear which could lead to osteolysis, as it is the case sometimes with other biocompatible alloys as stainless steels, titanium or cobalt-chromium alloys. [12]

In 1900, Payr already tried to use magnesium sheet to stabilize fracture, but this led to more operations. Then Lambotte made in 1907 four operations, where the bone was stabilized with magnesium nails. The four patients healed all per primam without any other complications than the formation of gas cavities due to the degradation of magnesium. But this drawback was the only one that Lambotte noticed from his experiment. In the X-ray imaging he made, one year after the operations, he observed the disappearance of the magnesium implant, and no hypertrophy of the bone. Then during thirty years other researchers developed the magnesium implants for the use of healing compound fractures, or fixing autologous grafts [11]. In 1948, Troitskii and Tsitrin noticed that the presence of magnesium could stimulate the formation of a callus by neutralizing the acidity in the tissue caused by inflammatory reactions. In order to prevent electrolytic corrosion, they advised, as Payr, that magnesium was also to be implanted alone.

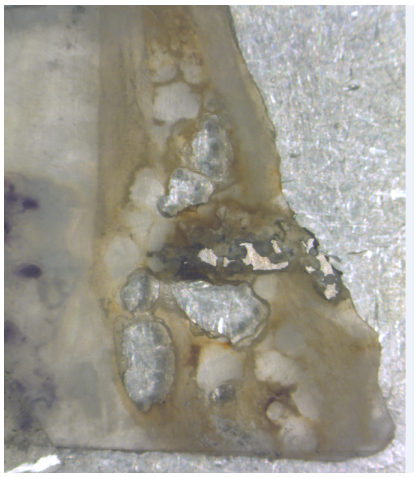

Figure 2.2: Implant with a high corrosion rate, the gas product by the corrosion of magnesium led to the formation of cavities in the bone

The difficulties with magnesium came from the cavities caused by the corrosion of magnesium which produces dihydrogen and from its too quick disappearance (see figure 2.2). The following equations are the theoretical corrosion reactions that happens in the body that leads to that gas production [12].

$$Mg(s) + 2H_2O \rightarrow Mg(OH)_2(s) + H_2(g) \tag{2.1}$$

$$Mg(s) + 2Cl^-(aq) \rightarrow MgCl_2 \tag{2.2}$$

$$Mg(OH)_2(s) + 2Cl^-(aq) \rightarrow MgCl_2 \tag{2.3}$$

Magnesium without coating will quickly react with water to form a layer of oxyde and dihydrogene. With high concentration of Cl^-, that oxide will react to form magnesium chloride and hydrogen gas. The rate of this reaction has a high influence on the bone reaction. The surface exposed also plays an important role in the degradation rate. Indeed, if the implant degrades too quickly, the bone is not going to be able to evacuate the gas formed, which would lead to the formation of cavities, which would indirectly damage the bone and needs more time to repair. Pure magnesium in physiological system with a pH of 7.4-7.6 and a high chloride environment degrade too quickly, the bone does not have time to heal and the gas production is too high to be eliminated by the bone. At the beginning of the research on magnesium, that was what dissuaded its development, but now, new ways exists to slow the reaction, by coating the implants, or by alloying it. This path is the path that Witte et al. took, by trying to alloy magnesium with aluminium or zinc and rare earth elements.[13] They observed an increased bone apposition along the implants, and when mechanical push out test were made, researchers found an increased interfacial strength [14] . Alloying enables to increase the mechanical properties of the implant, which is very brittle if used pure, and enhances the resistance of implant to corrosion.

2.3.2 The WZ21 magnesium alloy class

For this master thesis, only one type of magnesium alloy has been studied. It has been developed for the BRIC project, BioResorbable Implants for Children. This program was grounded by the trauma surgeon Annelie Weinberg at the medical University of Graz in collaboration with the Technical universities of Vienna and Graz, the University for Natural Ressources and Live Sciences Vienna and Heraeus Medical. The aim was to try for new ways of supporting the healing of bone by children and to shorten the time they spend in hospitals. With that perspective, implants that dissolve themselves are an interesting way of research.

	$\rho(g.cm^{-3})$	Young modulus (MPa)	Fracture toughness ($MPa.m^{\frac{1}{2}}$)
Human bone	1.8 - 2.1	3 - 20	3 - 6
Magnesium	1.74 - 2.0	41 - 45	15 - 40
Titanium	4 - 5	116	44 - 66

Table 2.4: Mechanical properties of Bone, magnesium and Titanium [15]

This WZ21 alloy has been chosen because of its rather slow degradation rate: 50% of the implant is still visible after 5 to 6 months and the complete degradation is only reached after 18 months [16]: but also for its mechanical properties that are closer of those of the bone than Titanium implant. Compared for example with the LV1 alloy that is almost 50% degraded in three months and totally degraded in 6 months, the WZ21 has a much slower degradation rate, which enables the bone to eliminate the hydrogen.

The implant composition is the following: WZ21 stands for Yttrium 2% and Zinc 1%, in mass weight on total and the rest Calcium 0.25%, Manganese, 0.15% and 96.60% in pure magnesium. The corrosion products are not harmful on the level of cells. The dimension of the pin inserted were the following [15]: a diameter of 1.6 mm and a length of 8 mm .

Chapter 3

Small Angle X-Ray Scattering

3.1 History of the X-ray diffraction techniques

In 1895 Röntgen discovered the X-ray, and since that day, the use of it has been extraordinarily various: thanks to it, one can gain informations on the meter scale, as X-ray are used to studied structures of some walls, centimeter scale to micrometer, the X-ray radiograph or computed tomography that is done by the doctor to know if a bone is broken, but also, and this is the point that we are going to develop, on the µm and even nanometer thanks to the method of X-ray diffraction which enable for example to discover the structure of the deoxyribonucleic acid, the DNA. X-ray are electromagnetic waves with a wavelength in the region of 1 Å ($10^{-10}m$).

First the differences between X-ray diffraction and X-ray scattering should be made [17]:

Scattering: deviation of radiation or moving particles from a straight path caused by one or more local non-uniformities in the medium through which they pass, influenced by the difference of the electron densities

Diffraction: apparent bending of waves around small obstacles and the spreading out of waves past small openings (involves interference), influenced by the lattice dimension of crystal.

But in the case of X-ray, the scattering is supposed to refer to amorphous materials, and diffraction to crystalline or periodic materials; usually, the two denominations are used without making a difference.

3.2 Ground principles: Bragg law

In this following pages, we are going to have a deeper look on the X-ray diffraction, as it is the technique that we used to study the nanostructure of bone.

The Bragg law states the conditions to have constructive interferences of X-rays diffracted from a crystal [17]:

$$n\lambda = 2d\sin(\theta) \tag{3.1}$$

with

- λ the wavelength,
- n an integer,

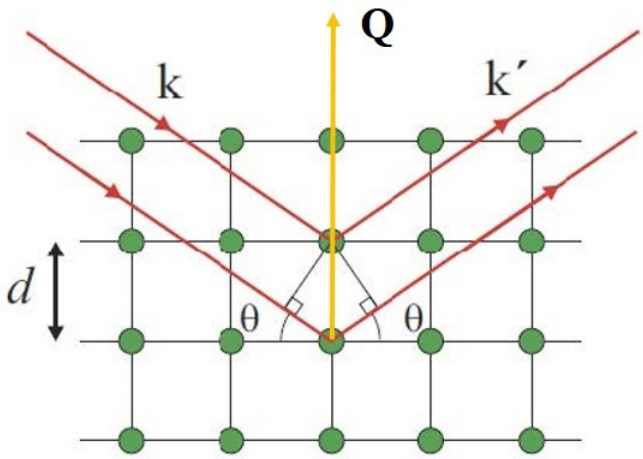

Figure 3.1: Bragg law condition for constructive interferences with k the incident X-ray and k′ the scattered one.[18]

- d the distance between the scattering planes,
- 2θ the angle at which the constructive interference happens or angle of diffraction.

The consequences of that equation is that the smaller is the wave length, the smaller are the details that can be studied. With X-ray wavelength being in the order or the Å, and even smaller, one can study structure of that size. Also, the larger is an diffracting object of size d, the smaller is the angle of diffraction.

The X-ray is scattered and the modification of its trajectory can be written with vector:

$$\vec{Q} = \vec{k} - \vec{k'} \tag{3.2}$$

with

- $\mid Q \mid = \frac{4\pi}{\lambda} \sin(\theta)$ the wave vector transfer,
- $\mid k \mid = \frac{2\pi}{\lambda}$ the incident wave vector,
- $\mid k' \mid = \frac{2\pi}{\lambda}$ the scattered wave vector as we consider an elastic scattering,

3.3 SAXS

Small Angle X-ray Scattering is the method used in this thesis. The use of this technique was initiated in 1937 by A. Guinier[19] and developped by Kratky and Porod with the introduction of the Kratky-Porod model [20]. It consists of studying the scattering at small angles, approximately till $2\theta = 10°$ which gives us access to information of the nanometer size. The very interesting point is that it also work with noncrystalline and non ordered materials. Through that study, the size, shape, inner surface, fractal dimension and orientation of the mineral particles can be gained. The following table 3.1 summarizes the advantages and disavantages of the Small Angle X-ray Scattering.

The SAXS analysis consists in studying the bidimensionnal pattern of the intensity projected on the detector, with that intensity being proportional to the number of X-ray photons scattered by the

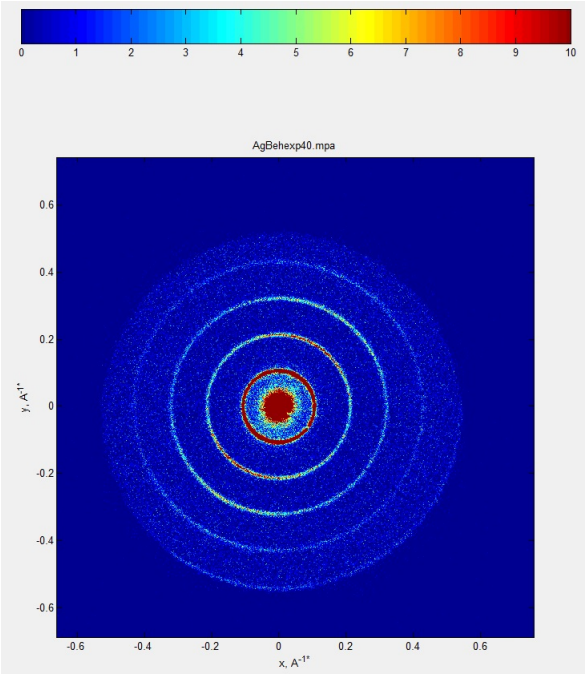

Figure 3.2: The diffraction image of AgBeh, this material is used for calibration as the condition for its scattering angle is known

Advantages	Difficulties
Not only ordered or crystalline materials	Interpretation of the curve harder through pattern that are not as clear as for crystalline material
Non destructive method	Background needs to be corrected
Integral method	Need for interpretation and modelling of the curve

Table 3.1: SAXS Advantages and difficulties [18]

material, which is in its self proportional to the constrast in electron density. An example of this pattern is shown on figure 3.2. In the case of bone, the scattering intensity is going to be mainly due to the hydroxyapatite, as it is the element in bone which has the higher electron density compared with void, collagen, or resin. In case of spherically symetric system or spherically average system, the intensity hitting the detector can generally be described as [17]:

$$I^{SAXS}(q) = \Delta\rho^2 V_p^2 \mid \mathcal{F}(q) \mid^2 \tag{3.3}$$

with

q: the scattering vector,

$\Delta\rho$ **:** the difference of electron density, between the element of the material here collagen and mineral,

V_p **:** the integrated volume of the particle,

$\mathcal{F}(q) = \frac{1}{V_p} \int_{V_p} e^{iqr} dr$ **:** the form factor of particle which depends of its shape and of its size.

3.3.1 Guinier approximation: small q

At small q compared to the characteristic size R of the particles, $qR \ll 1$, the form factor of the equation 3.3, can be approximated, which gives us the following equation:

$$I^{SAXS}(q) = \Delta\rho^2 V_p^2 e^{\frac{-q^2R^2}{5}} \tag{3.4}$$

This approximation, that was developed by Guinier, was first derived for spherical particles. The form factor of simple shapes can be computed for example for full sphere, rods or discs. In order to have a better understanding of the phenomenon, the notion of radius of gyration is introduced:

$$R_g = \frac{\int_{V_p} \rho(r) r^2 dV_p}{\int \rho(r) dV_p} \tag{3.5}$$

This will allow the extention of the results that are only valid for full sphere to other shape of particles in case of spherically averaged systems. . In the case of a sphere where $R_g^2 = \frac{3}{5}R^2$, the equation can be rewritten as: $I^{SAXS,sphere}(q) = \Delta\rho^2 V_p^2 e^{\frac{-q^2R_g^2}{3}}$ Nevertheless, it can be extended to other shape of particles, assuming that they are randomly oriented, they can be considered as sphere of a certain radius of gyration Rg. We can then deduce that for a random orientation of the particles and an arbitrary shape, the above equation gets: $I^{SAXS}(q) \approx \Delta\rho^2 V_p^2 e^{\frac{-q^2R_g^2}{3}}$ Assuming that $\Delta\rho$ and V_p do not change I_{SAXS} becomes

$$I^{SAXS}(q) = I_0 e^{\frac{-q^2R_g^2}{3}} \tag{3.6}$$

which allows us to identify the characteristic size if the shape is known.

The shape can be deduced also from the slope of the curve in the Guinier region on a log log graph, which is at small q, in the case of very high aspect ratio and of length of rod or platelets outside the visible range of scattering angles. With a slope of 0, the particles are full sphere, with a slope of -1, the particles are rods, with a slope of -2, platelets (see table 3.2).

3.3.2 Porod approximation: high q

At large q compared to the characteristic size R of the particles, $qR \gg 1$, the scattering curve has a decay of q^{-4} whatever the shape is, provided the interface is smooth. The intensity can then be rewritten in the following way:

$$I^{SAXSPorod}(q) = \frac{P}{q^4} + B \tag{3.7}$$

with

- P the Porod constant which is proportional to the inner surface S of the sample,
- and B the background noise due to diffuse scattering.

3.3.3 Invariants

The Porod constant is useful in order to compute the thickness of the particles. Indeed, using the following integral, 3.8, one has a access to an invariant, proportional to the volume of the particles.

$$I^{invariant} = \int_0^\infty q^2 I(q) dq \tag{3.8}$$

This $I^{invariant}$ depends on the scattering volume V of particles, the electron density contrast and the proportion of each phase. It does not depend on the structure, nor of the shape of the particles, but using the ratio of those two invariants, we obtain the following relation:

$$\frac{P}{I^{invariant}} = \frac{1}{\pi\phi(1-\phi)}\frac{S}{V} \tag{3.9}$$

with ϕ the mineral content of the sample.

This relation allows us to identify the characteristic size of the particles as $\frac{S}{V}$ is proportional to the T parameter. Assuming a mineralization of 50% and platelet shape and according to the litterature [21], we obtain the following equation:

$$T = \frac{V}{S} = \frac{4}{\pi P}\int_0^\infty q^2 I(q)dq \tag{3.10}$$

	Radius of gyration R_g	Slope in Guinier region
Sphere	$\sqrt{\frac{3}{5}}R$	0
Rod	$\sqrt{\frac{1}{2}}R$	-1
Platelet	$\sqrt{\frac{1}{12}}L$	-2

Table 3.2: Radius of gyration and Guinier exponents depending on the shape of the particles [17]

3.4 SAXS devices

The simplified device to make X-ray diffraction is the following (see figure 3.3):

- an X-ray source, that would produce a monochromatic, well collimated beam
- pinholes to reduce beam size and the divergence
- a vacuum chamber where the sample is put, so that the beam is not scattered by air molecules
- a detector to register the scattered photon.
- a photodiode in order to measure the absorption of the beam by the materials.

The figure 3.4 shows the device used for preliminary measurements to this study. Due to unexpected instrument downtime, the major part of the experiments had to be conducted at the SAXS laboratory of Prof. Peterlik, University of Vienna..

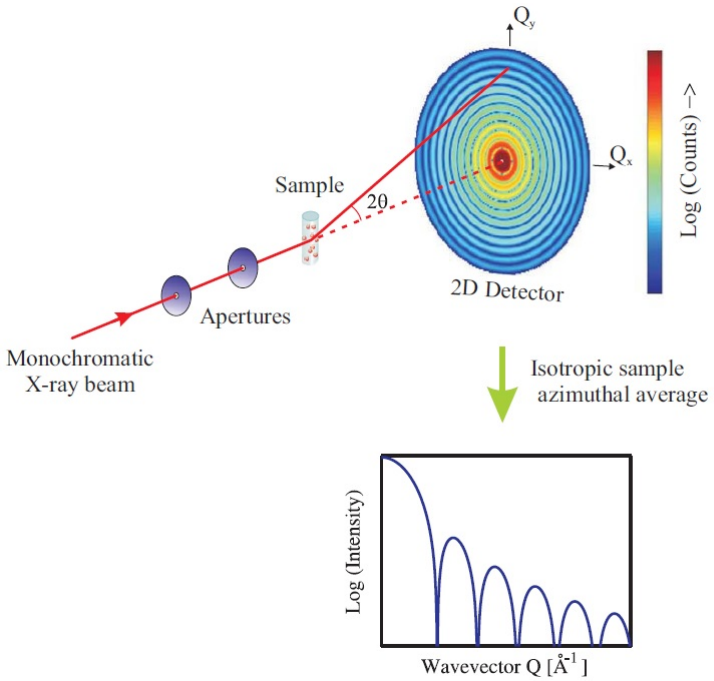

Figure 3.3: Schematic layout of a small-angle X-ray scattering instrument. A monochromatic X-ray beam is collimated using a set of apertures and then impinges on the sample. The scattered beam is detected on a two-dimensional, position sensitive detector (PSD). For isotropic samples, the scattering can be azimuthally averaged to produce a plot of scattered intensity versus wave vector transfer.[17]

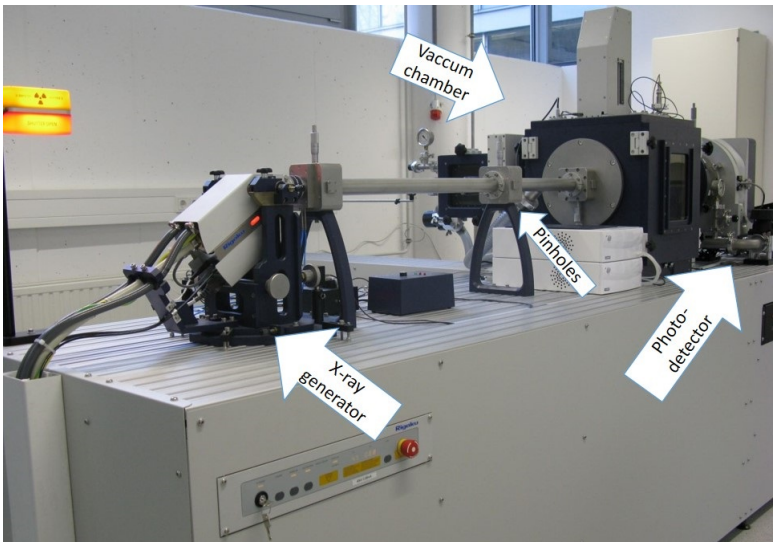

Figure 3.4: The SAXS device of the BOKU with its X-ray generator, its pinholes, its vaccum chamber where the sample is placed and the photo detector where the scattering pattern is recorded

Part II

Method

Chapter 4

The SAXS Experiment

4.1 Sample preparation

The bone were taken from six male Sprague-Dawley rats five weeks of age at the moment of the implantation at the medical university of Graz. They had an implant on each leg through all bone. Regular CT scans were made on the rats to see the evolution of the degradation of the implants and to try to see the formation of gas cavities in the bone. They were then sacrificed at different period of time reported in the table 4.1 .

Sample	Duration of implantation in months
4187	1
4172	3
4050	6
4165	9
4280	12
4340	18

Table 4.1: Duration of implantation of the WZ21 implants

After sacrifice, the bone were scanned, cut in two half and then reduced to slices which were used for an histological analysis, for micro nano indentation and for SAXS analysis. The bone were filled with resin and the thickness was then reduced by sanding in order to reach an optimal thickness, that minimize the absorption and maximize the scattering. Six samples were studied for this alloy.

4.2 SAXS method

The measurement were partly done at the University of Natural Resources and Applied Life Sciences Vienna and partly done at the University of Vienna.

Parameters for mapping

The beam size was 350 µm and the step size was 350 µm. Mapping was usually approximately made 4 mm above the implants and 4 mm under it on the full width. Calibration was done using Silver behenate powder.

SAXS device configuration

Configuration	Distance sample-detector (mm)	λ(Å)	Time/ point (s)
Long	300	1.5418	200

Table 4.2: Parameters of the SAXS device for the measurements

Range of q reached by the configuration: $0.015\,\text{Å}^{-1}$ to $0.71\,\text{Å}^{-1}$. Range of q effectively reached with the configuration : $0.043\,\text{Å}^{-1}$ to $0.4\,\text{Å}^{-1}$.

Background correction

The background was measured in places were only resin was present (see figure 4.1). We assumed that the thickness was constant and only the proportion of bone and resin was changing. Assuming also that intensity in the high value of q is only due to background, we can then correct each curve by normalizing the background.

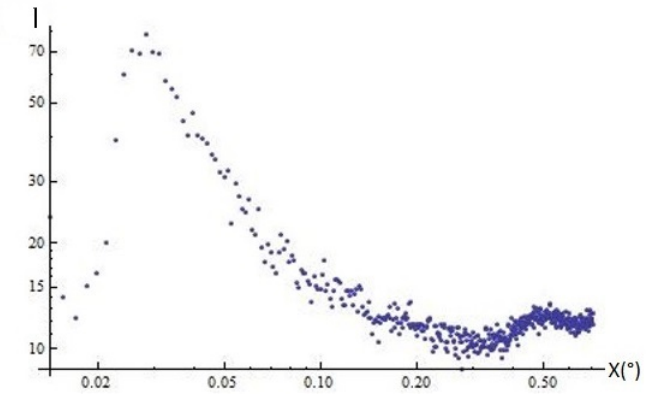

Figure 4.1: Background profile when radially integrated, arbitrary unit for the intensity

Chapter 5

Mathematical modeling of the integrated intensity

To get access to the information, the 2-dimensionnal pattern obtained on the detector must first be integrated. This can be done in two ways (see figure 5.1):

azimuthal integration : At each angle, the data or integrated along the radius,

$$I(\chi) = \int_0^q I(q, \chi) dq$$

through that integration, information about the orientation of the particles can be gained.

radial integration : At each radius, the data are integrated all over a concentric circle,

$$I(q) = \int_0^{360^\circ} I(q, \chi) d\chi$$

through that integration, information about the shape, size, inner surface and fractal dimension can be gained,

5.1 Azimuthal intensity integration

To be able to discriminate if there is a preferential orientation, the intensity is integrated azimuthally. If the particles have a preferential orientation, then, the X-ray photons are going to be scattered in preferential directions, which would mean that the 2D pattern projected on the detector is not going to be concentric circles. In the case of mineral platelets, once azimuthally integrated, the curve is going to be approximated by two Gaussian peaks separated by 180°(see figure 5.2). The parameters used to quantify the orientation of the particles are the following:

orientation : the degree at which the peak appear modulus 180 °,

degree of orientation : the inverse of the width at middle height of the Gaussian peaks.

The intensity is modeled by a double Gaussian curve:

$$I(\chi) = B + a(e^{-(\frac{(\chi-b)^2}{2*c^2}} + e^{-(\frac{(\chi-b-180)^2}{2*c^2}}) \tag{5.1}$$

where

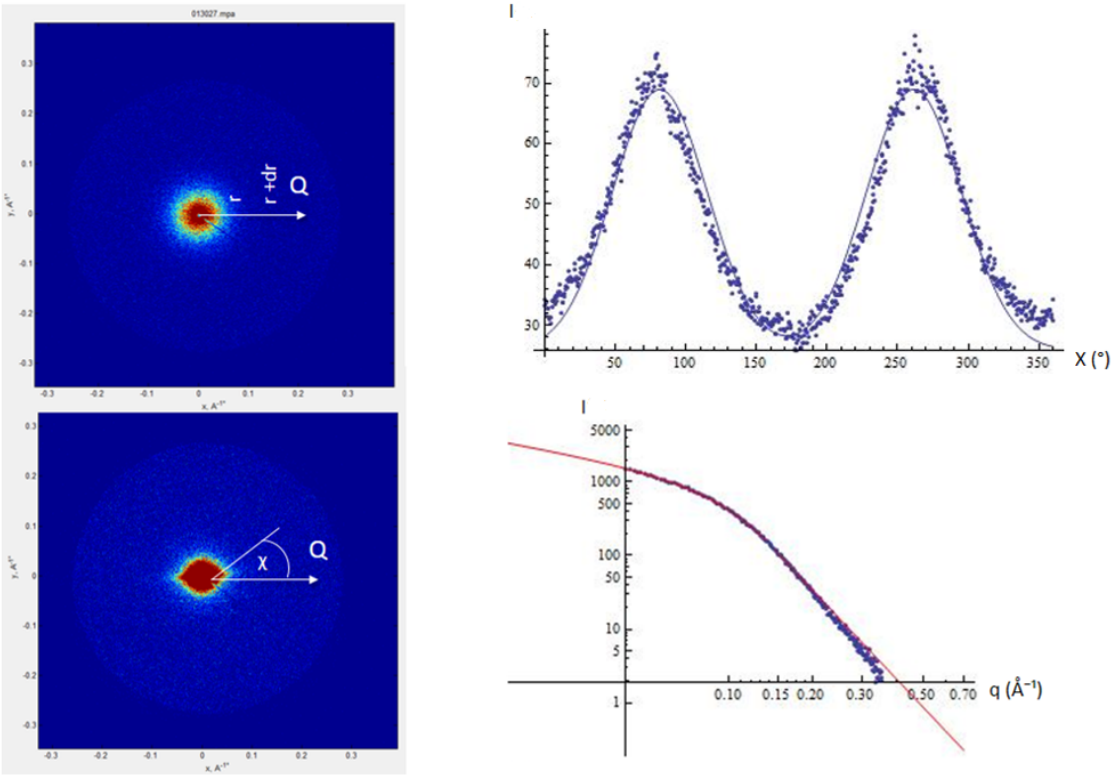

Figure 5.1: The two way of integrating the data, I in arbitrary unit

B: the background noise,

a: the height of the peak,

b: the position of one of the peak,

c: the width of the peak at middle height.

Then it can be deduced that the orientation is **b** and the degree of orientation is $\frac{1}{c}$ (see figure 5.3).

Detector with beam stop

The detector from the University of Natural Resources and Applied Life Sciences Vienna had a beam stop which created a shadow on the detector (see figure 5.4). That shadow had to be corrected before the analyze of the azimuthal intensity integration. The correction of the beam stop shadow was made by taking points 180°away from the shadow and adapting it to the local value. If the curve was anisotropic, then the correction was working well. If we had an isotropic point, then the correction was also valid, as the points were uniformly spread.

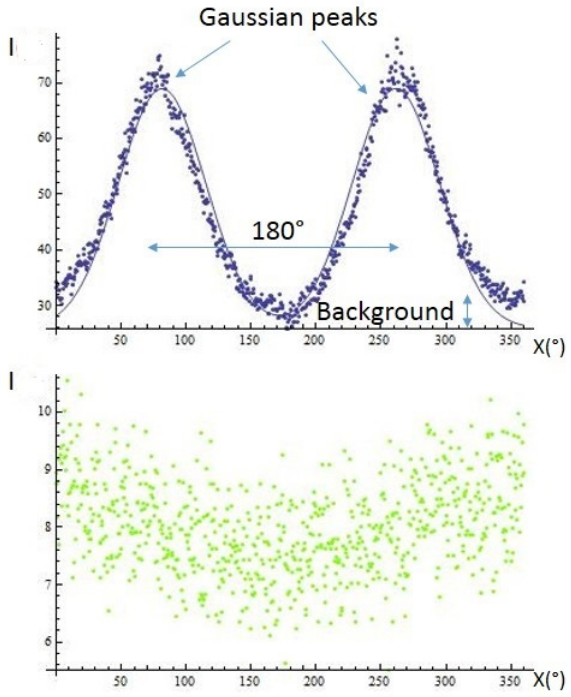

Figure 5.2: The difference between an isotropic point and an isotropic point, I arbitrary unit

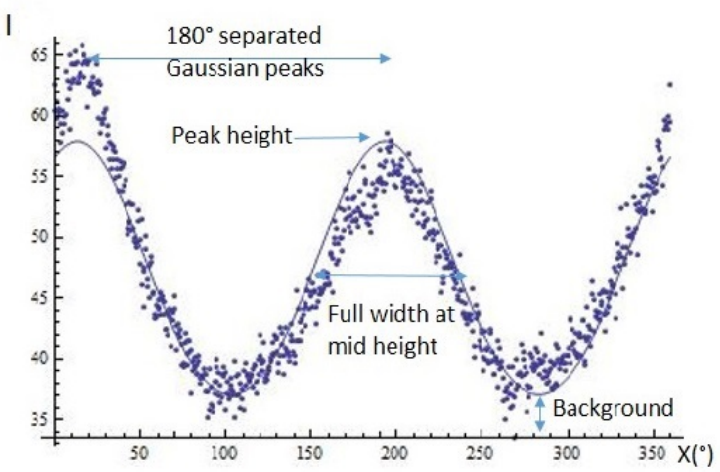

Figure 5.3: The different parameters of the fitting function, I arbitrary unit

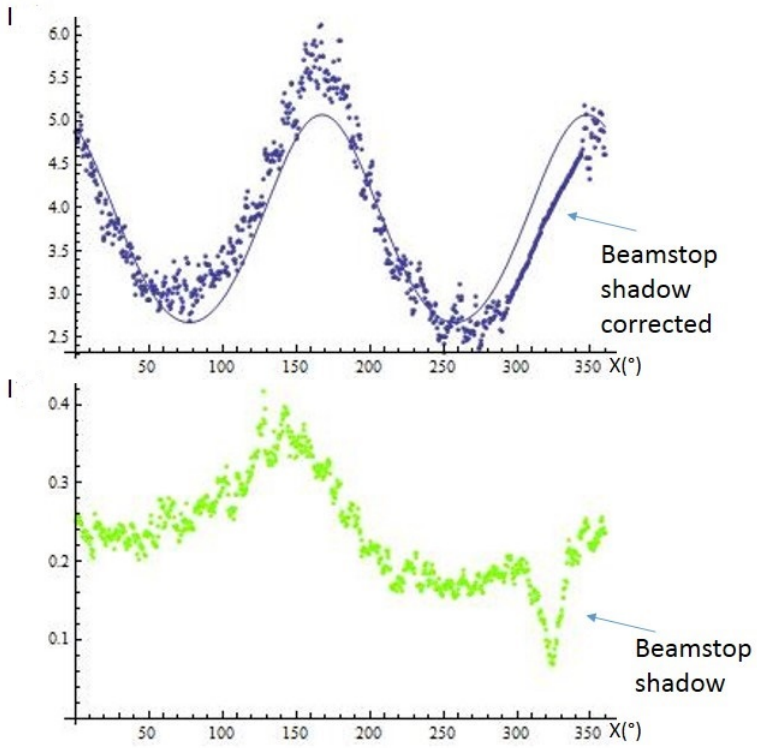

Figure 5.4: The beam stop influence, I arbitrary unit

5.2 Radial intensity integration

The radial integration enables to identify the thickness and the shape of the particles.

5.2.1 Determination of the T parameter

The first approach, and the classic one, to have an idea of the thickness is to use the T parameter, using the ratio that exists between the inner surface of particles and their volumes. According to literature [21]:

$$T = \frac{4}{\pi P} \int_0^\infty q^2 I(q) dq \tag{5.2}$$

with P the Porod constant at high q. As we do not have an access to the shape parameter and to all the curve from 0 to infinity, the curve needs to be extrapolated. Under qmin, its value is set to qmin, and above qmax till infinity, the value is set to $\frac{P}{q^4}$. [22] This approximation is biased by the fact that we do not have a constant mineralization rate and also because we assume the shape of the crystals to always be platelets.

5.2.2 Guinier Porod fitting: Hammouda model

Our second approach that we used has been developed mainly by two authors: G.Beaucage and B.Hammouda.[23, 24, 25, 26] and uses a combination of Guinier and Porod approximation, together with an option to take particle shape into account.

The curve is then modeled with the following equations (see figure 5.5): In the Guinier region, for

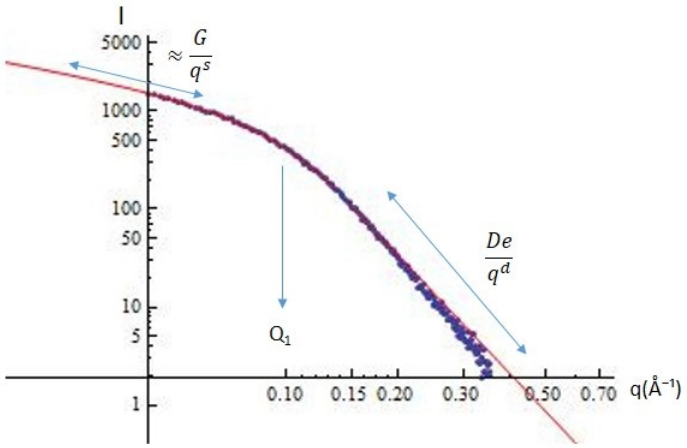

Figure 5.5: The parameters for the Guinier Porord fitting [23], I arbitrary unit

$q \leq Q_1$:

$$f_{guinier}(q) = \frac{G}{q^s} e^{\frac{-q^2 Rg^2}{3-s}} \tag{5.3}$$

and in the Porod region for $q \geq Q_1$

$$f_{porod}(q) = \frac{De}{q^d}. \tag{5.4}$$

with

s: the coefficient that will allow the identification of the shape of the particle also named α,

Rg: the radius of gyration of the particle,

De: the Porod constant $De = Ge^{\frac{-Q_1^2 Rg^2}{3-s}} Q_1^{d-s}$,

d: the slope coefficient in the Porod region, which was taken to be 4,

Q_1**:** the place where the curve is changing of slope $Q_1 = \frac{1}{Rg}(\frac{(d-s)(3-s)}{2})^{1/2}$.

The parameter on which, the program was free to move in order to fit the curve were:

- G,
- s or named α,
- Rg.

The results of the fitting to the Hammouda model that were used to access the thickness and shape were then the radius of gyration Rg, the shape parameter α.

5.2.3 Identification of thickness and shape with the Beaucage/Hammouda model

Once the curves were fitted, a few manipulations were still necessary to get the thickness and the shape. In case of the Hammouda model, an extrapolation on the thickness was made depending on the shape and of the radius of gyration. The following table 5.1 gives the value for shape known, assuming that the other dimensions are much larger than the thickness, and thus do not appear on our 2 D pattern (see figure 5.6) :

	Sphere	Rod	Platelet
α	0	1	2
Thickness function of Rg	$2 * \sqrt{\frac{5}{3}}Rg$	$2\sqrt{2}Rg$	$\sqrt{12}Rg$
$\frac{V}{S}$	$\frac{R}{3}$	$\frac{R}{2}$	$\frac{T}{2}$
T parameter	$\frac{6V}{S}$ Diameter	$\frac{4V}{S}$ Diameter	$\frac{2V}{S}$

Table 5.1: Radius of gyration, thickness and ration surface on volume depending on the shape of the particles

Extrapolation of the results

Then having α, as it was not always an integer equal to 0, 1 or 2 we extrapolate the thickness with the following formulas:

- between sphere and rod (0 and 1):

$$Thickness(\alpha) = (2\sqrt{2}Rg - 2\sqrt{\frac{5}{3}}Rg)\alpha + 2\sqrt{\frac{5}{3}}Rg \tag{5.5}$$

- between rod and platelets between (1 and 2):

$$Thickness(\alpha) = (\sqrt{12}Rg - 2\sqrt{2}Rg)(\alpha - 1) + 2\sqrt{2}Rg \tag{5.6}$$

- above 2:

$$Thickness(\alpha) = \sqrt{12}Rg \tag{5.7}$$

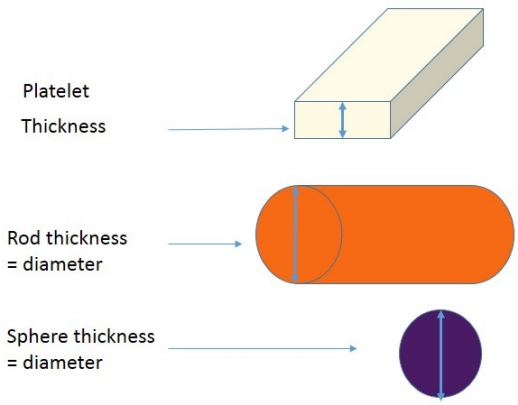

Figure 5.6: Signification of the thickness parameter depending on the shape of the particles

5.2.4 Segmentation on the data

To identify the different points on the mapping, the scattered intensity has been normalized:

$$I_{scattered} = \frac{\int_{q_{min}}^{q_{max}} I_{corrected}(q)dq}{I_{transmitted}} \tag{5.8}$$

If $I_{scattered}$ was too low, it means that there is not enough scattering material and thus, that the results are not consistent. If$I_{scattered}$ was too high, it means that the $I_{transmitted}$ is too low and thus that we do not have actually lot of data to analyze.

Through that discrimination it is possible to differentiate cortical bone (highly scattering with a strong absorbance) from spongious bone, and thus have a better analysis of the data (see table 5.2).

	Cortical Bone	Spongious bone	Void	Resin	Implant
Preferred Orientation	Highly oriented	Random orientation	No orientation	No orientation	No orientation
$I_{transmitted}$	Low	Medium	High	Medium	No transmission
$I_{scattered}$	High	Medium to low	No scattering	No scattering	No scattering

Table 5.2: Discrimination of the data through orientation, $I_{scattered}$ and $I_{transmitted}$

Part III

Results

Chapter 6

Time series for the WZ21 alloy pins

6.1 Pin implanted one month: sample 4187

The first sample was the bone of a rat where the implant has been implanted only for one month. In the figure 6.1 microscopic images of the sample are shown with absorption and scattering maps from the Small Angle X-ray Scattering. The figure 6.1.a shows the microscopic image of the slice of bone that was submitted to the SAXS analysis. The pin is still clearly visible and only superficially corroded. The black scale bar represent 1 mm. On the second microscopic image, the figure 6.1.b, is shown the mirror slice of bone that was dyed to be submitted to a histological analysis. The tissue which are pink are bone. This mirror image of our sample helped us to identify the nature of the point of the mapping, if it was cortical bone or spongious bone. Nevertheless, this mirror is exactly the same, as it was taken on the other half of the bone. The figure 6.1.c is the image of the transmitted intensity. This is equivalent to say that this image is an X-ray radiograph with a precision of 350 µm of the bone. It has only an arbitrary unit. The normalized scattered intensity is represented in figure 6.1.d. The absolute scattered intensity has been divided by the transmitted intensity. This scattered intensity is a measure of the amount of mineral particles in the beam. It can well be seen that the scattered intensity is correlated to the presence of cortical bone. On the edges of the implant, the scattered intensity seems to decrease. The figure 6.2 shows the results from the specific SAXS analysis. The mineral particle thickness (Å) derived from the Hammouda model (figure 6.2.a) seems to be lower near implant. The T parameter (Å) derived from the classic approach seems constant on all the sample and a little increase may be visible near implant. Since the Hammouda model is also sensitive to the shape of the particles in the Guinier region, the shape parameter can be represented on the graph 6.2.c . The shape parameter describes the shape of the particles with 0 being spherical particles, 1 rod like particles and 2 platelet like particles. It does not have a unit. This graph can give the impression that the particles tend to be more platelet like near implant. The last figure 6.2.d is the results of the azimuthal integrations. It represents the orientation of the particles with their degree of orientation as length. In the background is plotted the normalized scattered intensity, to help to visualize the nature of the point scanned. The orientation of the cortical bone is changing near implant.

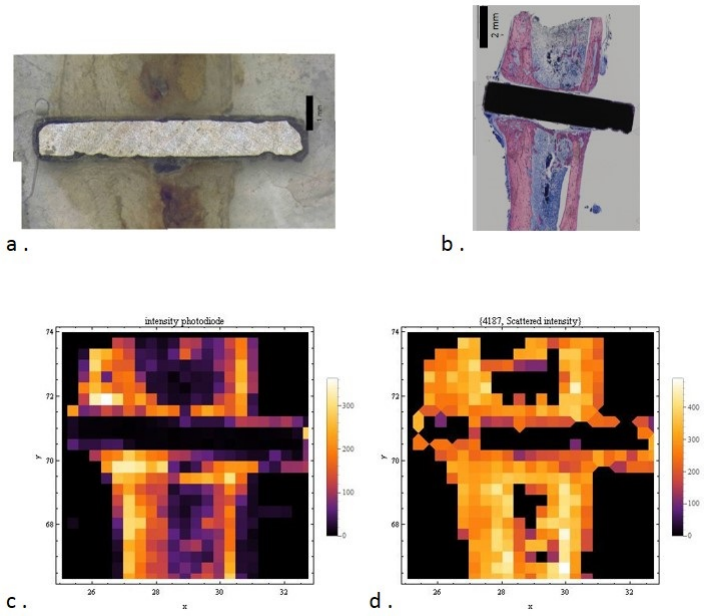

Figure 6.1: 1 month: a: microscopic image of the sample (scale bar 1 mm);
b: microscopic image of the dyed opposite slice of the bone (scale bar 2 mm);
c: the transmitted intensity (arbitrary unit);
d: the normalized scattered intensity (arbitrary unit).

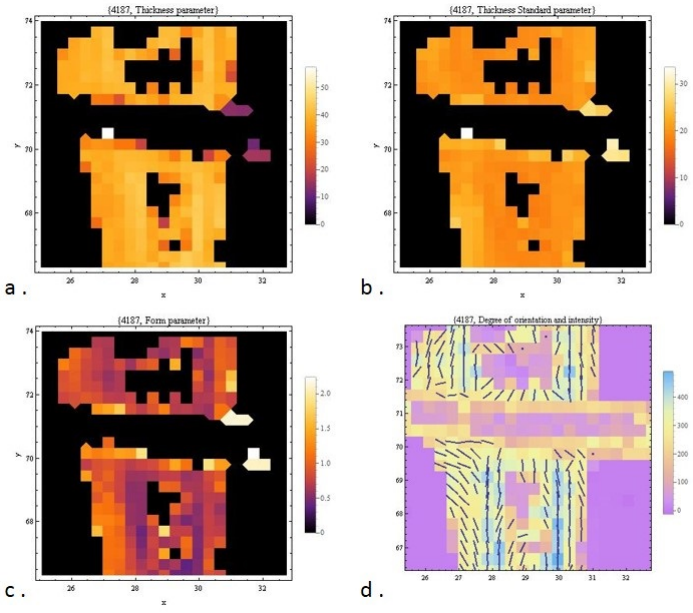

Figure 6.2: 1 month: a: the thickness computed with the Hammouda model (Å);
b: the T parameter (Å);
c: the shape parameter of the particles (no unit);
d: the orientation of the particles with the scattered intensity in background.

6.2 Pin implanted three months: sample 4172

In that sample, the implant was left in the bone for three months. It can be seen that it has already begun to dissolve, on the exterior of the bone (see figure 6.3.a). The corrosion is not only a uniform one, as it can be seen, the implant is also being more degraded on some localized parts. The histological microscopic image of the figure 6.3.b seems to show an irregular bone formation. The transmitted intensity seems to be higher under the implant (see figure 6.3.c), maybe in places where the implant was and where new bone is beginning to grow. The scattered intensity is higher in points where the cortical bone is (see figure 6.3.d). It can also be noticed that the thickness of the mineral particles near the implant seems to drop (figure 6.4.a). When compared with the T parameter in figure 6.4.b, the T seems to increase close to the implant, which is counterintuitive and thought to be due to the changed degree of mineralization rather than a real effect. The shape parameter of the particles near the implant also seems to increase in figure 6.4.c, which means more platelets like mineral near implant and needle like mineral in the rest of the bone. In the figure 6.4.d the bone is reorienting itself near implant to be, not in the direction of the long bone, but to be around the implant, as in the figure 6.2.d.

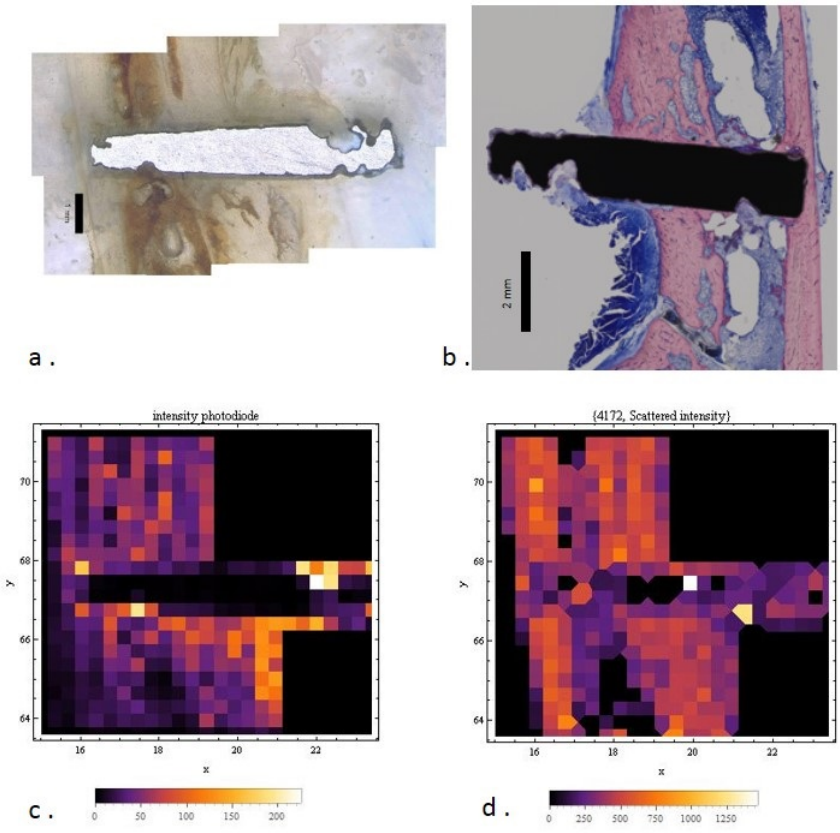

Figure 6.3: 3 months: a: microscopic image of the sample (scale bar 1 mm);
b: a microscopic image of the dyed opposite slice of the bone (scale bar 2 mm);
c: the transmitted intensity (arbitrary unit);
d: the normalized scattered intensity (arbitrary unit).

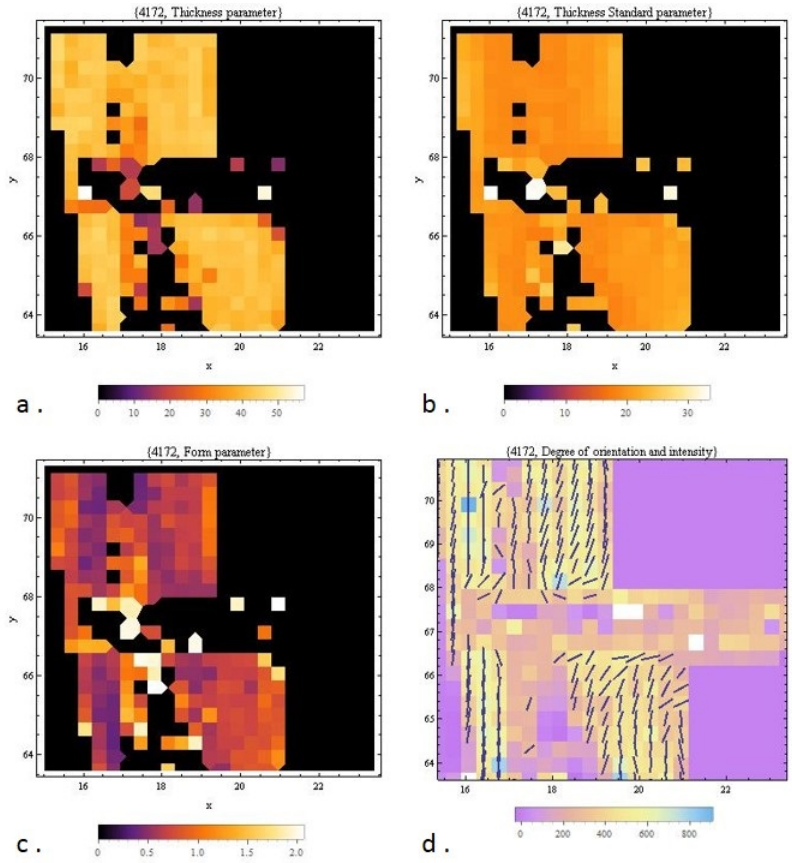

Figure 6.4: 3 months: a: the thickness computed with the Hammouda model (Å);
b: the T parameter (Å);
c: the shape parameter of the particles (no unit);
d: the orientation of the particles with the scattered intensity in background.

6.3 Pin implanted six months: sample 4050

In this sample, the pin, implanted for six months, is still visible but already half degraded in its center (see figure 6.5. In that sample it is clearly visible that the implant is degraded faster in the spongious bone than in the cortical bone (see figure 6.5.a and b). The region of the bone where the implant used to be is not highly scattering, but has a high transmitted intensity (figure 6.5.c and d), which means that it does not have lot of mineral. The thickness of the mineral particles computed by the Hammouda model is getting smaller near implant (see figure 6.5.f) and the shape parameter is getting higher near implant (figure 6.5.e), which means that the particles tend to be more platelet like near implant. In the figure 6.5.g, the T parameter increases slightly near implant near implant. The reorientation of the particles is also visible near implant (figure 6.5.h.)

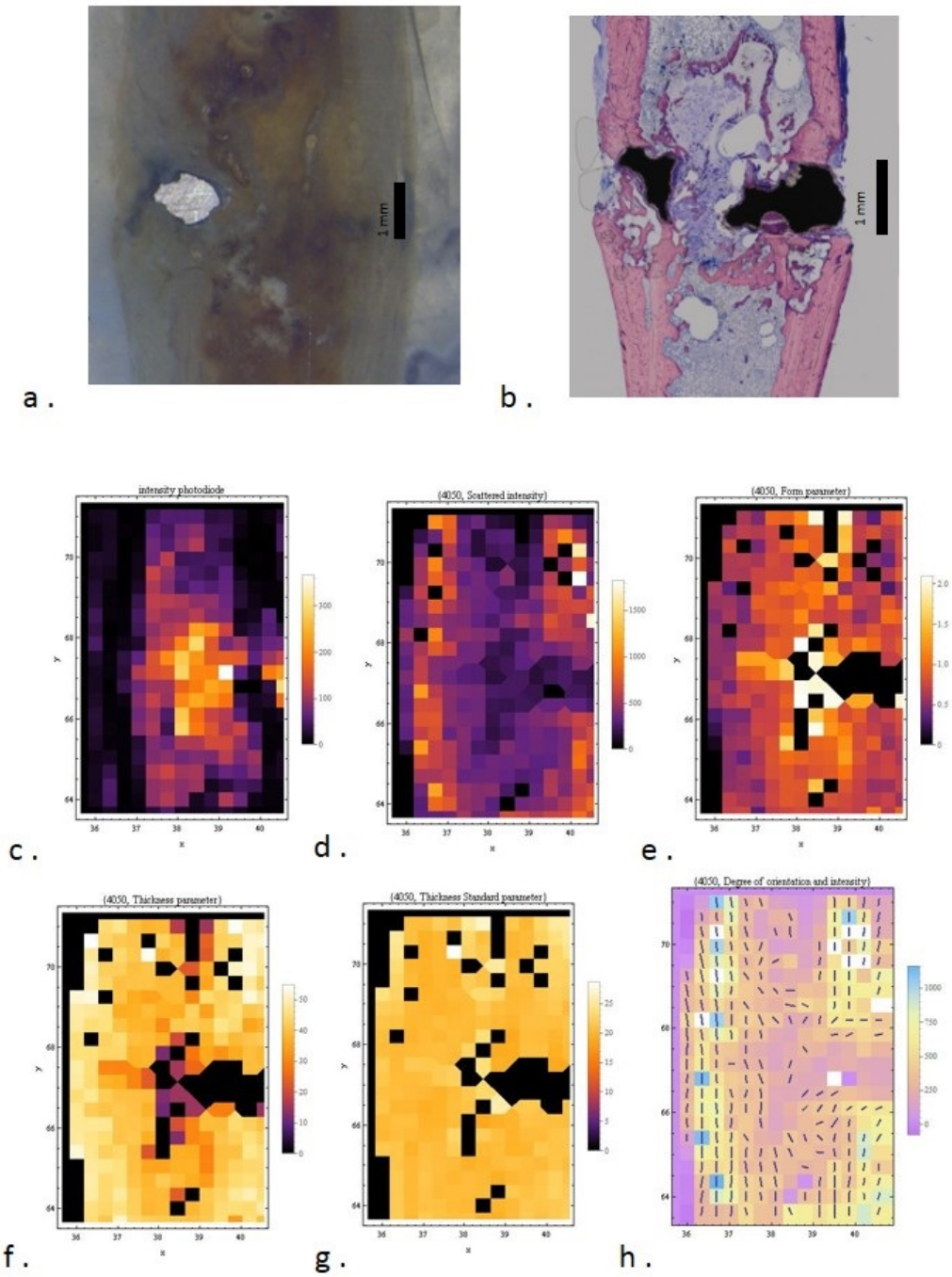

Figure 6.5: 6 months: a: a microscopic image of the sample (scale bar 1 mm);
b: a microscopic image of the dyed opposite slice of the bone (scale bar 1 mm);
c: the transmitted intensity (arbitrary unit);
d: the normalized scattered intensity (arbitrary unit):
e: the shape parameter of the particles (no unit);
f: the thickness computed with the Hammouda model (Å);
g: the T parameter (Å);
h: the orientation of the particles with the scattered intensity in background.

6.4 Pin implanted nine months: sample 4165

The pin was implanted for nine months, and what remains of the pin is very small. A cavity which was formed in the bone is also visible (see figure 6.6.a and b). The transmitted intensity is very strong in the region where the bone has newly grown (figure 6.6.c) as in the sample where the pin was implanted for 6 months (figure 6.5.c) The scattering intensity is very strong in cortical bone (figure 6.6.d) as in the sample 4050 (figure 6.5.d) and 4172 (figure 6.3.d). The thickness of the particles fitted with the Hammouda model seems to decrease near implant (figure6.7.a) when the T parameter seems rather constant (figure 6.7.b). The bone particles seem to be more platelets like in newly formed bone, which is in places where the implant was (figure 6.7.c). The particles have reoriented themselves around the implant in the figure 6.7.d. At position where the implant used to be, the orientation is still perturbed but it looks like the bone is already beginning to get the crystals in the main direction.

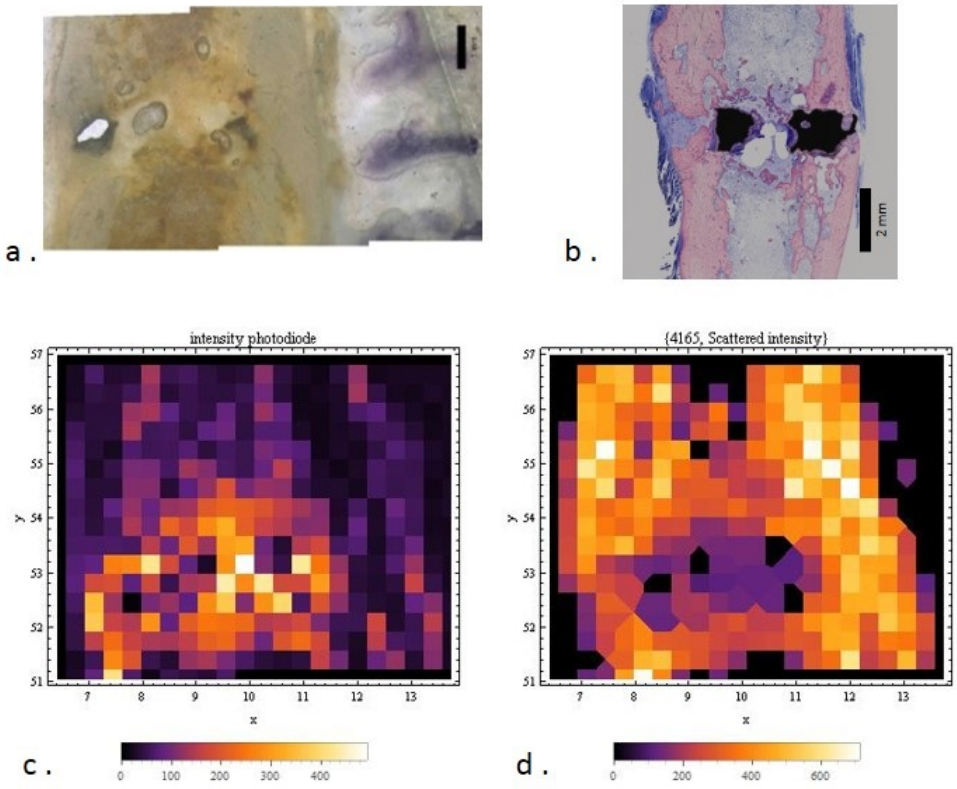

Figure 6.6: 9 months: a: microscopic image of the sample (scale bar 1 mm);
b: microscopic image of the dyed opposite slice of the bone (scale bar 2 mm);
c: the transmitted intensity (arbitrary unit);
d: the normalized scattered intensity (arbitrary unit).

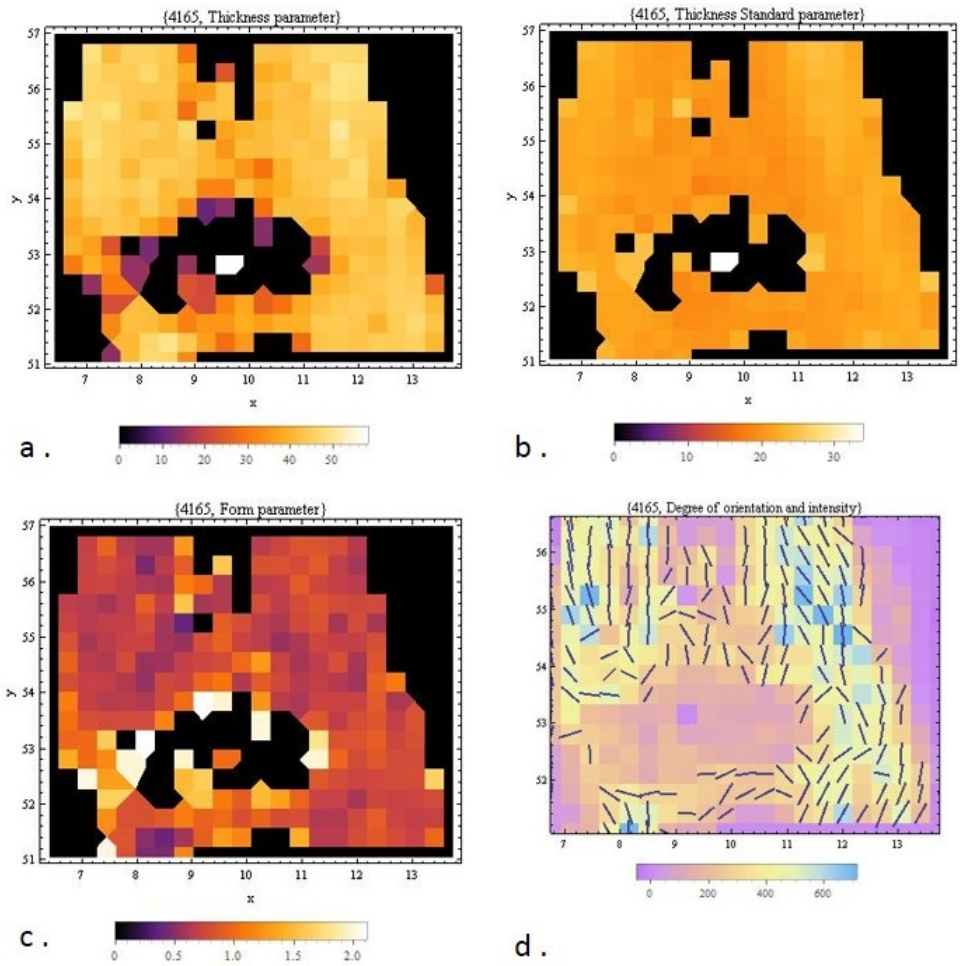

Figure 6.7: 9 months: a: the thickness computed with the Hammouda model (Å);
b: the T parameter (Å);
c: the shape parameter of the particles (no unit);
d: the orientation of the particles with the scattered intensity in background.

6.5 Pin implanted twelve months: sample 4280

That pin was less degraded in that sample after twelve months of implantation than the sample 4165 with 9 months (See figure 6.8.a and b compared with figure 6.6.a and b). Nevertheless, it is well visible that the pin has more degraded in the spongious bone than in the cortical bone. We do not see any cavity due to gas formation. The transmitted intensity is very high in the region of newly formed bone, *i. e.* where the implant has already begun to degrade (figure 6.8.c) and the scattering intensity is maximal in the cortical bone (See figure 6.8.d). The thickness of the particles computed with the Hammouda method tends to decrease in the newly formed bone as it is visible on the figure 6.9.a . The T parameter has some changes near the implant but that changes are not significant as it can be seen on the figure 6.9.b . The shape tends to increase in newly formed bone, as the figure 6.9.c seems to show. Bone is again adapting the orientation of the particles near implants in figure 6.9.d, and the perturbation of orientation compared to the main direction of the bone does not seem to be corrected.

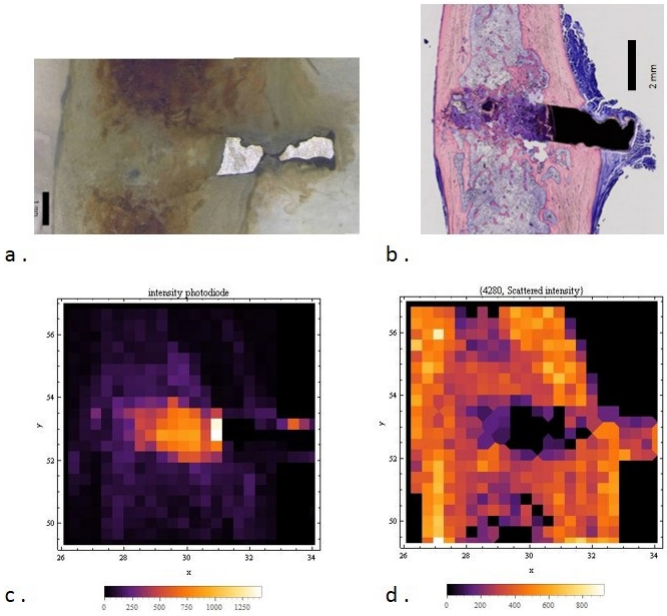

Figure 6.8: 12 months: a: microscopic image of the sample (scale bar 1 mm);
b: microscopic image of the dyed opposite slice of the bone (scale bar 2 mm);
c: the transmitted intensity (arbitrary unit);
d: the normalized scattered intensity (arbitrary unit).

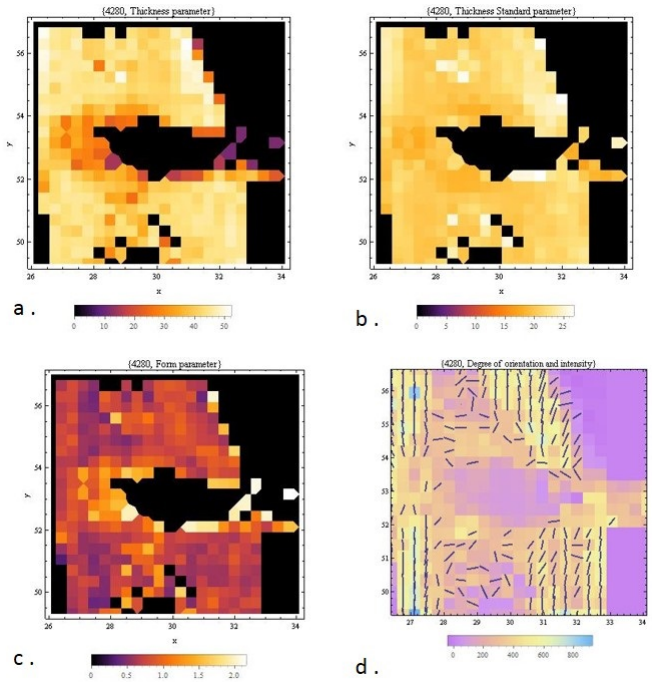

Figure 6.9: 12 months: a: the thickness computed with the Hammouda model (Å);
b: the T parameter (Å);
c: the shape parameter of the particles (no unit);
d: the orientation of the particles with the scattered intensity in background.

6.6 Pin implanted eighteen months: sample 4340

The pin was implanted for 18 months and had totally dissolved during that period of time as the figure 6.10.a and 6.10.b show it. The bone did not perfectly rebuild itself, as it can very well be seen on the dyed histological photography: it has made a loop , which would then weaken the bone. This weakness is visible on the transmitted intensity graph, figure 6.10.c . Nevertheless the bone has build new cortical bone which scatters as much as old cortical bone: on the figure 6.10.d the old cortical bone being the points that are away from the center of the sample where the implant was and which is now the new cortical bone. Nevertheless, the bone shape is pretty consistent in all sample, and the orientation follows the newly formed cortical bone. The thickness of the particles computed with the Hammouda model, nor the T parameter, do not seem to depend of the position of the implant (figure 6.11.a and b), which is contrasting with the other sample with shorter dwelling time. The shape parameter describing the particles shape also seems independent of the position of the implant on the figure 6.11.c. The orientation of the particles (figure 6.11.d), when correlated with the microscopic images 6.10.c and 6.10.d seem to follow the structure of cortical bone.

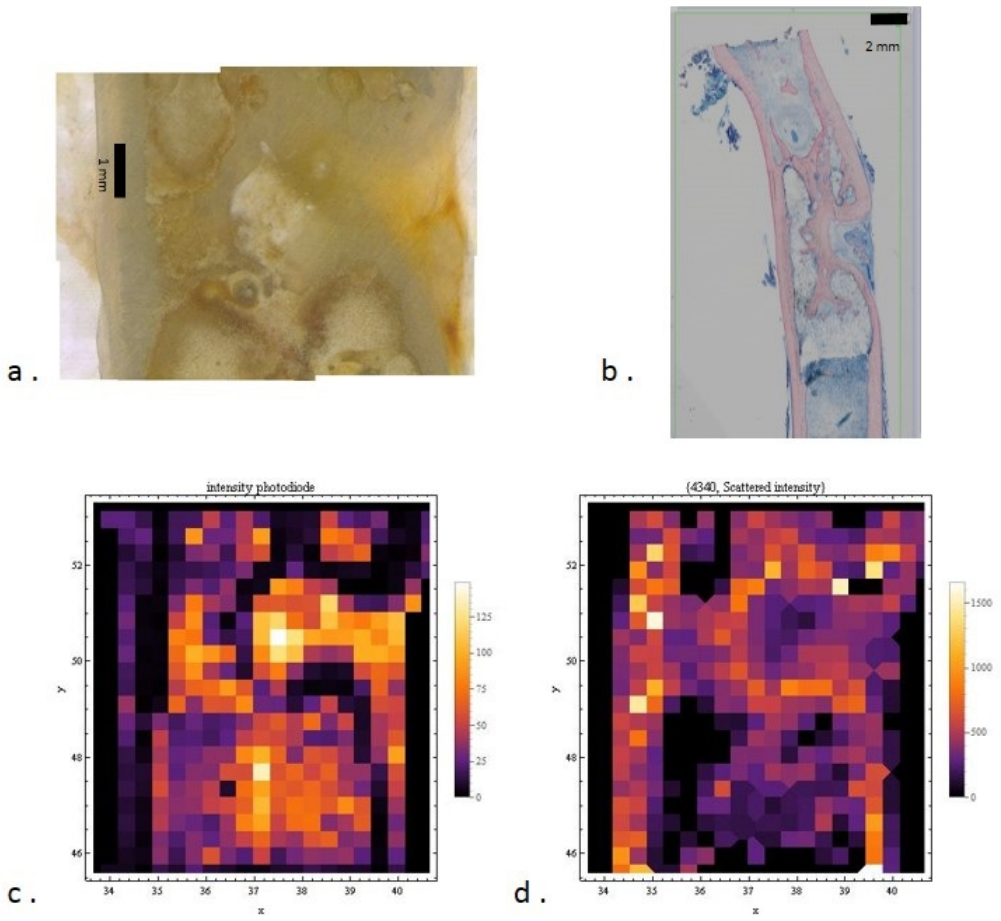

Figure 6.10: 18 months: a: microscopic image of the sample (scale bar 1 mm);
b: microscopic image of the dyed opposite slice of the bone(scale bar 2 mm);
c: the transmitted intensity (arbitrary unit);
d: the normalized scattered intensity (arbitrary unit).

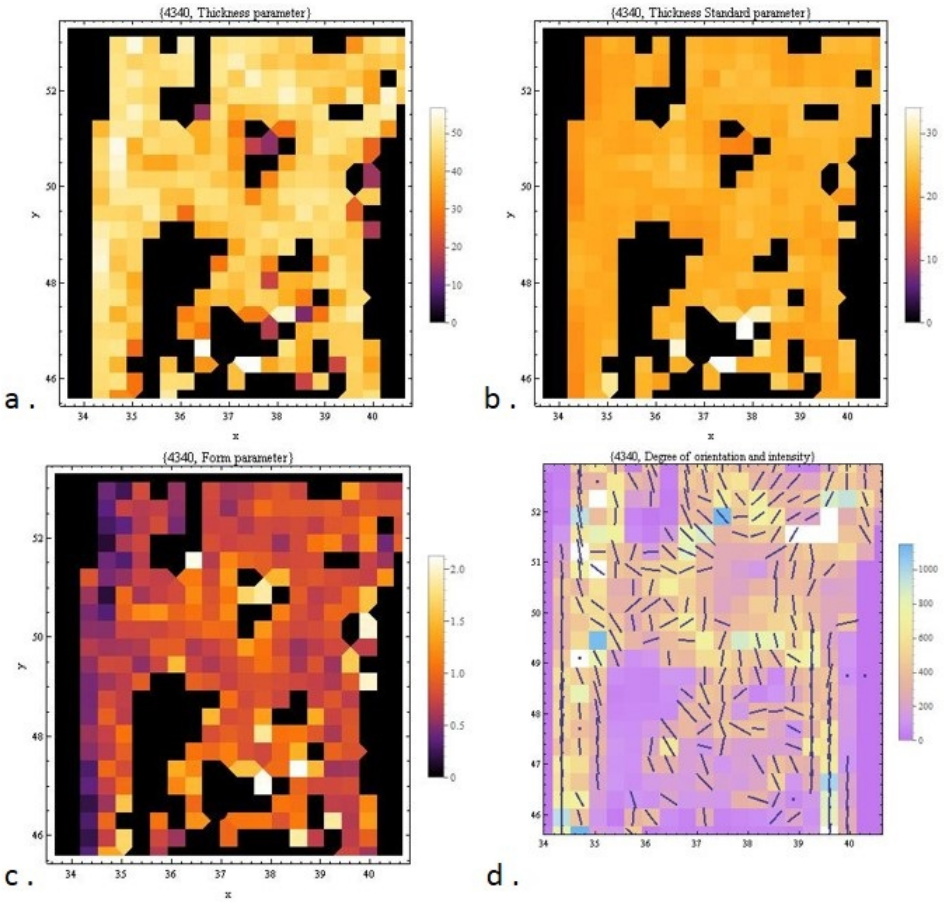

Figure 6.11: 18 months: a: the thickness computed with the Hammouda model (Å);
b: the T parameter (Å);
c: the shape parameter of the particles (no unit);
d: the orientation of the particles with the scattered intensity in background.

Part IV

Discussion

Chapter 7

Evolution of the parameters

Discussion of the time evolution

In the previous part, each sample was studied individually, which, makes the analysis dependent on the natural individual variation. In this part, more general tendencies are going to be shown.

7.1 Difference cortical and spongious bone

In the spongious bone, the metabolism is higher and there is more blood circulation, which could easily explain why the pin is often more degraded in the spongious bone than in the cortical bone, for example, the sample 4050, 4165, 4280 (see figure 7.1.c ,d, and e). Indeed, as, there is more blood, the evacuation of the degradation product is made quicker, which constantly displaces the state of equilibrium of the Mg corrosion. The reaction has then a higher degradation rate.

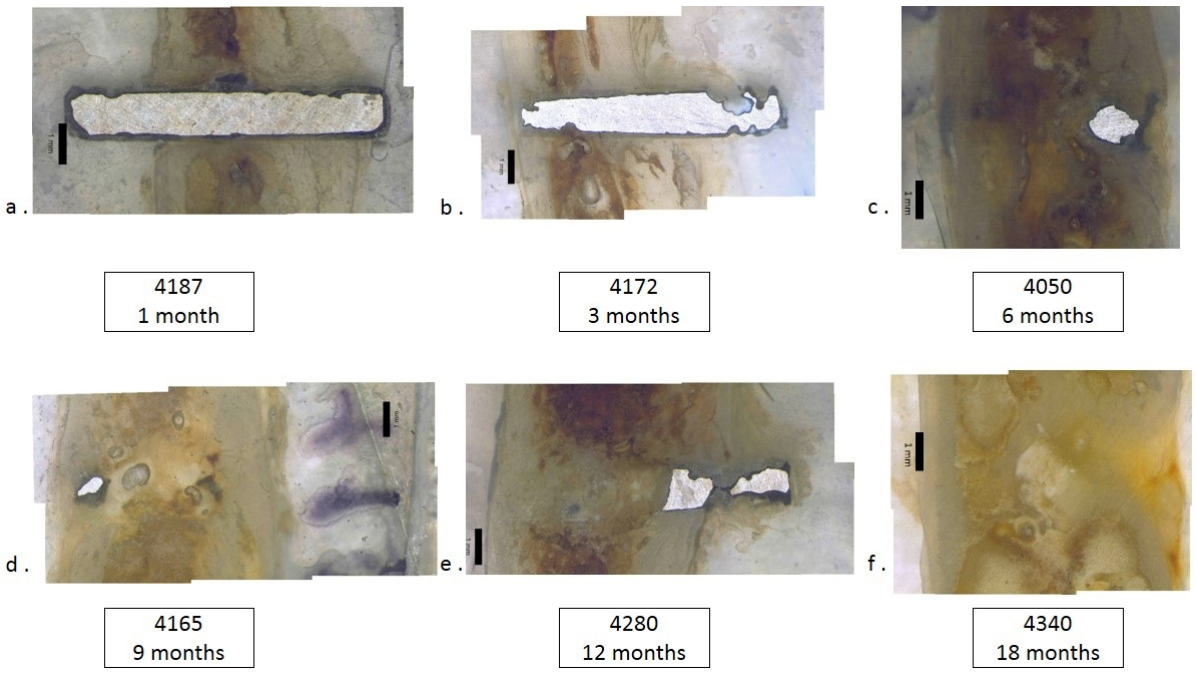

Figure 7.1: The pin states after 1, 3, 6, 9, 12 and 18 months of implantation (scale bar 1 mm) (respectively a, b, c, d, e, f

Denomination of cortical bone and newly formed bone

For the following analysis of the parameter to have a better view of the influence of the implant, two types of data points on the mapping were taken: the so called newly formed bone (in green in figure 7.2) and the cortical bone (in blue in figure 7.2). The newly formed bone is the bone that grew in place where the implant was and had degraded. The cortical bone are the points of the bone that form the outer layer of the bone. It can be seen that the denomination of newly formed bone has been only considered for sample with implantation time longer than 3 months.

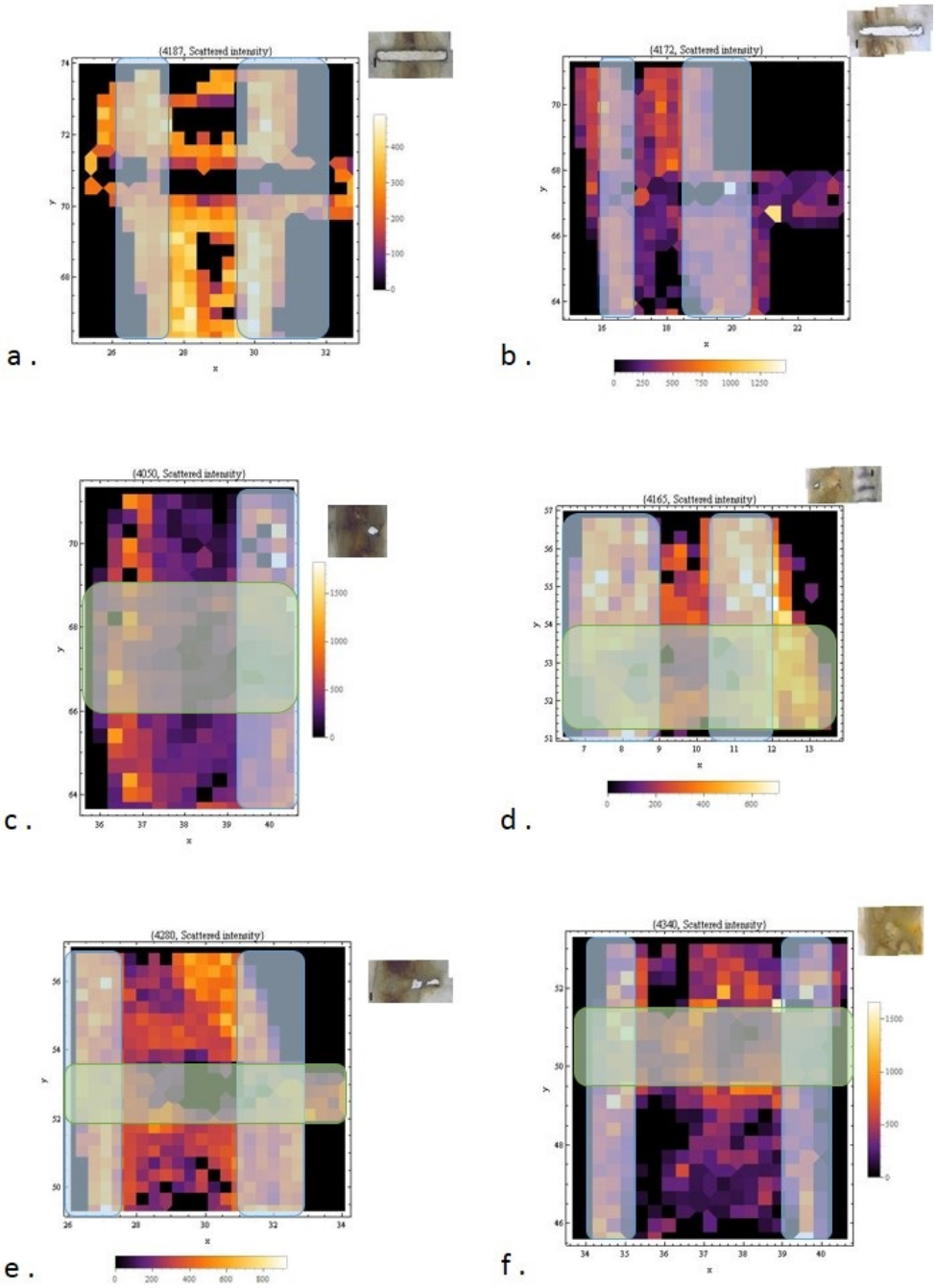

Figure 7.2: In green were the so called newly formed bone and in blue the zone for the cortical bone. Bones with dewlling time of 1, 3, 6, 9, 12 and 18 months, respectiveley a, b, c, d, e and f.

7.2 The scattered intensity

The scattered intensity is a parameter which gives information on the relative amount of mineral, which provides in our bone sample the most scattering contrasts, as it is the material with the higher differences of electron density, compared to void, collagen or resin. As said earlier, the scattered intensity that is studied here has been normalized with the transmitted intensity to be independent of the thickness of material it goes through. The evolution in the newly formed bone is not very clear, although a tendency can be guessed in some sample: it seems that the scattered intensity is decreasing near implant in figure 7.3.a, 7.3.b and 7.3.c . This drop of scattered intensity can be explained by a drop of mineralization near implant. Indeed with growing bone, the first elements that are present are not crystals but first the collagen fibers, that would form the callus. This callus is then going to be mineralized but its degree of mineralization is lower than mature bone. So it would be logical to have a drop of mineralization near implant. When the evolution of the scattered intensity as a function to the distance to the implant is studied in the cortical bone, some sample show the same tendency, figure 7.4.c and 7.4.d . This drop in the scattered intensity could be correlated to the evolution of the T parameter near implant (cf section 7.6.1).

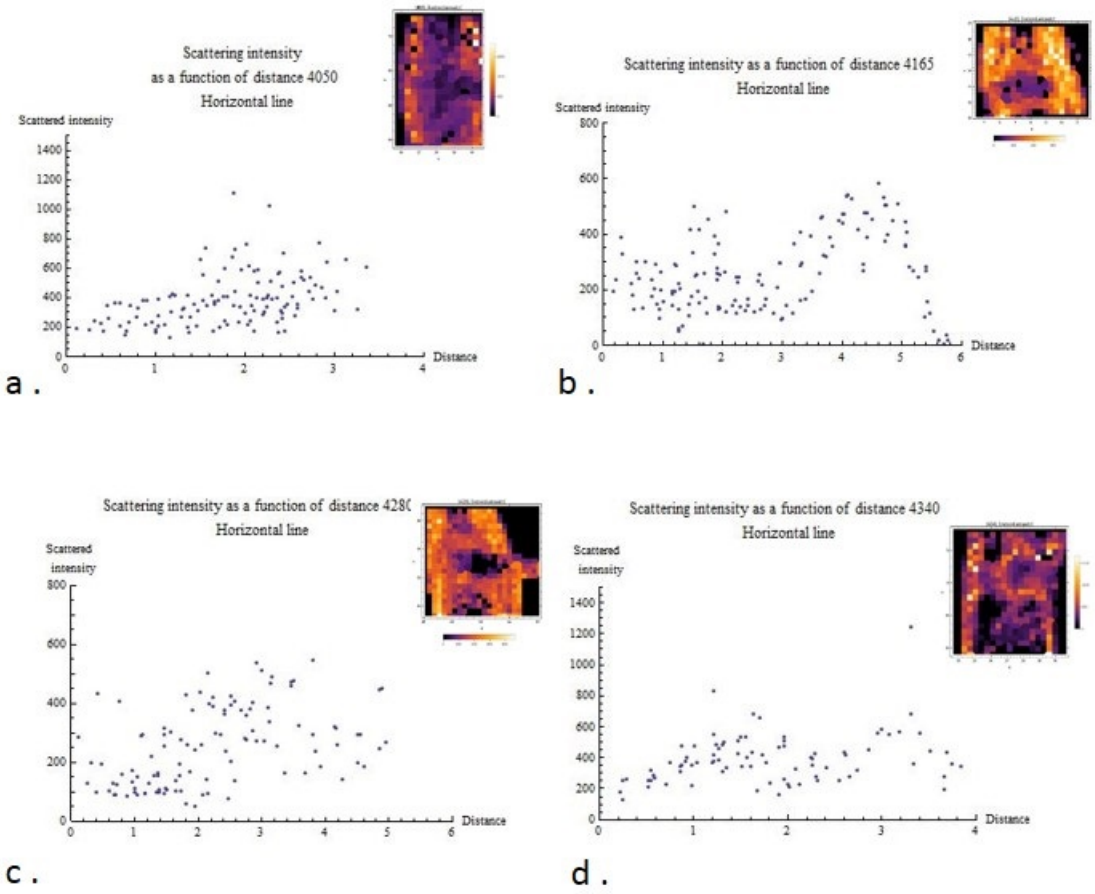

Figure 7.3: Scattered intensity (Arbitrary unit) as a function of the distance to the implant (mm) in the newly formed bone
a: 6 months implantation; b: 9 months implantation; c: 12 months implantation; d: 18 months implantation.

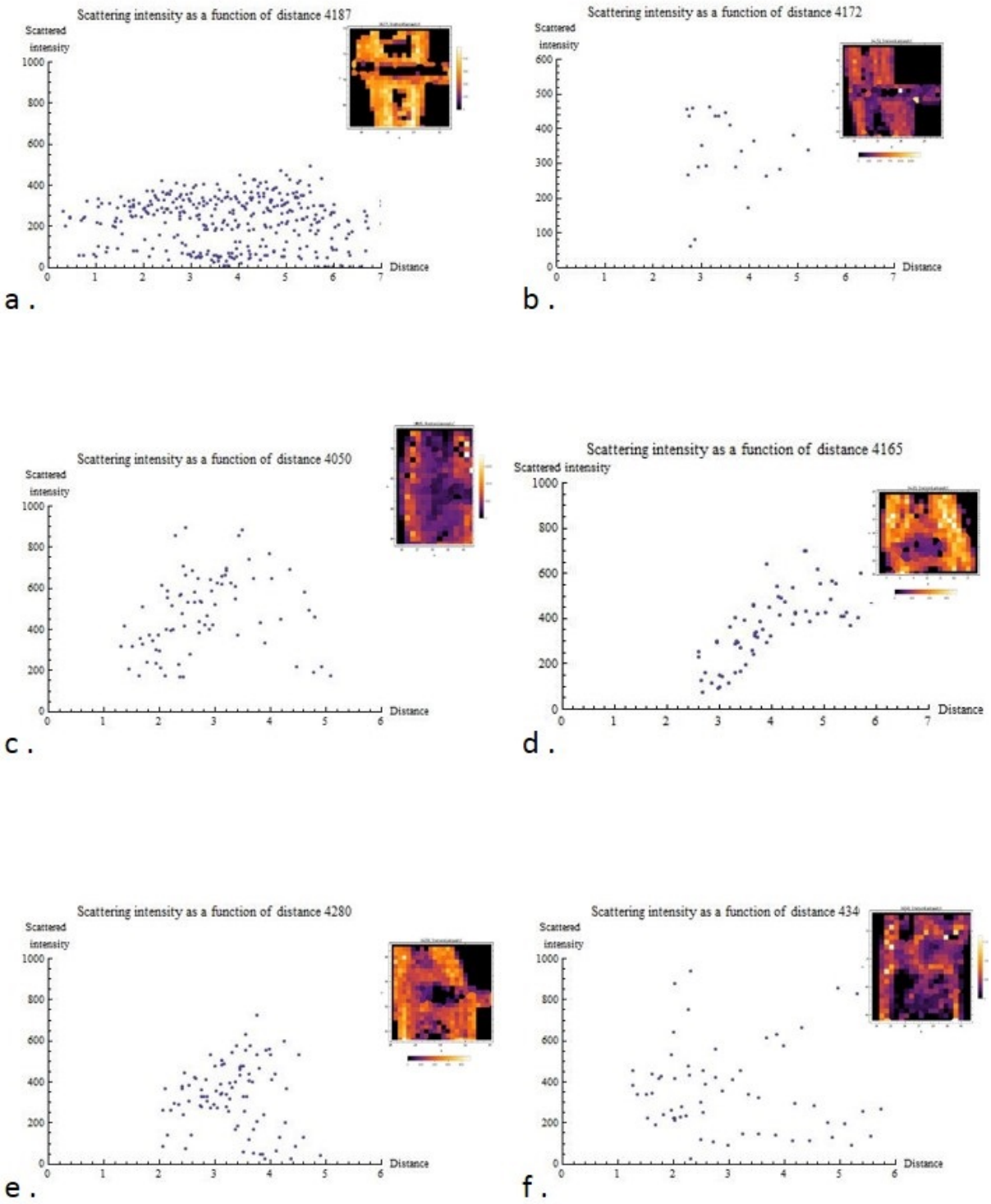

Figure 7.4: Scattered intensity (Arbitrary unit) as a function of the distance to the implant (mm) in the cortical bone
a: 1 month implantation; b: 3 months implantation; c: 6 months implantation; d: 9 months implantation; e: 12 months implantation; f: 18 months implantation.

7.3 Thickness of the particles computed with the Hammouda model Evolution near Implant

The thickness of the particles is an indicator of the age of the particles till a certain thickness which is the thickness of a mature bone particle. Indeed, the older a particle is, the more mineral would have been formed, and then the thicker the particles is going to be. In the figure 7.5.a, b and d, it seems that near implant, the thickness is getting smaller, which would be logical, as it is newly formed particles. This impression is also due to the fact that near implant, the dispersion of the value of the particle's thickness seems larger than away from the implant (figure 7.5.a, b and d). Nevertheless, that tendency is not visible in all bone as the bone with a dwelling time of 12 months (figure 7.5.c9, where that tendency is not visible.
In cortical bone, it seems that near implant, the thickness is more variable and smaller than away from the implant: in figure 7.6.b, c, d and e, respectively 3, 6, 9 and 12 months of implantation time. Nevertheless, all sample do not seem to have an increasing thickness size with increasing distance to the implant as the bones implanted for 1 and 18 months (respectively figure 7.6.a and f), where no relation seems to exist between thickness of the particles and the distance to the implant. This could be explain for the first one, that in one month, the bone did not have time to grow new particles. For the second case where no influence seems to exist between distance and thickness, this could be explain by the fact that the bone particles have all attained their mature size and thus, that the thickness of the particles is independent of its age.

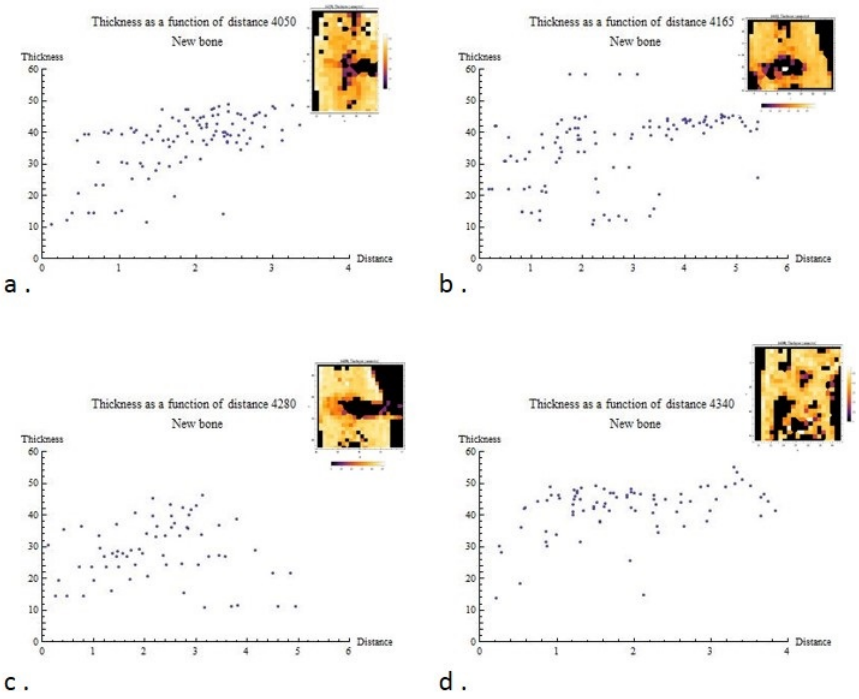

Figure 7.5: Thickness (Å) as a function of distance to the implant (mm) in newly formed bone
a: 6 months implantation; b: 9 months implantation; c: 12 months implantation; d: 18 months implantation.

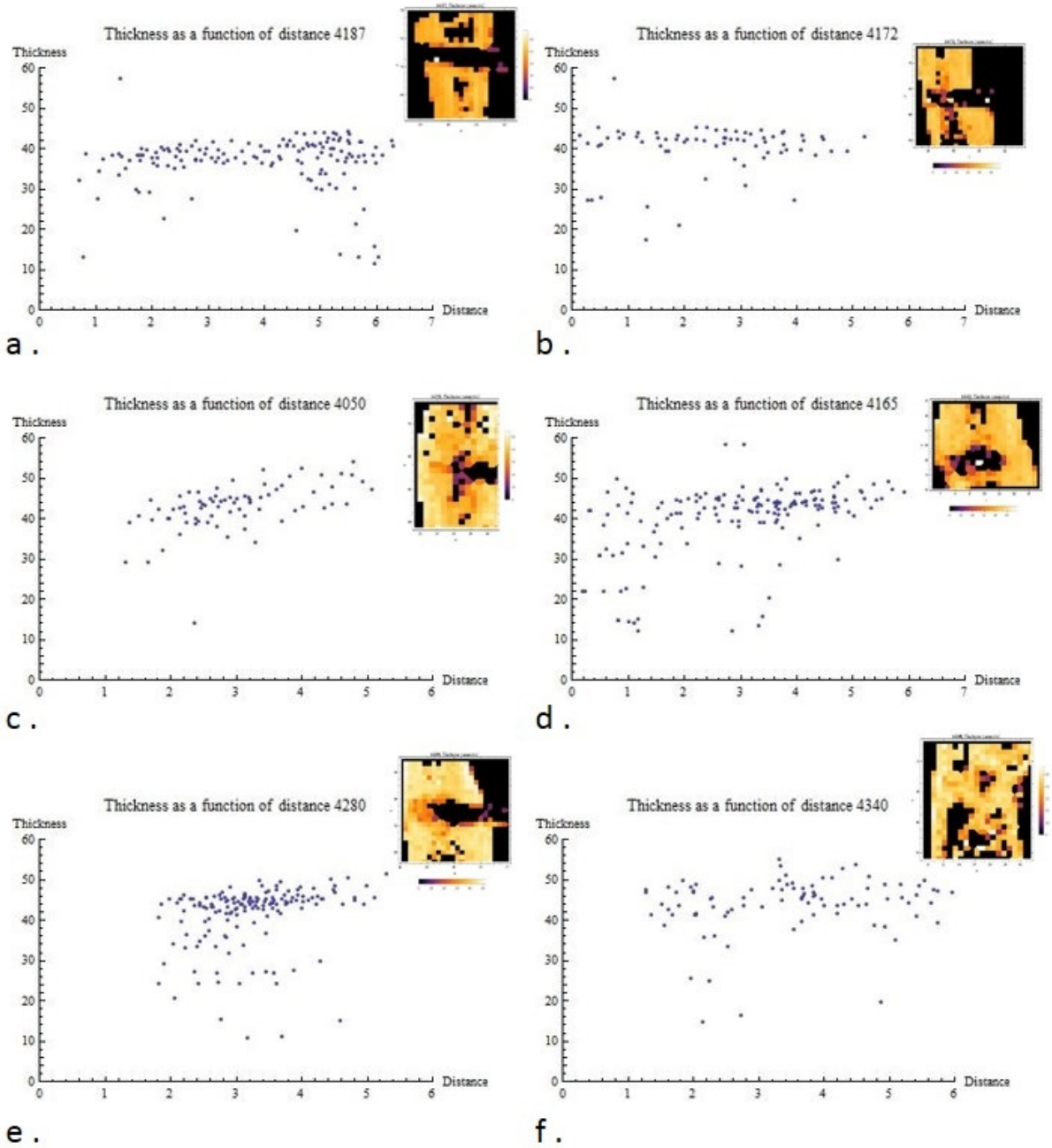

Figure 7.6: Thickness (Å) as a function of distance to the implant (mm) in cortical bone
a: 1 month implantation; b: 3 months implantation; c: 6 months implantation; d: 9 months implantation; e: 12 months implantation; f: 18 months implantation.

7.4 The shape parameter α computed with the Hammouda model

7.4.1 Needle like particles and platelets like particles

The α parameter used to describe the shape has been extracted of the 2D diffraction pattern by the fitting of the radial integration to the Hammouda model which is sensitive to the shape. The value of the shape parameter gave us mainly value of α between 0 and 2 at the maximum with a majority of the data points being between 0 and 1 which means that the particles have a shape between a sphere and a rod, which is an ellipsoid (see figure 7.7). Studying human bone, we would have expected the particles to be more platelets like [1, 3], but as the bone studied were bones from rats, those results are actually consistent [21],as rats and mice bones tends to have particles which are more needle like than platelets like.

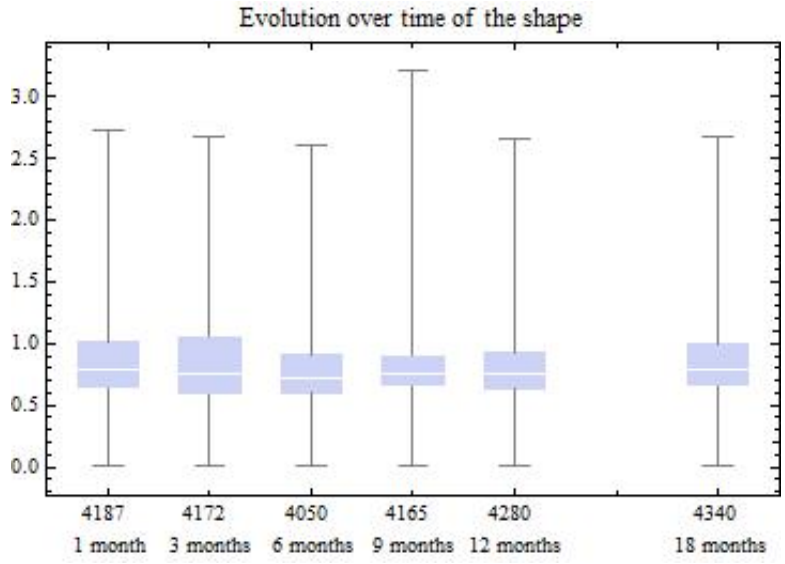

Figure 7.7: Shape parameter (no unit) as a function of duration of implantation of the pin;
The white line is the median, the two extrema of the blue box are respectively, 25% and 75% of the data points of the mapping and the extremities of the black bar are the extrem values of the shape parameter

7.4.2 Influence of the distance to the implant

As it can be seen on those graphs, the shape parameter dispersion seems to increase near the implant in cortical bone (see figure 7.8.b c and d) and in newly formed bone (see figure 7.9a, b and d). This higher dispersion has the effect that the shape parameter seems to increase near implant, which means that the particles are more platelet like near implant and more ellipsoidal like away from the implant.

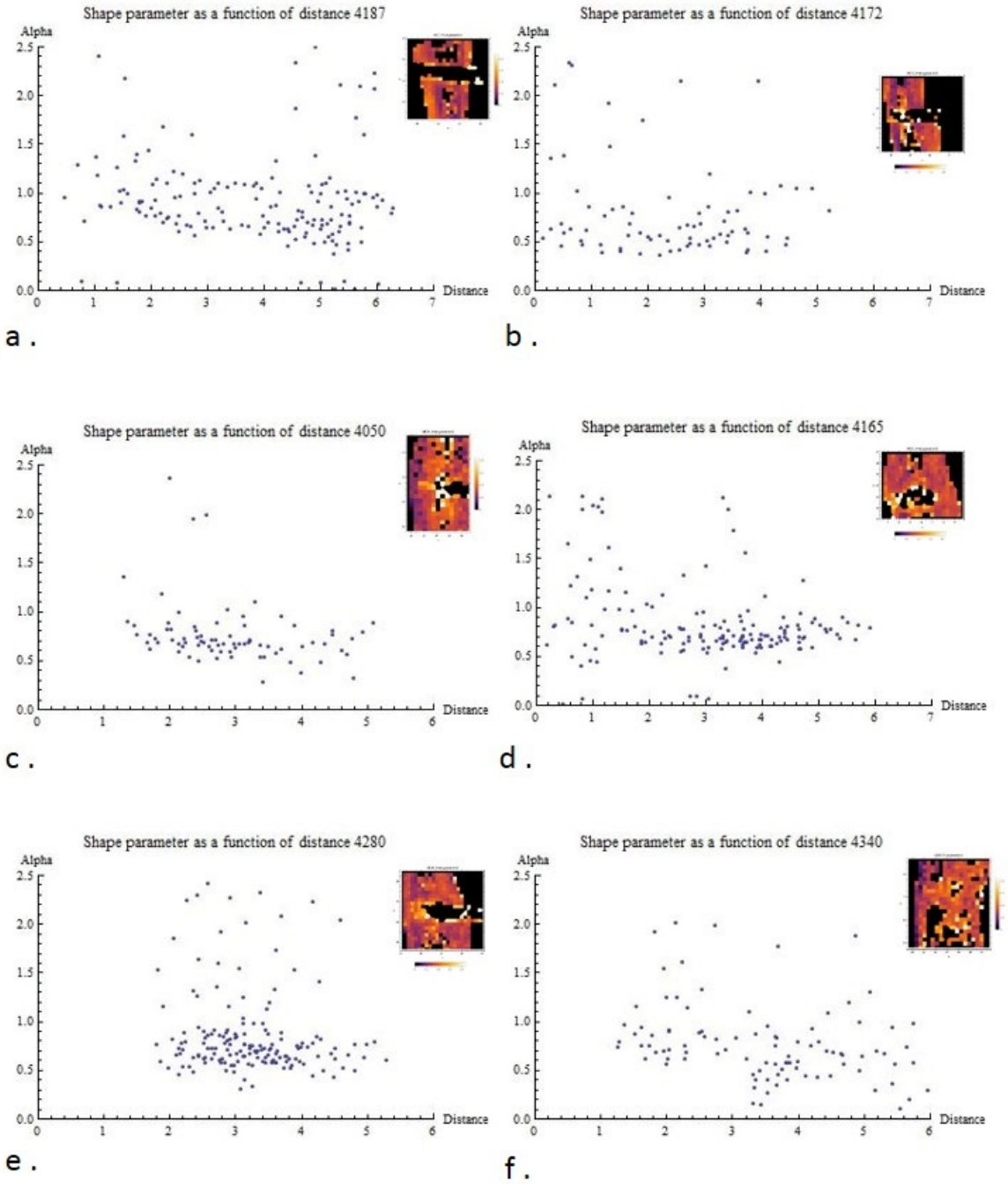

Figure 7.8: Shape parameter (no unit) as a function of the distance to the implant (mm) in cortical bone
a: 6 months implantation; b: 9 months implantation; c: 12 months implantation; d: 18 months implantation.

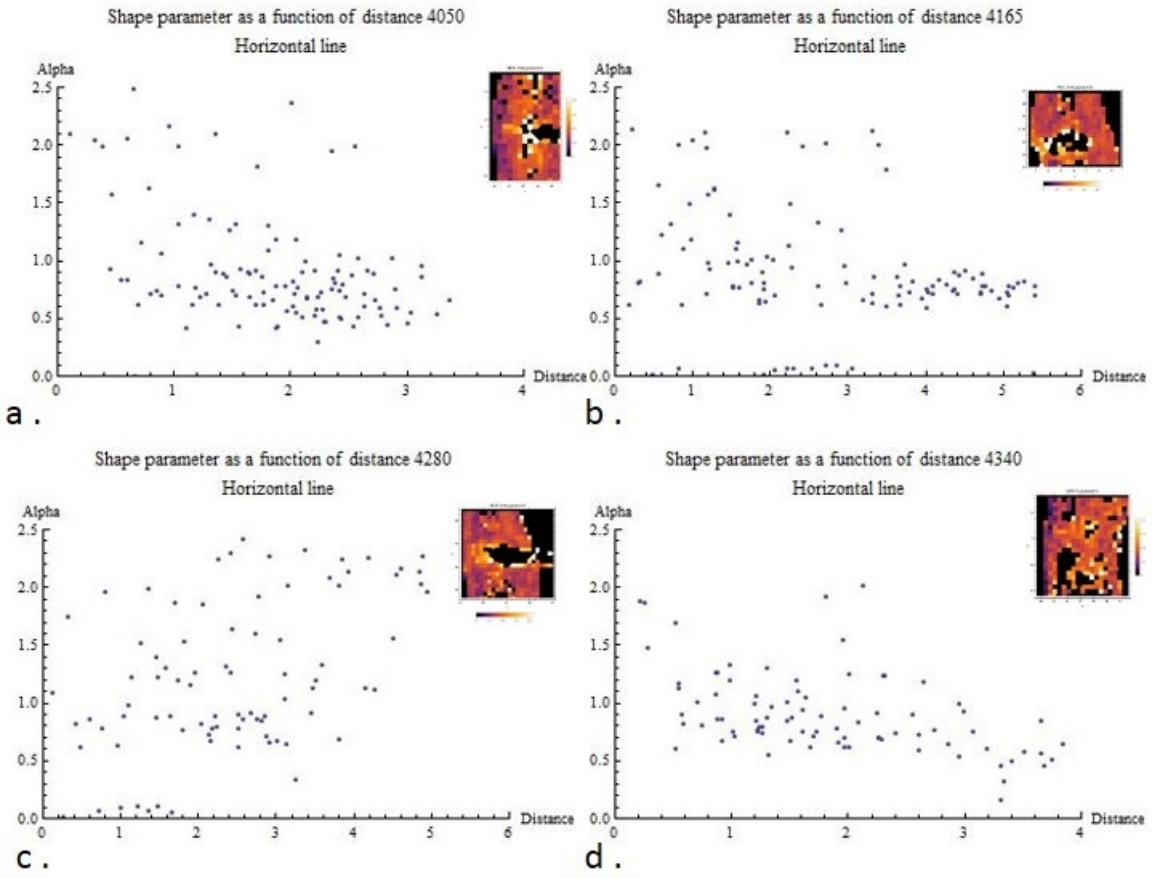

Figure 7.9: Shape parameter (no unit) as a function of the distance to the implant (mm) in newly formed bone

7.4.3 Guinier slope fitting influence on the shape parameter α

The shape parameter α is fitted in the Guinier region, which is the region of low q. This region can appear extended in logarithmic scale, but is in reality very narrow and only a few points issued from the radial integration of the diffraction pattern are present in that region. Indeed the data range for the radial integration runs from $0.042\,\text{Å}^{-1}$ to $0.4\,\text{Å}^{-1}$ and the Guinier region runs usually from $0.04\,\text{Å}^{-1}$ to $0.1\,\text{Å}^{-1}$ when the Porod region runs from $0.1\,\text{Å}^{-1}$ to $0.4\,\text{Å}^{-1}$, which is five times larger. Would it be a small difference in the integrated points, which would make the integrated intensity more high, this would have for consequence an increase of the shape parameter. As we do not have lot of data in that region of the integration, the variability is high for the shape parameter found with the Hammouda model. Moreover, near the implant the scattering intensity is smaller, which means less integrated points on which the data could be fitted, then the increase of the shape parameter near the implant is to be taken with caution. The figure 7.10, shows how the shape parameter can be shifted.

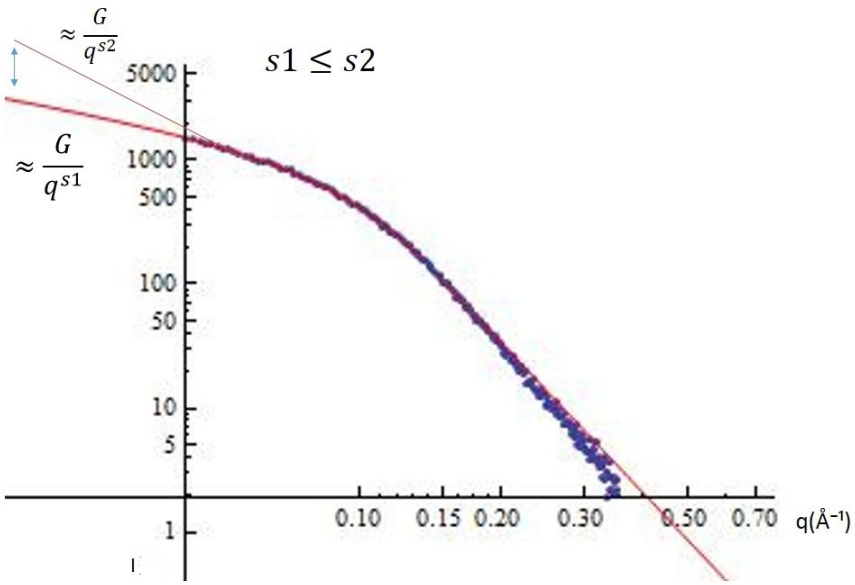

Figure 7.10: Influence of the data in the Guinier region on the shape parameter found with the Hammouda model

7.5 Orientation parameter

The preferred orientation of the mineral particles in bone is known to follow the principal directions of the load and therefore indicates how the bone is reacting to the presence of the implant. If the bone was not even noticing the presence of the pin, the main orientation would only be the one of the long bone. This is not what we observe in most of our samples. Indeed, in cortical bone near implant, it seems, that the particles are preferably oriented along the implant directions. This can be measured with the orientation deviation from the long bone direction. In figure 7.11.a, c, d and f it can be seen that the deviation is higher near implant than away from it. When that deviation is computed for newly formed bone in figures 7.12.b, c and d, it seems that there is not preferred direction of orientation, except for the figure 7.12.a where a cluster of points seems to aggregate at above 1.5 mm away from the implant.

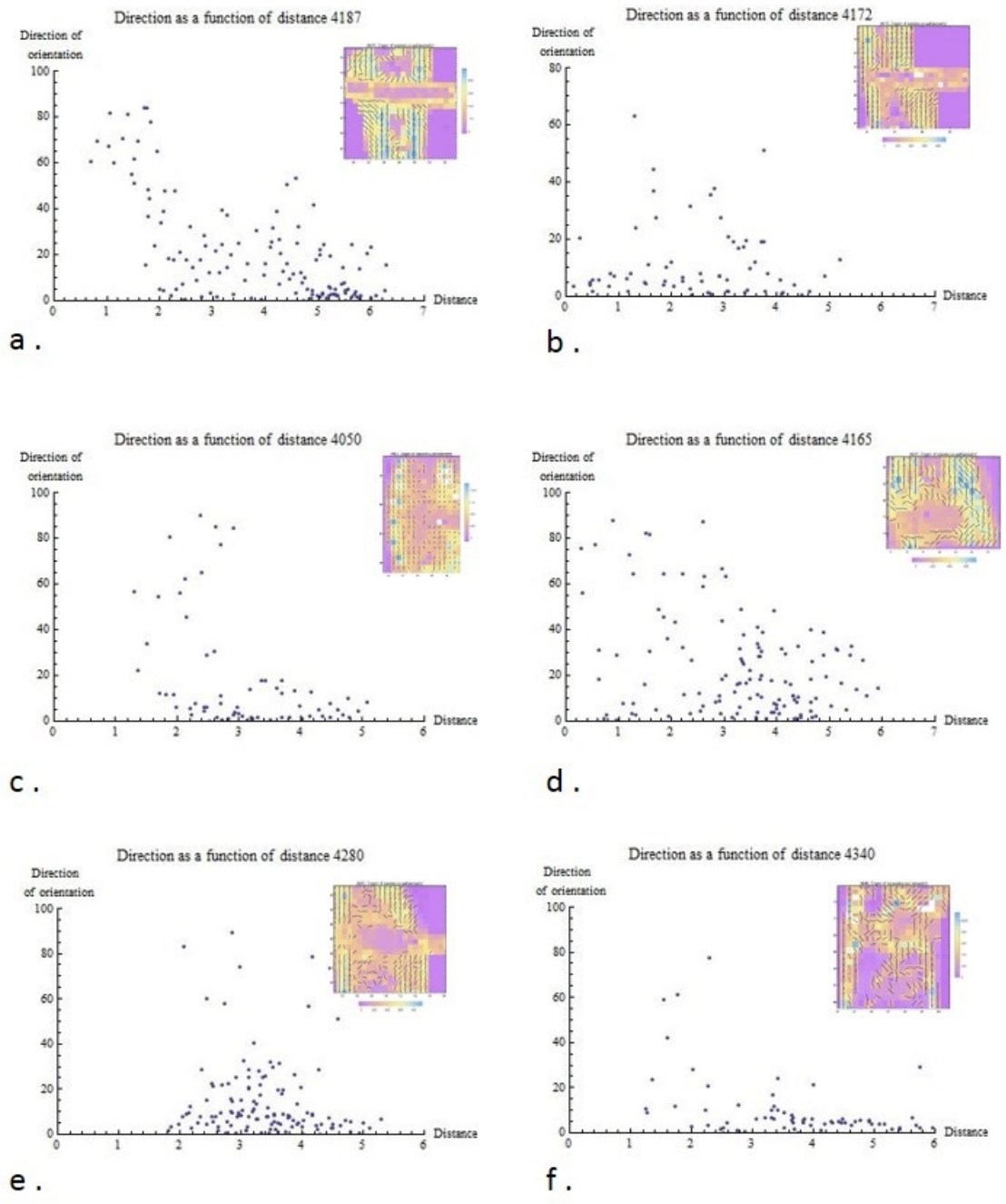

Figure 7.11: Orientation deviation (°) to the longitudinal direction of the bone, as a function to the distance to the implant (mm) in cortical bone
a: 1 month implantation; b: 3 months implantation; c: 6 months implantation; d: 9 months implantation; e: 12 months implantation; f: 18 months implantation.

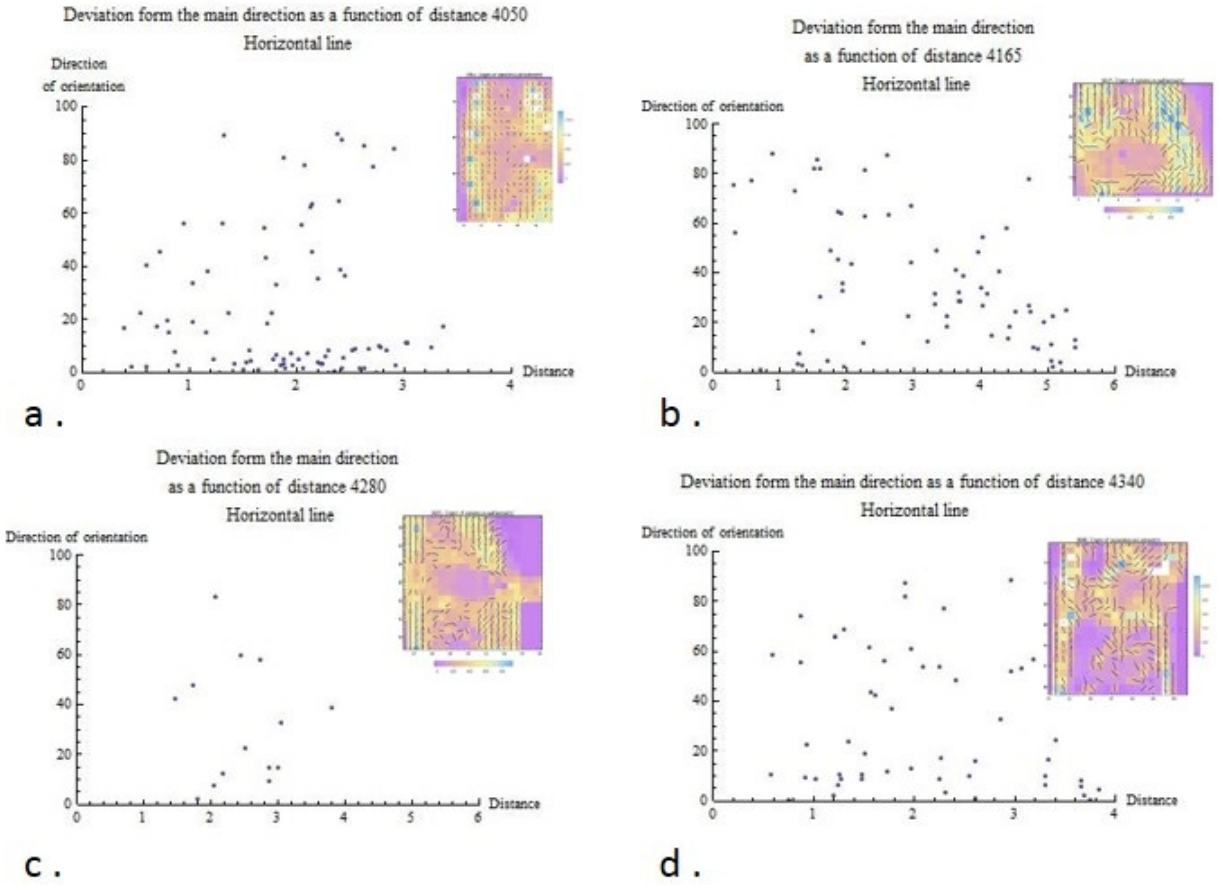

Figure 7.12: Orientation deviation (°) to the longitudinal direction of the bone, as a function to the distance to the implant (mm) in newly formed bone
a: 6 months implantation; b: 9 months implantation; c: 12 months implantation; d: 18 months implantation.

7.6 Comparison of the thickness derived from the Hammouda model and the T parameter

7.6.1 Evolution of the T parameter near implant

During this master thesis, the thickness has been computed directly from the integrated curve, by using the Hammouda model. Nevertheless, the results have been compared with the standard way of computing thickness, using the T parameter [21]. When compared, the two parameters were different, a difference from a factor two (see table 7.1), but also different was the evolution near implant, with a decrease of the thickness size near implant for the thickness computed with the Hammouda model and sometimes a small increase of the T parameter near implant (See figures 7.13.b, d and f or 7.14. a and b).

The difference of behavior in the T parameter results near implant can be explained through the degree of mineralization. Indeed near implant and in newly formed bone, the scattered intensity is lower than in the rest of the bone, which is correlated to a lower mineral amount as mineral is the most scattering material in bone. But the T parameter depends on the degree of mineralization ϕ,

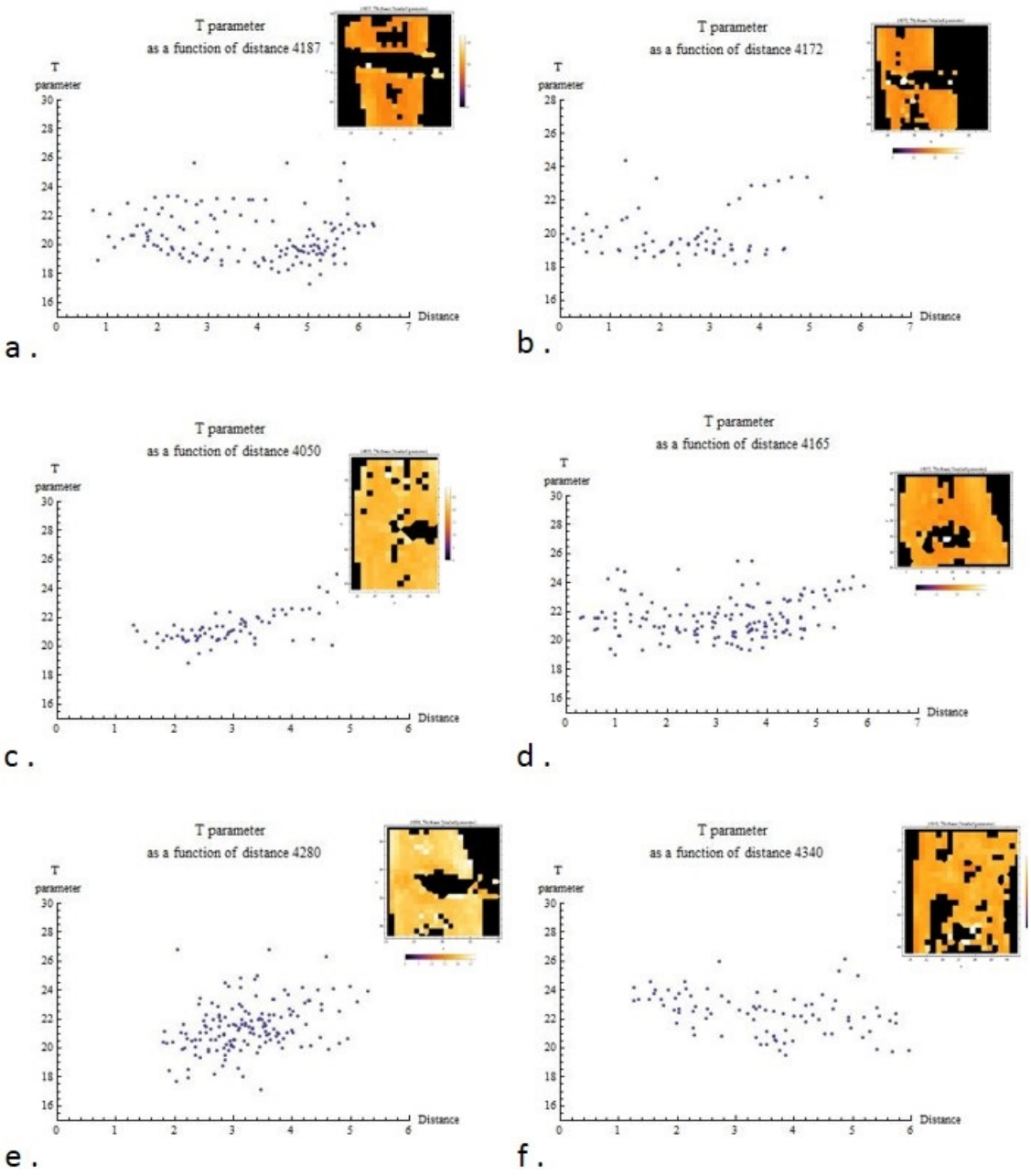

Figure 7.13: T parameter (Å) as a function of the distance to the implant(mm) in cortical bone
a: 1 month implantation; b: 3 months implantation; c: 6 months implantation; d: 9 months implantation; e: 12 months implantation; f: 18 months implantation.

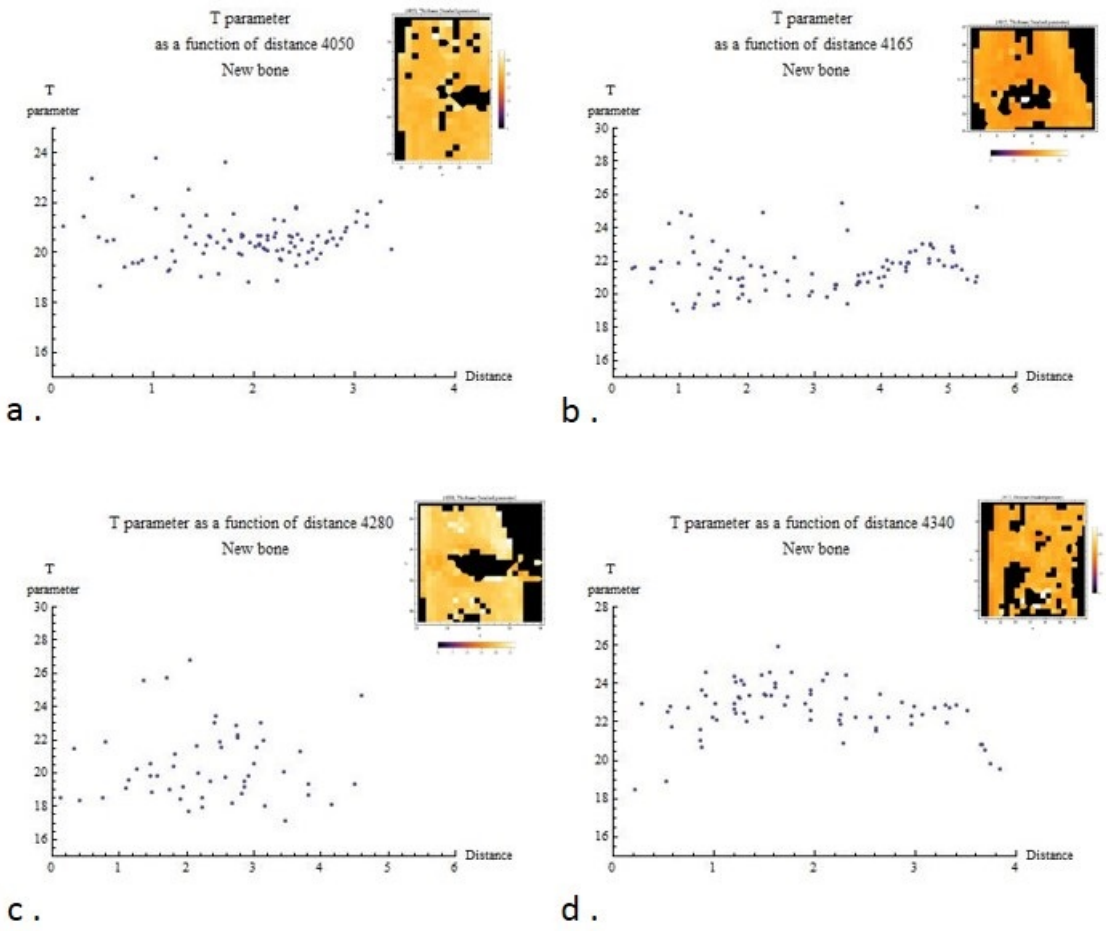

Figure 7.14: T parameter (Å) as a function of the distance to the implant(mm) in newly formed bone a: 6 months implantation; b: 9 months implantation; c: 12 months implantation; d: 18 months implantation.

and this degree is assumed to be constant and equal to 50%:

$$T = \frac{P}{I^{invariant}} = \frac{1}{\pi\phi(1-\phi)}\frac{S}{V} \tag{7.1}$$

and if the degree of mineralization is dropping, the thickness should increase as T is conversely proportional to the degree of mineralization. Thus the difference of evolution that we can see in figures 7.13 and 7.14.

The difference of value between the thickness computed from the Hammouda model and the T parameter can be explained by the fact that the T parameter is defined as a correlation length, which is not exactly equal to the thickness but can be interpreted as a measure of the thickness.

7.6.2 Comparison of the thickness from the Hammouda model and of the T parameter

Even if the value of the thickness computed with the Hammouda model and of the T parameter are not the same, the evolution over time of the two thickness parameters are similar (see table 7.1 and figures 7.15 and 7.16): a tendency to increase of the mean thickness and of the T parameter over time, tendency that is in the range of the standard deviation, thus to be taken with caution.

Sample	Months	Mean (standard deviation) on thickness computed with the Hammouda model (Å)	Mean (standard deviation) on the T parameter (Å)
4187	1	36.45 (7.18)	20.38 (2.20)
4172	3	38.00 (8.41)	20.52 (2.18)
4050	6	39.67 (8.50)	20.97 (1.38)
4165	9	39.65 (9.05)	21.51 (1.56)
4280	12	39.45 (8.28)	21.18 (1.69)
4340	18	42.50 (7.60)	22.88 (1.84)

Table 7.1: Comparison of the model to obtain thickness

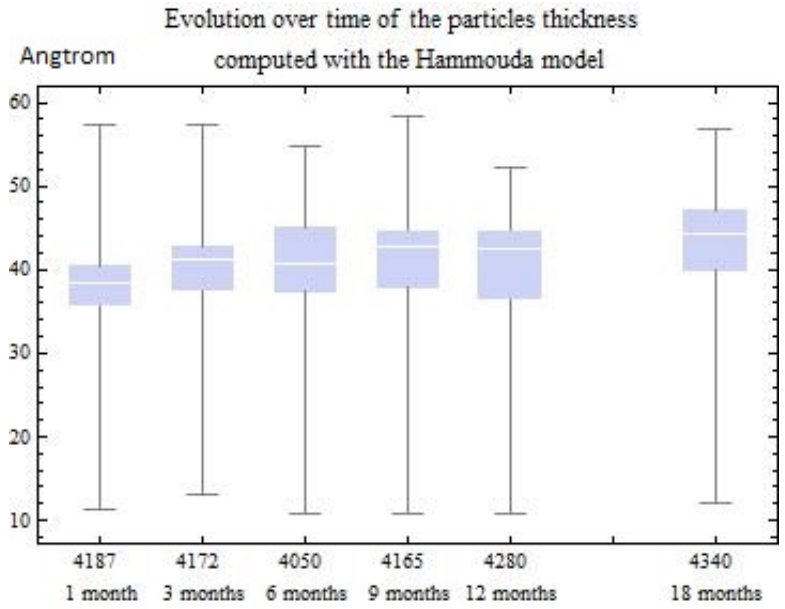

Figure 7.15: Evolution of the thickness of the particles computed with the Hammouda model (Å) over time
The white line is the median, the two extrema of the blue box are respectively, 25% and 75% of the data points of the mapping and the extremities of the black bar are the extrem values of the shape parameter

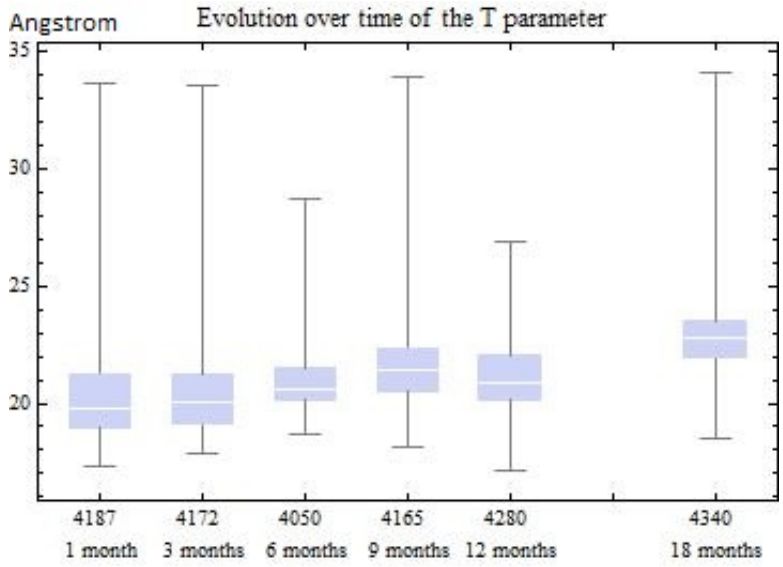

Figure 7.16: Evolutionof the T parameter (Å) over time
The white line is the median, the two extrema of the blue box are respectively, 25% and 75% of the data points of the mapping and the extremities of the black bar are the extrem values of the shape parameter

Part V

Conclusion

Conclusion

This master thesis was part of the BRIC project (BioResorbable Implants for Children). A promising implant is a magnesium alloyed pin from the WZ21 class. this master thesis aimed to observe the reaction of the nanostructure of rats bone to the implantation and degradation of that bio resorbable magnesium pin. The reaction was to be quantified with criteria on size, shape, and orientation of the mineral crystals that constitute bone on the nanoscopic level. Six rats were implanted with the pin for a period of 1, 3, 6, 9, 12 and 18 months. The implanted bones were then removed and prepared in slices to be then analyzed with histological techniques, Small Angle X-ray Scattering. The six bone samples were scanned with the Small Angle X-ray Scattering technique at the University of Natural Resources and Life Sciences Vienna and at the University of Vienna. For each sample a mapping of at least 300 points of dimension 350 µm by 350 µm was made, which represents approximately data 4 mm of bone above and under the implant. From those SAXS experiment were obtained 2D diffraction patterns. Those patterns were integrated first radially then azimuthally to be then fitted, in order to identify, the thickness of the minerals, their shape and their direction of orientation. The radial integration enabled to identify, the mean thickness and shape of the particles present in the scanned points, when the azimuthal integration made possible the characterization of the orientation of the particles. Two models were compared for computing the thickness of the particles. The first model was the Hammouda model that used the fitting of the radial integration, the thickness was computed from the shape of the curve in the Guinier and in the Porod regions. The second model used the invariants of the radial integration and the result of that model was the T parameter. The experiment also gave information on the relative mineralization in each sample. It has been observed:

- that the degradation rate of the WZ21, is slow enough to prevent the formation of gas cavities,
- that the bone is reacting by forming new crystals, whose thickness grows over time to stabilize between 12 and 18 months,
- that the bone is reacting by orienting near implant the crystals parallel to the implant directions, and that this difference of orientation is no more visible after 18 months,
- that the bone is forming more platelets like particles near implant,
- that the new bone is less mineralized but this difference disappears over time.

The variation of thickness over time, found with the two models were both in the range of the standard deviation and thus were to be taken with caution.

Next development of the project

The first development is to study the behavior of bone with other alloy, for example a fast degrading one, to see the reaction of the bone on a long term. This is going to be done at the BOKU with LV1 magnesium alloy pins. The next development for the project, is going to be the study of the sample through X-Ray fluorescence to get to know how the magnesium and other part of the alloy are spread out. Indeed with the SAXS analysis, we gained information on the bone crystals reaction, but no information could be gained on the dispersion of the magnesium, and of the other part of the alloy. This complementary study will allow to see how the bone is evacuating the pin corrosion products. This part of the project is going to take place at the Technical University Vienna.

In conclusion, in my opinion, the WZ21 alloy is a promising alloy for the pediatric orthopedic surgery and the SAXS technic a good complementary way to study bone's reaction to implantation.

Difficulties and experience gained

This master thesis has been a very interesting and enriching experience, with difficulties I had to overcome, but which enabled me to have a better understanding of the phenomenon I studied. The first difficulty I met was to get to understand the principle of SAXS, and the only way to go past that difficulty was actually to get to work with the experiment, to understand what was the influence of each parameter. In the end, I am really amazed by the information that the SAXS could give and by the possibility of the device. The second difficulty was to use Mathematica, and to handle the different types of data. This has been a true brainteaser, but it has also been the better way to understand how to manipulate the data.

Part VI

Appendix

Appendix A

Mathematica files

A.1 Complete file

```
(*4340*)
(*initializarion of the time*)
t0 = TimeUsed[];
name = 4340;
(* variables are cleared*)
Clear[files, FileNameList, FileNameList1, inxy, pathin, pathin1, xpt, ypt, ext, l,
    Filename, FileNameList2, i, imax, in, xmin, xmax, dx, ymin, ymax, dy, z, intensity,
    intensitygraph, lxy, intense2];

(*Copy of the directory to manipulate it without having to change the original data*)
DeleteDirectory["C:\\Users\\ogier\\Desktop\\DATA\\4340_IntegrationKopie",DeleteContents
    -> True];
pathin1 = "C:\\Users\\ogier\\Desktop\\DATA\\4340_Integration";

pathin = CopyDirectory[pathin1,"C:\\Users\\ogier\\Desktop\\DATA\\4340_IntegrationKopie"];
len = StringLength[pathin1];

(*importation of the file of the radial integration Selection of the file of interest
first radial integrated file*)
files = FileNames[{"Bone_*_*radial.plt"}, FileNameJoin[{pathin}]];
FileNameList = FileNameTake[#, -1] & /@ files;
len2 = StringLength[FileNameList[[1]]];

(* Modification of the extension of the file to have it in txt so we can manipulate them
    *)
FileNameList1 =
  RenameFile[#, StringInsert[StringDrop[#, -3], ".txt", len + len2 + 3(*length of the
      name of the file*)]] & /@ files;
(*Only the name is taken*)
FileNameList2 = FileNameTake[#, -1] & /@ FileNameList1;
(*Ordering of the file to manipulate them in the order by which they have been scanned
    first number of character in the file name before the three characteristics number
    004 for example and second one, the number of character after that number*)
f[str_] := {str, StringDrop[StringDrop[str, 12], -7]};
FileNameList = SortBy[Map[f, FileNameList2], Last][[All, 1]];
(*number of points measured*)
imax = Length[FileNameList];
```

```
31
32 (*obtention of the azimuthal integration*)
33 filesazi = FileNames[{"Bone_*_*azi.plt"}, FileNameJoin[{pathin}]];
34 (* Modification of the extension of the file to have it in txt so we can manipulate them
       *)
35 inter = FileNameTake[#, -1] & /@ filesazi;
36 len2azi = StringLength[inter[[1]]];
37 FileNameList1azi = RenameFile[#, StringInsert[StringDrop[#, -3], ".txt", len +
       len2(*lenght of the name of the file without the extension*)]] & /@ filesazi;
38 (*Only the name is taken*)
39 FileNameList2azi = FileNameTake[#, -1] & /@ FileNameList1azi;
40 (*Ordering of the file to manipulate them in the order by which they have been scanned
       first number of character in the file name before the three characteristics number
       004 for example and second one, the number of character after that number *)
41 fazi[str_] := {str, StringDrop[StringDrop[str, 7], -7]};
42 FileNameListazi = SortBy[Map[fazi, FileNameList2azi], Last];
43
44 (*Thanks to the intensity file and the histological and photo, you have deduced where was
       the implant, you should then have this coordinates in the following lines it is
       going to be useful for computation of the distance to the implant influence *)
45 For[i = 0, i < 7, i++,
46  If[ToExpression[StringSplit[Import[
47        FileNames["Implant*txt",
48          FileNameJoin[
49           "C:\\Users\\ogier\\Desktop\\DATA\\background_file"]][[1]]
50        ]][[5*i + 1]] == name,
51   yimplantmin = ToExpression[StringSplit[Import[
52        FileNames["Implant*txt",
53          FileNameJoin[
54           "C:\\Users\\ogier\\Desktop\\DATA\\background_file"]][[1]]
55        ]][[5*i + 2]];
56   yimplantmax = ToExpression[StringSplit[Import[
57        FileNames["Implant*txt",
58          FileNameJoin[
59           "C:\\Users\\ogier\\Desktop\\DATA\\background_file"]][[1]]
60        ]][[5*i + 3]];
61   ximplantmin = ToExpression[StringSplit[Import[
62        FileNames["Implant*txt",
63          FileNameJoin[
64           "C:\\Users\\ogier\\Desktop\\DATA\\background_file"]][[1]]
65        ]][[5*i + 4]];
66   ximplantmax = ToExpression[StringSplit[Import[
67        FileNames["Implant*txt",
68          FileNameJoin[
69           "C:\\Users\\ogier\\Desktop\\DATA\\background_file"]][[1]]
70        ]][[5*i + 5]];]
71  ]
72
73
74 (*Define Background File here*)
75 backgroundimp3 =
76   ToExpression[
77    StringSplit[
78     Import["C:\\Users\\ogier\\Desktop\\DATA\\background_file\\Bone_2_\
```

```
377radial.txt", {"Lines", Range[17, 507, 1]}, Path -> pathin]]];

backgroundimp1 = Drop[backgroundimp3, None, 1];
backgroundimp = Drop[backgroundimp1, None, {2}];
backgroundimp =
  backgroundimp[[All, {1, 2}]] = backgroundimp[[All, {2, 1}]];

backg = ListLogLogPlot[backgroundimp, PlotRange -> All]
intbackground3 = Drop[backgroundimp, None, {1}];

intbackgroundsave = intbackground3;
Length[intbackgroundsave];
intbackground2 = Drop[intbackground3, -135];
intbackground = Drop[intbackground2, 340];

(*Creation of a list to stock the results*)
l = {};
l1 = {};
l2 = {};
l3 = {};
l4 = {};
ldistance = {};
lscatter = {};
lcorr = {};
lcorrfit = {};
lhisto = {};
lintense = {};
 l1azi = {};
 lazi = {};

 ldistanceazi = {};
lxy = {};
(*results files, etc...*)
intensity =
  OpenWrite[
   "C:\\Users\\ogier\\Desktop\\DATA\\4340_Integration\\intensity.txt"];
results =
  OpenWrite[
   "C:\\Users\\ogier\\Desktop\\DATA\\4340_Integration\\radialresults.\
txt"];
intensityforazi =
  OpenWrite[
   "C:\\Users\\ogier\\Desktop\\DATA\\4340_Integration\\iscat.txt"];
Results =
  OpenWrite[
   "C:\\Users\\ogier\\Desktop\\DATA\\4340_Integration\\aziresults.\
txt"];
(*number of the last line to import in the azimuthal integration*)
lastlinepltfile = 737;

(*obtention of the xy coordinate*)
filesxy = FileNames[{"*.csv"}, FileNameJoin[{pathin}]];
FileNameListxy = FileNameTake[#, -1] & /@ filesxy;
Filenamexy = Part [FileNameListxy, 1];
```

```
133 inxy = Import[filesxy[[1]], Path -> pathin];
134
135 (*loop on all the points measured*)
136 For[i = 1, i < imax + 1, i++,
137  Clear[Rg, d, s, G, q, De, Q1, nlm, int, datfit, datplot, fguinier, fporod, in, dat, dat1
        , raw, qlist, inti2, inti, ratio, scale, inbackgroundscale, hintergrundkorrigiert,
       hint, intcorrected, radcorrected, corr, xpt, ypt, valuepeak, valueangle, backgazi,
       ext, intense2, datazi, inazi];
138  Filename = FileNameList[[i]];
139  (*obtention of intensity in q=0 photodiode intensity*)
140  inint = ToExpression[
141    StringSplit[
142     Import[FileNameList[[i]], {"Lines", Range[17, 18, 1]},
143      Path -> pathin]]];
144  datint = inint;
145  intense2 = datint[[1, 2]];
146
147  z == WriteString[intensity, Filename, "␣\t␣", intense2, "\n"];
148  (*obtention of x and y of the points*)
149  ext = Part[inxy, i][[1]];
150  xpt = ToExpression[StringSplit[ext][[3]]];
151  ypt = ToExpression[StringSplit[ext][[4]]];
152  distance = ((Min[{yimplantmax - ypt,
153          yimplantmin - ypt}])^2 + (Min[{ximplantmax - xpt,
154          ximplantmin - xpt}])^2)^0.5;
155  lintense = AppendTo[lintense, {xpt, ypt, intense2}];
156  lxy = AppendTo[lxy, {xpt, ypt}];
157
158  If[intense2 == 0,
159   l = AppendTo[l, {Filename, xpt, ypt, 0, 0, 0, 0, 0, 0, 0, 0, 0, 0}];
160   ,
161
162   (*Obtention of the data
163   first radial integrated data*)
164   in = ToExpression[
165     StringSplit[
166      Import[FileNameList[[i]], {"Lines", Range[17, 507, 1]},
167       Path -> pathin]]];
168   dat = Drop[in, None, 1];
169   dat1 = Drop[dat, None, {2}];
170   dat1 = dat1[[All, {1, 2}]] = dat1[[All, {2, 1}]];
171   raw = ListLogLogPlot[dat1, PlotRange -> All];
172   qlist = Drop[dat1, None, {2}];
173   inti2 = Drop[dat1, None, {1}];
174
175   (*This determines the range of background normalisation*)
176   inti = Drop[inti2, -135];
177   inti = Drop[inti, 340];
178
179   ratio = inti/intbackground;
180   scale = Mean[ratio];
181   intbackgroundscale = scale * {intbackgroundsave};
182   intbackgroundscale = Flatten[Flatten[intbackgroundscale]];
183   hintergrundkorrigiert =
```

```
    Transpose[Insert[Transpose[qlist], intbackgroundscale, 2]];
  hint = ListLogLogPlot[hintergrundkorrigiert, PlotRange -> All];

  intcorrected = inti2 - intbackgroundscale;
  intcorrected = Flatten[intcorrected];

  radcorrected = Transpose[Insert[Transpose[qlist], intcorrected, 2]];
  corr = ListLogLogPlot[radcorrected, PlotRange -> All];
  (*Show[corr,raw,backg];*)
  (*Number of datapoints to drop for the fitting*)
  datfit = Drop[radcorrected, 20];
  datfit = Drop[datfit, -250];
  (*calculation of the scattered intensity as the ration of the sum \
of the intensity of the curve and the intensity of the photodiode
   and writting of it for the azimuthal integration*)
  itotal = Part[Total[datfit], 2];
  scatteredintensity = itotal/intense2;

  iscat ==
   WriteString[intensityforazi, FileNameList[[i]], "\t",
    scatteredintensity, "\n"];

  datplot = ListLogLogPlot[datfit, PlotRange -> All];

  (*begining of the loop to filter data*)
  (*first step,
  exclude the data that are not coherent through intensity*)
  If[scatteredintensity < 100 || scatteredintensity > 2000,

   Print["FileName: ", Filename, "(x,y):(", xpt, ",", ypt,
    "), Non coherent because of scattered intensity: ",
    scatteredintensity];
   Unprotect[Out ]; Clear[Out];
   put ==
    WriteString[results, FileNameList[[i]], "\t",
     "non coherent because of scattered intensity ", "\n"];
   datplot = ListLogLogPlot[datfit, PlotRange -> All];
   donnee =
    ListLogLogPlot[dat1[[All, {1, 2}]],
     PlotStyle -> RGBColor[1, 0, 0]];
   l = AppendTo[
     l, {Filename, xpt, ypt, distance, intense2, itotal,
      scatteredintensity, 0, 0, 0, 0}];
   scatteredintensity = 0;
   Rg = 0;
   s = 0;
   l1 = AppendTo[l1, {xpt, ypt, 0}];
   l2 = AppendTo[l2, {xpt, ypt, 0}];
   l3 = AppendTo[l3, {xpt, ypt, 0}];
   lscatter = AppendTo[lscatter, {xpt, ypt, scatteredintensity}];
   Print[Show[datplot, PlotRange -> All]],

   (*definition of the fit function and fitting*)
   fguinier = G/q^s*Exp[(-q^2*Rg^2)/(3 - s)];
```

```
238     fporod = De/q^d;
239
240     Q1 = 1/Rg*((d - s)*(3 - s)/2)^1/2;
241     De = G*Exp[-Q1^2*Rg^2/(3 - s)]*Q1^(d - s);
242     int = Piecewise[{{fguinier, q < Q1}, {fporod, q >= Q1}}];
243     d = 4;
244     (*fitting*)
245     nlm = NonlinearModelFit[datfit,
246       int, {{Rg, 10}, {G, Max[datfit]*0.6}, {s, 1.5}}, q];
247
248     Rg = Abs[Rg] /. nlm["BestFitParameters"];
249     G = G /. nlm["BestFitParameters"];
250     s = s /. nlm["BestFitParameters"];
251
252     (*Then evicition of non coherent values*)
253     If[s <= 0 || s > 3.5 || Rg < 3 || G < 0 || Rg > 21 ||
254       NotElement[G, Reals] || NotElement[Rg, Reals] ||
255       NotElement[s, Reals],
256      Print["FileName:␣", FileNameList[[i]], "(x,y):(", xpt, ",", ypt,
257       ")", "␣,␣Non␣coherent␣fit␣because␣of␣Rg␣or␣s:␣(", Rg, ",", s,
258       "␣)␣,␣scattered␣intensity:␣", scatteredintensity];
259      datplot = ListLogLogPlot[datfit, PlotRange -> All];
260      donnee =
261       ListLogLogPlot[dat1[[All, {1, 2}]],
262        PlotStyle -> RGBColor[1, 0, 0]];
263      l = AppendTo[
264        l, {Filename, xpt, ypt, distance, intense2, itotal,
265         scatteredintensity, s, Rg, 0, 0}];
266      Rg = 0;
267      s = 0;
268      l1 = AppendTo[l1, {xpt, ypt, s}];
269      l2 = AppendTo[l2, {xpt, ypt, Rg}];
270      l3 = AppendTo[l3, {xpt, ypt, 0}];
271      lscatter = AppendTo[lscatter, {xpt, ypt, scatteredintensity}];
272      Print[Show[datplot, PlotRange -> All]]
273       Unprotect[Out ]; Clear[Out];
274      put ==
275       WriteString[results, FileNameList[[i]], "␣\t", Rg, "␣\t", G,
276        "␣\t", s, "␣\t", d, "␣\t", Q1, "␣\t", De, scatteredintensity,
277        "\t", "non␣coherent␣because␣of␣rg␣or␣s␣", "\n"];,
278
279
280     (*Calculation of the Porod constant,
281     then the Kratky integral to gain access to the thickness as \
282 calculated usually placed here so only integration when there should \
283 be a fit*)
284      nlm["FittedModel"];
285      J = Integrate[4/\[Pi]*q^2*nlm[q], {q, 0.001, 0.4}] +
286        4/\[Pi]*0.001^3*nlm[0.001]/2 + De/0.4*4/\[Pi];
287      If[Element[J, Reals],
288       Q1;
289       De;
290       Tstandard = J/De;
291       (*loop to select the data that are the most scattering,
```

```
292       mainly cortical bone to have them computing the distance*)
293       If[scatteredintensity < 400,
294        If[s > 0 && s < 1,
295         (*interpolation to know the thickness depending of s and Rg*)
296         T = ((2^1.5 - 2 (5/3)^0.5))*Rg*s + 2 (5/3)^0.5*Rg;
297         l1 = AppendTo[l1, {xpt, ypt, s}];
298         l2 = AppendTo[l2, {xpt, ypt, T}];
299         l3 = AppendTo[l3, {xpt, ypt, Tstandard}];
300         lhisto = AppendTo[lhisto, {s, Rg, T, Tstandard}];
301         ldistance = AppendTo[ldistance, {distance, s, T, Rg}];
302         lcorr = AppendTo[lcorr, {s, Rg}];
303         lcorrfit = AppendTo[lcorrfit, {s, Rg}];
304         lscatter = AppendTo[lscatter, {xpt, ypt, scatteredintensity}];
305         l =
306          AppendTo[
307           l, {Filename, xpt, ypt, distance, intense2, itotal,
308            scatteredintensity, s, Rg, T, Tstandard}];
309        nlm["FittedModel"]
310         Print["Filename", FileNameList[[i]], "␣Rg␣", Rg, "␣;␣s␣", s,
311          "␣T␣", T, "␣Tstandard␣", Tstandard, "(x,y):(", xpt, ",",
312          ypt, "),scattered␣intensity:␣", scatteredintensity];
313
314         Print[
315          Show[datplot,
316           LogLogPlot[nlm[q], {q, 0.01, 0.7},
317            PlotStyle -> RGBColor[1, 0, 0]], PlotRange -> All]]
318         Unprotect[Out ]; Clear[Out]
319          put ==
320         WriteString[results, FileNameList[[i]], "␣\t", Rg, "␣\t", G,
321          "␣\t", s, "␣\t", d, "␣\t", Q1, "␣\t", De, "\t",
322          scatteredintensity, "\n"];,
323        If[s >= 1 && s <= 2,
324         (*interpolation to know the thickness depending of s and Rg*)
325
326
327         T = ((12^0.5 - 2^1.5))*Rg*(s - 1) + 2^1.5*Rg;
328
329         l1 = AppendTo[l1, {xpt, ypt, s}];
330         l2 = AppendTo[l2, {xpt, ypt, T}];
331         l3 = AppendTo[l3, {xpt, ypt, Tstandard}];
332
333         lhisto = AppendTo[lhisto, {s, Rg, T, Tstandard}];
334         ldistance = AppendTo[ldistance, {distance, s, T, Rg}];
335         lcorr = AppendTo[lcorr, {s, Rg}];
336         lcorrfit = AppendTo[lcorrfit, {s, Rg}];
337         lscatter = AppendTo[lscatter, {xpt, ypt, scatteredintensity}];
338         nlm["FittedModel"]
339          Print["Filename", FileNameList[[i]], "␣Rg␣", Rg, "␣;␣s␣", s,
340           "␣T␣", T, "␣Tstandard␣", Tstandard, "(x,y):(", xpt, ",",
341           ypt, "),scattered␣intensity:␣", scatteredintensity];
342         l =
343          AppendTo[
344           l, {Filename, xpt, ypt, distance, intense2, itotal,
345            scatteredintensity, s, Rg, T, Tstandard}];
```

```
346          Print[
347           Show[datplot,
348            LogLogPlot[nlm[q], {q, 0.01, 0.7},
349             PlotStyle -> RGBColor[1, 0, 0]], PlotRange -> All]]
350          Unprotect[Out ]; Clear[Out]
351           put ==
352          WriteString[results, FileNameList[[i]], "␣\t", Rg, "␣\t", G,
353           "␣\t", s, "␣\t", d, "␣\t", Q1, "␣\t", De, "\t",
354           scatteredintensity, "\n"];,
355          If[s > 2 && s <= 3,
356          (*interpolation to know the thickness depending of s and Rg*)
357
358
359          T = 12^0.5*Rg;
360
361          l1 = AppendTo[l1, {xpt, ypt, s}];
362          l2 = AppendTo[l2, {xpt, ypt, T}];
363          l3 = AppendTo[l3, {xpt, ypt, Tstandard}];
364
365          lhisto = AppendTo[lhisto, {s, Rg, T, Tstandard}];
366          ldistance = AppendTo[ldistance, {distance, s, T, Rg}];
367          lcorr = AppendTo[lcorr, {s, Rg}];
368          lcorrfit = AppendTo[lcorrfit, {s, Rg}];
369          lscatter = AppendTo[lscatter, {xpt, ypt, scatteredintensity}];
370          l =
371           AppendTo[
372            l, {Filename, xpt, ypt, distance, intense2, itotal,
373             scatteredintensity, s, Rg, T, Tstandard}];
374          nlm["FittedModel"]
375
376           Print["Filename", FileNameList[[i]], "␣Rg␣", Rg, "␣;␣s␣", s,
377            ",␣T␣", T, ",␣Tstandard␣", Tstandard, "(x,y):(", xpt, ",",
378            ypt, "),scattered␣intensity:␣", scatteredintensity];
379
380          Print[
381           Show[datplot,
382            LogLogPlot[nlm[q], {q, 0.01, 0.7},
383             PlotStyle -> RGBColor[1, 0, 0]], PlotRange -> All]]
384          Unprotect[Out ]; Clear[Out]
385           put ==
386          WriteString[results, FileNameList[[i]], "␣\t", Rg, "␣\t",
387           G, "␣\t", s, "␣\t", d, "␣\t", Q1, "␣\t", De, "\t",
388           scatteredintensity, "\n"];
389          ]]]
390
391        ,(*if it is not cortical bone*)
392        If[s > 0 && s < 1,
393         (*interpolation to know the thickness depending of s and Rg*)
394         T = ((2^1.5 - 2*(5/3)^0.5))*Rg*s + 2*(5/3)^0.5*Rg;
395
396         l1 = AppendTo[l1, {xpt, ypt, s}];
397         l2 = AppendTo[l2, {xpt, ypt, T}];
398         l3 = AppendTo[l3, {xpt, ypt, Tstandard}];
399          l =
```

```
400          AppendTo[
401           l, {Filename, xpt, ypt, distance, intense2, itotal,
402            scatteredintensity, s, Rg, T, Tstandard}];
403          lhisto = AppendTo[lhisto, {s, Rg, T, Tstandard}];
404          lcorr = AppendTo[lcorr, {s, Rg}];
405          lcorrfit = AppendTo[lcorrfit, {s, Rg}];
406          lscatter = AppendTo[lscatter, {xpt, ypt, scatteredintensity}];
407          nlm["FittedModel"]
408           Print["Filename", FileNameList[[i]], "␣Rg␣", Rg, "␣;␣s␣", s,
409            ",␣T␣", T, ",␣Tstandard␣", Tstandard, "(x,y):(", xpt, ",",
410            ypt, "),scattered␣intensity:␣", scatteredintensity];
411
412          Print[
413           Show[datplot,
414            LogLogPlot[nlm[q], {q, 0.01, 0.7},
415             PlotStyle -> RGBColor[1, 0, 0]], PlotRange -> All]]
416           Unprotect[Out ]; Clear[Out]
417            put ==
418           WriteString[results, FileNameList[[i]], "␣\t", Rg, "␣\t", G,
419            "␣\t", s, "␣\t", d, "␣\t", Q1, "␣\t", De, "\t",
420            scatteredintensity, "\n"];,
421          If[s >= 1 && s <= 2,
422           (*interpolation to know the thickness depending of s and Rg*)
423
424
425           T = ((12^0.5 - 2^1.5))*Rg*(s - 1) + 2^1.5*Rg;
426
427           l1 = AppendTo[l1, {xpt, ypt, s}];
428           l2 = AppendTo[l2, {xpt, ypt, T}];
429           l3 = AppendTo[l3, {xpt, ypt, Tstandard}];
430            l =
431            AppendTo[
432             l, {Filename, xpt, ypt, distance, intense2, itotal,
433              scatteredintensity, s, Rg, T, Tstandard}];
434           lhisto = AppendTo[lhisto, {s, Rg, T, Tstandard}];
435           lcorr = AppendTo[lcorr, {s, Rg}];
436           lcorrfit = AppendTo[lcorrfit, {s, Rg}];
437           lscatter = AppendTo[lscatter, {xpt, ypt, scatteredintensity}];
438           nlm["FittedModel"]
439            Print["Filename", FileNameList[[i]], "␣Rg␣", Rg, "␣;␣s␣", s, ",␣T␣", T, ",␣
                 Tstandard␣", Tstandard, "(x,y):(", xpt, ",", ypt, "),scattered␣intensity:␣",
                  scatteredintensity];
440
441           Print[
442            Show[datplot,
443             LogLogPlot[nlm[q], {q, 0.01, 0.7},
444              PlotStyle -> RGBColor[1, 0, 0]], PlotRange -> All]]
445            Unprotect[Out ]; Clear[Out]
446             put ==
447            WriteString[results, FileNameList[[i]], "␣\t", Rg, "␣\t", G,
448             "␣\t", s, "␣\t", d, "␣\t", Q1, "␣\t", De, "\t",
449             scatteredintensity, "\n"];,
450           If[s > 2 && s <= 3,
451            (*interpolation to know the thickness depending of s and Rg*)
```

```
452
453
454           T = 12^0.5*Rg;
455
456           l = AppendTo[
457             l, {Filename, xpt, ypt, distance, intense2, itotal,
458              scatteredintensity, s, Rg, T, Tstandard}];
459           l1 = AppendTo[l1, {xpt, ypt, s}];
460           l2 = AppendTo[l2, {xpt, ypt, T}];
461           l3 = AppendTo[l3, {xpt, ypt, Tstandard}];
462
463           lhisto = AppendTo[lhisto, {s, Rg, T, Tstandard}];
464           lcorr = AppendTo[lcorr, {s, Rg}];
465           lcorrfit = AppendTo[lcorrfit, {s, Rg}];
466           lscatter = AppendTo[lscatter, {xpt, ypt, scatteredintensity}];
467           nlm["FittedModel"]
468
469            Print["Filename", FileNameList[[i]], "␣Rg␣", Rg, "␣;␣s␣", s,
470              "␣,␣T␣", T, "␣,␣Tstandard␣", Tstandard, "(x,y):(", xpt, ",",
471              ypt, "),scattered␣intensity:␣", scatteredintensity];
472
473           Print[
474            Show[datplot,
475
476              LogLogPlot[nlm[q], {q, 0.01, 0.7},
477               PlotStyle -> RGBColor[1, 0, 0]], PlotRange -> All]]
478            Unprotect[Out ]; Clear[Out]
479             put ==
480            WriteString[results, FileNameList[[i]], "␣\t", Rg, "␣\t",
481             G, "␣\t", s, "␣\t", d, "␣\t", Q1, "␣\t", De, "\t",
482             scatteredintensity, "\n"];
483           ]          ]          ]          ],
484           l =
485         AppendTo[
486          l, {Filename, xpt, ypt, distance, intense2, itotal,
487           scatteredintensity, s, Rg, T, 0}];
488       ]     ]     ];
489
490   Clear[g, valueangle, valuepeak, a, b, c, backgazi, x, inazi, datazi];
491   (*here are treated the azimuthal integration*)
492
493
494   (*Obtention of the integrated data of one point which begin at the 17th line, and  end
          at the line you should look for it in one file*)
495   inazi =
496    ToExpression[
497     StringSplit[
498      Import[FileNameListazi[[i, 1]], {"Lines",
499        Range[17, lastlinepltfile, 1]}, Path -> pathin]]];
500   datazi = inazi;
501   backgazi = Min[ Part[datazi[[All, 2]]]];
502   valuepeak = Max[ Part[datazi[[All, 2]]]];
503
504   valueangle =
```

```
    Part[Pick[datazi[[All, 1]], datazi[[All, 2]], valuepeak], 1];

  (*selection on scattering intensity*)
  If[scatteredintensity > 400 && scatteredintensity < 2000,
      If[valuepeak <= 0.005 ,
    zazi ==
     WriteString[Results, Filename, "␣;␣", "␣Not␣consistent␣value␣\n"];
    donneeazi =
     ListPlot[inazi[[All, {1, 2}]], PlotStyle -> RGBColor[1, 0, 0]];

    Print["FileName:␣", Filename,
      "␣Value␣not␣consistent␣because␣intensity:␣␣",
      scatteredintensity, "(␣", xpt, ",␣", ypt, "␣)␣\n"]
     Print[Show[donneeazi, PlotRange -> All]]
     (* for the vector plot*)
     (*Degree of orientation*)
     Clear[degoforient, bfit];
    degoforient = 0;
    (*Direction of orientation*
    1=90degree real space, 0=0degree real space, -1=
    90 degree realspace*)
    bfit = 0;
     lazi =
     AppendTo[
      lazi, {{xpt,
        ypt}, {{degoforient*Cos[bfit Degree],
         degoforient*Sin[bfit Degree]}, scatteredintensity}}];
     l1azi =
     AppendTo[
      l1azi, {{xpt, ypt}, {degoforient*Cos[bfit Degree],
        degoforient*Sin[bfit Degree]}}];

    OrVec = {direction, degoforient};
    l = Insert[l, 0, {i, -1}];
    l = Insert[l, 0, {i, -1}];
    ,


    valueangle =
     Part[Pick[datazi[[All, 1]], datazi[[All, 2]], valuepeak], 1];
    (*Test to know where might be the peak to apply the right fitting \
function*)
    If [valueangle <= 45,
     g = backgazi + a*E^-(((x - b)^2)/(2 c^2)) +
       a*E^-(((x - b - 180)^2)/(2 c^2)) +
       a*E^-(((x - b - 360)^2)/(2 c^2)),
      If[45 < valueangle <= 135,
       g = backgazi + a*E^-(((x - b)^2)/(2 c^2)) +
         a*E^-(((x - b - 180)^2)/(2 c^2)),
        If[135 < valueangle <= 225,
         g =
          backgazi + a*E^-(((x - b + 180)^2)/(2 c^2)) +
           a*E^-(((x - b - 180)^2)/(2 c^2)) + a*E^-(((x - b)^2)/(2 c^2)),
         If[225 < valueangle <= 315,
```

```
559         g =
560          backgazi + a*E^-(((x - b)^2)/(2 c^2)) +
561           a*E^-(((x - b + 180)^2)/(2 c^2)),
562          If[315 < valueangle <= 360,
563           g = backgazi + a*E^-(((x - b)^2)/(2 c^2)) +
564             a*E^-(((x - b + 180)^2)/(2 c^2)) +
565             a*E^-(((x - b + 360)^2)/(2 c^2))]]]];
566       Fitfunctionazi[x_] = g;
567
568       (*fitting*)
569       nlmazi =
570        NonlinearModelFit[datazi[[All, {1, 2}]],
571         Fitfunctionazi[x], {{a, valuepeak}, {b, valueangle}, c}, x,
572         VarianceEstimatorFunction -> (Mean[#^2] &)];
573       nlmazi["BestFitParameters"];
574       Rsq = nlmazi["RSquared"];
575       ARsq = nlmazi["AdjustedRSquared"];
576       AIC = nlmazi["AIC"];
577       AICc = nlmazi["AICc"];
578       BIC = nlmazi["BIC"];
579       cerr = nlmazi["ParameterErrors"];
580       afit = a /. nlmazi["BestFitParameters"];
581       bfit = b /. nlmazi["BestFitParameters"];
582       cfit = c /. nlmazi["BestFitParameters"];
583       dfit = backgazi /. nlmazi["BestFitParameters"];
584
585       (*ctriterium for isotropy*)
586       If[cerr[[3]] > 0.83 || cfit < 2,
587        Print["FileName:␣", Filename, "␣,␣Point␣is␣isotrope.(␣", xpt,
588         "␣,␣", ypt, "␣)␣" ];
589        Clear[degoforient, bfit];
590        (* for the vector plot*)
591        (*Degree of orientation*)
592        degoforient = 0;
593        (*Direction of orientation*
594        1=90degree real space, 0=0degree real space, -1=
595        90 degree realspace*)
596        bfit = 0;
597         lazi =
598         AppendTo[
599          lazi, {{xpt,
600            ypt}, {{degoforient*Cos[bfit Degree],
601             degoforient*Sin[bfit Degree]}, scatteredintensity}}];
602        l1azi = AppendTo[
603          l1azi, {{xpt, ypt}, {degoforient*Cos[bfit Degree],
604            degoforient*Sin[bfit Degree]}}];
605
606
607        OrVec = {direction, degoforient};
608        (*graph*)
609        donneeazi =
610         ListPlot[inazi[[All, {1, 2}]],
611          PlotStyle -> RGBColor[0.5, 1.5, 0]];
612        Print[Show[donneeazi, PlotRange -> All]]
```

```
613
614         zazi == WriteString[Results, Filename, "␣;␣isotrope␣", "\n"];
615       l = Insert[l, 0, {i, -1}];
616       l = Insert[l, 0, {i, -1}];
617       ,
618
619       (*Degree of orientation*)
620       degoforient = 1/cfit;
621       (*Direction of orientation*
622       1=90degree real space, 0=0degree real space, -1=
623       90 degree realspace*)
624       direction = Cos[bfit Degree];
625        lazi =
626        AppendTo[
627         lazi, {{xpt,
628           ypt}, {{degoforient*Cos[bfit Degree],
629            degoforient*Sin[bfit Degree]}, scatteredintensity}}];
630        l1azi =
631        AppendTo[
632         l1azi, {{xpt, ypt}, {degoforient*Cos[bfit Degree],
633           degoforient*Sin[bfit degree]}}];
634
635       OrVec = {direction, degoforient};
636        ldistanceazi =
637        AppendTo[ ldistanceazi, {distance, degoforient, Mod[bfit, 180]}];
638       l = Insert[l, degoforient, {i, -1}];
639       l = Insert[l, Mod[bfit, 180], {i, -1}];
640
641       Print["FileName:␣", Filename, "␣,␣background:␣", backgazi,
642        "␣␣,␣peak␣height:␣", afit, "␣␣,␣peak␣position␣(deg):␣", bfit,
643        "␣␣,␣peak␣width:␣", cfit,
644        "␣,␣standard␣deviation␣on␣peak␣width:␣", cerr[[3]],
645        ",␣scattered␣intensity:␣", scatteredintensity, "(␣", xpt, ",␣",
646        ypt, "␣)" ];
647
648       (*graph*)
649       fittedcurve = Plot[nlmazi[x], {x, 0, 360}];
650       donneeazi = ListPlot[datazi[[All, {1, 2}]]];
651       Print[Show[donneeazi, fittedcurve, PlotRange -> All]];
652
653
654       zazi ==
655        WriteString[Results, Filename, "␣;␣", afit, "␣;␣", bfit, "␣;␣",
656         cfit, "␣;␣", dfit, "␣;␣", degoforient, "␣;␣", direction, "␣;␣",
657          OrVec, "\n"];
658       ]     ]
659     ,
660           If[valuepeak <= 0.005,
661      zazi ==
662       WriteString[Results, Filename, "␣;␣", "␣Not␣consistent␣value␣\n"];
663      donneeazi =
664       ListPlot[inazi[[All, {1, 2}]], PlotStyle -> RGBColor[1, 0, 0]];
665
666      Print["FileName:␣", Filename,
```

```
667       "␣Value␣not␣consistent␣because␣intensity:␣␣",
668       scatteredintensity, "(␣", xpt, ",␣", ypt, "␣)␣\n"]
669      Print[Show[donneeazi, PlotRange -> All]]
670      (* for the vector plot*)
671      (*Degree of orientation*)
672      Clear[degoforient, bfit];
673     degoforient = 0;
674     (*Direction of orientation*
675     1=90degree real space, 0=0degree real space, -1=
676     90 degree realspace*)
677     bfit = 0;
678      lazi =
679      AppendTo[
680       lazi, {{xpt,
681         ypt}, {{degoforient*Cos[bfit Degree],
682          degoforient*Sin[bfit Degree]}, scatteredintensity}}];
683      l = Insert[l, 0, {i, -1}];
684     l = Insert[l, 0, {i, -1}];
685     l1azi = AppendTo[
686       l1azi, {{xpt, ypt}, {degoforient*Cos[bfit Degree],
687         degoforient*Sin[bfit Degree]}}];
688
689     OrVec = {direction, degoforient};
690     ,
691     valueangle =
692      Part[Pick[datazi[[All, 1]], datazi[[All, 2]], valuepeak], 1];
693     (*Test to know where might be the peak*)
694     If [valueangle <= 45,
695      g = backgazi + a*E^-(((x - b)^2)/(2 c^2)) +
696        a*E^-(((x - b - 180)^2)/(2 c^2)) +
697        a*E^-(((x - b - 360)^2)/(2 c^2)),
698      If[45 < valueangle <= 135,
699       g = backgazi + a*E^-(((x - b)^2)/(2 c^2)) +
700         a*E^-(((x - b - 180)^2)/(2 c^2)),
701       If[135 < valueangle <= 225,
702        g =
703         backgazi + a*E^-(((x - b + 180)^2)/(2 c^2)) +
704          a*E^-(((x - b - 180)^2)/(2 c^2)) + a*E^-(((x - b)^2)/(2 c^2)),
705        If[225 < valueangle <= 315,
706         g =
707          backgazi + a*E^-(((x - b)^2)/(2 c^2)) +
708           a*E^-(((x - b + 180)^2)/(2 c^2)),
709         If[315 < valueangle <= 360,
710          g = backgazi + a*E^-(((x - b)^2)/(2 c^2)) +
711            a*E^-(((x - b + 180)^2)/(2 c^2)) +
712            a*E^-(((x - b + 360)^2)/(2 c^2))]]]]];
713     Fitfunctionazi[x_] = g;
714     nlmazi =
715      NonlinearModelFit[datazi[[All, {1, 2}]],
716       Fitfunctionazi[x], {{a, valuepeak}, {b, valueangle}, c}, x,
717       VarianceEstimatorFunction -> (Mean[#^2] &)];
718     nlmazi["BestFitParameters"];
719     Rsq = nlmazi["RSquared"];
720     ARsq = nlmazi["AdjustedRSquared"];
```

```
721     AIC = nlmazi["AIC"];
722     AICc = nlmazi["AICc"];
723     BIC = nlmazi["BIC"];
724     cerr = nlmazi["ParameterErrors"];
725     afit = a /. nlmazi["BestFitParameters"];
726     bfit = b /. nlmazi["BestFitParameters"];
727     cfit = c /. nlmazi["BestFitParameters"];
728     dfit = backgazi /. nlmazi["BestFitParameters"];
729     (*ctriterium for isotropy*)
730     If[cerr[[3]] > 0.83 || cfit < 2,
731      Print["FileName: ", Filename, "  , Point is isotrope.( ", xpt,
732       ", ", ypt, " ) " ];
733      Clear[degoforient, bfit];
734      (* for the vector plot*)
735      (*Degree of orientation*)
736      degoforient = 0;
737      (*Direction of orientation*
738      1=90degree real space, 0=0degree real space, -1=
739      90 degree realspace*)
740      bfit = 0;
741       lazi =
742       AppendTo[
743        lazi, {{xpt,
744          ypt}, {{degoforient*Cos[bfit Degree],
745           degoforient*Sin[bfit Degree]}, scatteredintensity}}];
746      l1azi = AppendTo[
747        l1azi, {{xpt, ypt}, {degoforient*Cos[bfit Degree],
748          degoforient*Sin[bfit Degree]}}];
749
750      l = Insert[l, 0, {i, -1}];
751      l = Insert[l, 0, {i, -1}];
752      OrVec = {direction, degoforient};
753      (*graph*)
754      donneeazi =
755       ListPlot[inazi[[All, {1, 2}]],
756        PlotStyle -> RGBColor[0.5, 1.5, 0]];
757      Print[Show[donneeazi, PlotRange -> All]]
758
759        zazi == WriteString[Results, Filename, " ; isotrope ", "\n"];
760      ,
761
762      (*Degree of orientation*)
763      degoforient = 1/cfit;
764      (*Direction of orientation*
765      1=90degree real space, 0=0degree real space, -1=
766      90 degree realspace*)
767      direction = Cos[bfit Degree];
768       lazi =
769       AppendTo[
770        lazi, {{xpt,
771          ypt}, {{degoforient*Cos[bfit Degree],
772           degoforient*Sin[bfit Degree]}, scatteredintensity}}];
773       l1azi =
774       AppendTo[
```

```
        l1azi, {{xpt, ypt}, {degoforient*Cos[bfit  Degree],
          degoforient*Sin[bfit  Degree]}}];

      OrVec = {direction, degoforient};
      l = Insert[l, degoforient, {i, -1}];
      l = Insert[l, Mod[bfit, 180], {i, -1}];

      Print["FileName: ", Filename,  "  , background: ", backgazi,
       "  ,  peak height: ", afit, "  ,  peak position (deg): ", bfit,
       "  ,  peak width: ", cfit,
       "  ,  standard deviation on peak width: ", cerr[[3]],
       ",  scattered intensity: ", scatteredintensity, "( ", xpt, ",  ",
       ypt, " )" ];

      (*graph*)
      fittedcurve = Plot[nlmazi[x], {x, 0, 360}];
      donneeazi = ListPlot[datazi[[All, {1, 2}]]];
      Print[Show[donneeazi, fittedcurve, PlotRange -> All]];


      zazi ==
       WriteString[Results, Filename, "  ;  ", afit, "  ;  ", bfit, "  ;  ",
        cfit, "  ;  ", dfit, "  ;  ", degoforient, "  ;  ", direction, "  ;  ",
         OrVec, "\n"];
      ]    ]   ]  ] ]

(*creation of the histogramme*)
lhalpha = {};
lhRg = {};
lhT = {};
lhTstandard = {};
lhalpha =
  Flatten[Drop[Drop[Drop[lhisto, None, {2}], None, {2}], None, {2}]];
lhRg = Flatten[
   Drop[Drop[Drop[lhisto, None, {3}], None, {3}], None, {1}]];
lhT = Flatten[
   Drop[Drop[Drop[lhisto, None, {1}], None, {1}], None, {2}]];
lhTstandard =
  Flatten[Drop[Drop[Drop[lhisto, None, {1}], None, {1}], None, {1}]];

graphlhalpha =
  Histogram[lhalpha, 10, "Count",
   PlotLabel -> {name, "Alpha mean" , Mean[lhalpha] , "median ",
     Median[lhalpha]}];
graphlhRg =
  Histogram[lhRg, 10, "Count",
   PlotLabel -> {name, "Rg mean" , Mean[lhRg], "  median , ",
     Median[lhRg] }];
graphlhT =
  Histogram[lhT, 10, "Count",
   PlotLabel -> {name, "T mean" , Mean[lhT], " median " ,
     Median[lhT]}];
graphlhTstandard =
  Histogram[lhTstandard, 10, "Count",
```

```
829     PlotLabel -> {name, "Tstandard mean " , Mean[lhTstandard],
830       " median " , Median[lhTstandard ]}];
831 Show[graphlhalpha]
832 Show[graphlhRg]
833 Show[graphlhT]
834 Show[graphlhTstandard]
835 (*creation of the distance dependence graph*)
836 distancealpha =
837   ListPlot[Drop[Drop[ldistance, None, {3}], None, {3}],
838    PlotLabel -> {name, " distance to implant Alpha"},
839    AxesLabel -> {"Distance", "Alpha"}];
840 distanceT =
841   ListPlot[Drop[Drop[ldistance, None, {2}], None, {3}],
842    PlotLabel -> {name, " distance to implant T"},
843    AxesLabel -> {"Distance", "T"}];
844 distanceRg =
845   ListPlot[Drop[Drop[ldistance, None, {2}], None, {2}],
846    PlotLabel -> {name, " distance to implant Rg"},
847    AxesLabel -> {"Distance", "Rg"}];
848 distancedof =
849   ListPlot[Drop[ ldistanceazi, None, {3}],
850    PlotLabel -> {name, " distance to implant Degree of orientation"},
851    AxesLabel -> {"Distance", "DOF"}];
852 distancedir =
853   ListPlot[Drop[ ldistanceazi, None, {2}],
854    PlotLabel -> {name, " distance to implant direction"},
855    AxesLabel -> {"Distance", "direction of orientation"}];
856 Show[distancedof]
857 Show[distancedir]
858 Show[distancealpha]
859 Show[distanceRg]
860 Show[distanceT]
861 (*loop to fill the graph with value =0 where we do not have data*)
862 xmin = Min[Drop[lxy, None, {2}]];
863 xmax = Max[Drop[lxy, None, {2}]];
864 ymin = Min[Drop[lxy, None, {1}]];
865 ymax = Max[Drop[lxy, None, {1}]];
866 dx = 0.35;
867 dy = 0.35;
868 y1 = Round[(ymax - ymin)/dy + 2];
869 x1 = Round[(xmax - xmin)/dx + 2];
870 (*ratio to have square data points*)
871 z1 = y1/x1;
872 For[j = 0, j < (ymax - ymin)/dy + 2, j++,
873  For[k = 0, k < (xmax - xmin)/dx + 2, k++,
874   y = ymin + j*dy;
875   x = xmin + k*dx;
876   sel = Select[lxy, # == {x, y} &]
877     If[Length[sel] < 1,
878      l1 = AppendTo[l1, {x - dx, y, 0}];
879      l2 = AppendTo[l2, {x - dx, y, 0}];
880      l3 = AppendTo[l3, {x - dx, y, 0}];
881      lscatter = AppendTo[lscatter, {x - dx, y, 0}];
882      lazi = AppendTo[lazi, {{x - dx, y}, {{0, 0}, 0}}];
```

```
      l1azi = AppendTo[ l1azi, {{x - dx, y}, {0, 0}}];
      lintense = AppendTo[lintense, {x - dx, y, 0}];
      ]]]

(*Creation of the array and graphical representation*)
intensitygraph =
 ListDensityPlot[lintense, FrameLabel -> {"x", "y"},
  PlotRange -> Full, PlotLegends -> Automatic,
  ColorFunction -> "SunsetColors", InterpolationOrder -> 0,
  PlotLabel -> "intensity photodiode", AspectRatio -> z1]

alphaparameter =
 ListDensityPlot[l1, FrameLabel -> {"x", "y"}, PlotRange -> Full,
  PlotLegends -> Automatic, ColorFunction -> "SunsetColors",
  InterpolationOrder -> 0, PlotLabel -> {name, "Form parameter"},
  AspectRatio -> z1]
Tparameter =
 ListDensityPlot[l2, FrameLabel -> {"x", "y"}, PlotRange -> Full,
  PlotLegends -> Automatic, ColorFunction -> "SunsetColors",
  InterpolationOrder -> 0, PlotLabel -> {name, "Thickness parameter"},
   AspectRatio -> z1]
Tstandardparameter =
 ListDensityPlot[l3, FrameLabel -> {"x", "y"}, PlotRange -> Full,
  PlotLegends -> Automatic, ColorFunction -> "SunsetColors",
  InterpolationOrder -> 0,
  PlotLabel -> {name, "Thickness Standard parameter"},
  AspectRatio -> z1]
scatteredgraph =
 ListDensityPlot[lscatter, FrameLabel -> {"x", "y"},
  PlotRange -> Full, PlotLegends -> Automatic,
  ColorFunction -> "SunsetColors", InterpolationOrder -> 0,
  PlotLabel -> {name, "Scattered intensity"}, AspectRatio -> z1]
fessai[s_] :=
  Piecewise[{{Mean[lhT]/((2^1.5 - (5/3)^0.5)*s + (5/3)^0.5),
     s < 1}, {Mean[lhT]/((12^0.5 - 2^1.5)*(s - 1) + 2^1.5), s >= 1}}];
gessai = Plot[fessai[s], {s, 0, 2}, PlotRange -> Full];
corrgraph =
 ListPlot[lcorr, Frame -> True, FrameLabel -> {"alpha", "Thickness"},
  PlotRange -> Full]
(*fitting of alpha and Rg*)
line = Fit[lcorrfit, {1, zi}, zi];

graph1 = ListVectorDensityPlot[lazi, FrameLabel -> {"x", "y"},
  VectorStyle -> {Thick, Arrowheads[0]}, VectorScale -> Small,
  PlotRange -> {{xmin, xmax}, {ymin, ymax}},
  PlotLabel -> {name, "Degree of orientation and intensity"},
  ColorFunction -> "Pastel", Mesh -> 5, VectorPoints -> {x1, y1},
  AspectRatio -> z1 ]
graphvector =
  ListVectorPlot[l1azi, FrameLabel -> {"x", "y"},
   VectorStyle -> {Thick, Arrowheads[0]}, VectorScale -> Small,
   PlotRange -> {{xmin, xmax}, {ymin, ymax}},
   VectorPoints -> {x1, y1}, AspectRatio -> z1];
graphintensity =
```

```
937   ListDensityPlot[lscatter,
938    PlotLabel -> {name, "Degree of orientation and intensity"},
939    PlotLegends -> Automatic, InterpolationOrder -> 0,
940    ColorFunction -> "Pastel",
941    PlotRange -> {{xmin - dx, xmax + dx}, {ymin - dy, ymax + dy}},
942    ClippingStyle -> Red, AspectRatio -> z1];
943 graphintensity2 =
944   ListDensityPlot[lscatter,
945    PlotLabel -> {name, "Degree of orientation and intensity"},
946    PlotLegends -> Automatic, InterpolationOrder -> 1,
947    ColorFunction -> "Pastel",
948    PlotRange -> {{xmin, xmax}, {ymin, ymax}}, ClippingStyle -> Red,
949    AspectRatio -> z1];
950 graph = Show[graphintensity, graphvector]
951 graph2 = Show[graphintensity2, graphvector]
952
953
954 Show[ListPlot[lcorrfit, PlotStyle -> Blue, Frame -> True,
955   FrameLabel -> {"alpha", "Rg"}], Plot[line, {zi, 0, 3}], gessai]
956 (*here the directorry where the picture are going to be saved is written*)
957 SetDirectory["C:\\Users\\ogier\\Desktop\\Mathematica\\Image"];
958 Export["4340_beamstopintensity.jpg", intensitygraph];
959 Export["4340_alpha_radial.jpg", alphaparameter];
960 Export["4340_T_radial.jpg", Tparameter];
961 Export["4340_T_standard_radial.jpg", Tstandardparameter];
962 Export["4340_scatteredintensity.jpg", scatteredgraph];
963 Export["4340_correlation.jpg", corrgraph];
964 Export["4340_histo_alpha.jpg", graphlhalpha];
965 Export["4340_histo_T.jpg", graphlhT];
966 Export["4340_histoT_standard.jpg", graphlhTstandard];
967 Export["4340_histo_Rg.jpg", graphlhRg];
968 Export["4340_histo_distancealpha.jpg", distancealpha];
969 Export["4340_histo_distanceT.jpg", distanceT];
970 Export["4340_histo_distanceRg.jpg", distanceRg];
971 Export["4340_orientation_intensity.jpg", graph];
972 Export["4340_orientation_intensity_joli.jpg", graph1];
973 Export["4340_orientation_interpolated.jpg", graph2];
974 Export["4340_orientation_degree.jpg", distancedof];
975 Export["4340_orientation_direction.jpg", distancedir];
976 Export["4340_data.xls", l, "XLS"];
977
978 Close["C:\\Users\\ogier\\Desktop\\DATA\\4340_Integration\\intensity.txt"];
979 Close["C:\\Users\\ogier\\Desktop\\DATA\\4340_Integration\\iscat.txt"];
980 Close["C:\\Users\\ogier\\Desktop\\DATA\\4340_Integration\\\
981 radialresults.txt"];
982 Close[  "C:\\Users\\ogier\\Desktop\\DATA\\4340_Integration\\\
983 aziresults.txt"];
984 t = TimeUsed[] - t0
```

A.2 Statistical analysis

```
1 xmin1 = 34;
2 xmax1 = 35;
3 xmin2 = 39;
```

```
xmax2 = 40;
ymin1 = 63;
ymax1 = 72;
\!\(\*
ButtonBox["InstallJava",
BaseStyle->"Link",
ButtonData->"paclet:JLink/ref/InstallJava"]\)[];
Path2 = "C:\\Users\\ogier\\Desktop\\Mathematica\\Image";
SetDirectory[Path2];
l4340 = Import["4340_data.xls", Path -> Path2][[1]];
(*direction*)
data4340ddir = {};
l4340ddir =
  Drop[Drop[Drop[l4340, None, {5, 11}], None, {3}], None, {1}];
For[i = 1, i < Length[l4340ddir] + 1, i++,
 If[(l4340ddir[[i]][[1]] > xmin1 && l4340ddir[[i]][[3]] > 0 &&
     l4340ddir[[i]][[1]] < xmax1) || (l4340ddir[[i]][[1]] > xmin2 &&
     l4340ddir[[i]][[3]] > 0 && l4340ddir[[i]][[1]] < xmax2) ,
  data4340ddir =
   AppendTo[
    data4340ddir, {l4340ddir[[i]][[2]], l4340ddir[[i]][[4]]}];]

m = 90;
For[i = 1, i < Length[data4340ddir] + 1, i++,
 data4340ddir[[i]][[2]] = Abs[m - data4340ddir[[i]][[2]]];]

lpdir = ListPlot[data4340ddir,
   PlotLabel -> "Direction as a function of distance 4340",
   AxesLabel -> {"Distance", "Direction \n of orientation"},
   PlotRange -> {{0, 6}, {0, 100}}] ;
lpdir
Export["4340_d_dir.jpg", lpdir];

(*degree of orientation*)
data4340ddof = {};
l4340ddof =
  Drop[Drop[Drop[Drop[l4340, None, {13}], None, {5, 11}], None, {3}],
   None, {1}];
For[i = 1, i < Length[l4340ddof] + 1, i++,
 If[(l4340ddof[[i]][[1]] > xmin1 && l4340ddof[[i]][[3]] > 0 &&
     l4340ddof[[i]][[1]] < xmax1) || (l4340ddof[[i]][[1]] > xmin2 &&
     l4340ddof[[i]][[3]] > 0 && l4340ddof[[i]][[1]] < xmax2),
  data4340ddof =
   AppendTo[
    data4340ddof, {l4340ddof[[i]][[2]], l4340ddof[[i]][[3]]}];]


lpdof = ListPlot[data4340ddof,
   PlotLabel ->
    "Degree of orientation as a function of distance 4340",
   PlotRange -> {{0, 6}, {0, 0.04}},
   AxesLabel -> {"Distance", "DOF"}] ;
lpdof
Export["4340_d_dof.jpg", lpdof];
```

```
58
59 (*shape*)
60 data4340ds = {};
61 l4340ds =
62   Drop[Drop[Drop[Drop[l4340, None, {9, 13}], None, {5, 7}],
63     None, {3}], None, {1}];
64 For[i = 1, i < Length[l4340ds] + 1, i++,
65  If[(l4340ds[[i]][[1]] > xmin1 && l4340ds[[i]][[3]] > 0 &&
66      l4340ds[[i]][[1]] < xmax1) || (l4340ds[[i]][[1]] > xmin2 &&
67      l4340ds[[i]][[3]] > 0 && l4340ds[[i]][[1]] < xmax2 ) ,
68   data4340ds =
69     AppendTo[data4340ds, {l4340ds[[i]][[2]], l4340ds[[i]][[3]]}];]]
70
71 lps = ListPlot[data4340ds,
72    PlotLabel -> "Shape␣parameter␣as␣a␣function␣of␣distance␣4340",
73    AxesLabel -> {"Distance", "Alpha"},
74    PlotRange -> {{0, 6}, {0, 2.5}}] ;
75 lps
76 Export["4340_d_s.jpg", lps];
77 (*Thickness*)
78 data4340dT = {};
79 l4340dT =
80   Drop[Drop[Drop[Drop[l4340, None, {11, 13}], None, {5, 9}],
81     None, {3}], None, {1}];
82 For[i = 1, i < Length[l4340dT] + 1, i++,
83  If[(l4340dT[[i]][[1]] > xmin2 && l4340dT[[i]][[3]] > 0 &&
84      l4340dT[[i]][[1]] < xmax2 ) || (l4340dT[[i]][[1]] > xmin1 &&
85      l4340dT[[i]][[3]] > 0 && l4340dT[[i]][[1]] < xmax1 ),
86   data4340dT =
87     AppendTo[data4340dT, {l4340dT[[i]][[2]], l4340dT[[i]][[3]]}];]]
88
89 lpT = ListPlot[data4340dT,
90    PlotLabel -> "Thickness␣as␣a␣function␣of␣distance␣4340",
91    PlotRange -> {{0, 6}, {0, 60}}, AxesLabel -> {"Distance", "T"}] ;
92 lpT
93 Export["4340_d_T.jpg", lpT];
94 (*Thickness with invariant*)
95
96 data4340dTst = {};
97 l4340dTst =
98   Drop[Drop[Drop[Drop[l4340, None, {12, 13}], None, {5, 10}],
99     None, {3}], None, {1}];
100 For[i = 1, i < Length[l4340dTst] + 1, i++,
101  If[(l4340dTst[[i]][[1]] > xmin2 && l4340dTst[[i]][[3]] > 0 &&
102      l4340dTst[[i]][[1]] < xmax2 ) || (l4340dTst[[i]][[1]] > xmin1 &&
103      l4340dTst[[i]][[3]] > 0 && l4340dTst[[i]][[1]] < xmax1 ),
104   data4340dTst =
105     AppendTo[
106      data4340dTst, {l4340dTst[[i]][[2]], l4340dTst[[i]][[3]]}];]]
107
108 lpTst = ListPlot[data4340dTst,
109    PlotLabel ->
110     "Thickness␣computed␣with␣invariant␣\n␣as␣a␣function␣of␣distance␣\
111 4340", PlotRange -> {{0, 6}, {15, 30}},
```

```
    AxesLabel -> {"Distance", "T"}] ;
lpTst
Export["4340_d_Tst.jpg", lpTst];

(*scattering*)
data4340dscat = {};
l4340dscat =
  Drop[Drop[Drop[Drop[l4340, None, {8, 13}], None, {5, 6}],
    None, {3}], None, {1}];
For[i = 1, i < Length[l4340dscat] + 1, i++,
 If[(*(l4340dscat[[i]][[1]] > xmin1 &&l4340dscat[[i]][[3]]>0 &&
  l4340dscat[[i]][[1]]<
  xmax1)||*)(l4340dscat[[i]][[1]] > xmin2 &&
    l4340dscat[[i]][[3]] > 0 && l4340dscat[[i]][[1]] < xmax2 ) ,
  data4340dscat =
    AppendTo[
     data4340dscat, {l4340dscat[[i]][[2]], l4340dscat[[i]][[3]]}];]]

lpscat = ListPlot[data4340dscat,
   PlotLabel -> "Scattering intensity as a function of distance 4340",
    PlotRange -> {{0, 6}, {0, 1000}},
   AxesLabel -> {"Distance", "Scattered \n intensity"}] ;
lpscat
Export["4340_d_scat.jpg", lpscat];
```

A.3 Azimuthal integration with beam stop

```
Clear[a, b, c, d, e, i, j, k, l, l1, l2, liste, DropFront, DropBack,  pathin, imax, files
    , filestrans, FileNameListtrans, FileNameList, Results, Filename, in, intrans,
    fulldata, datprel, dat, backg,  Fitfunction, nlm, afit, bfit, cfit, dfit, degoforient
    , coef, valuepeak, value2, direction, OrVec, x , z , xmin, xmax, dx, ymin, ymax, dy,
    Beamstopstart, Beamstopend, t0, ttotal];
ClearAll;
(* In order to have a good fitting, please take care to have 720 points for the azimuthal
     integration in the SaxsGui script for automatisation*)
t0 = TimeUsed[]
(*Obtention of the files to analyse*)
pathin = "C:\\Users\\ogier\\Desktop\\DATA\\4182_SAXS_BOKU";
files = FileNames[{"*aziintxy.csv"}, FileNameJoin[{pathin}]];
filestrans = FileNames[{"*trans.csv"}, FileNameJoin[{pathin}]];
FileNameList = FileNameTake[#, -1] & /@ files;
FileNameListtrans = FileNameTake[#, -1] & /@ filestrans;

imax = Length[FileNameList];
DropFront = 0;
DropBack = 0;
Beamstopstart = 295; (* in degree*);
Beamstopend = 357.5;
xmin = 17;
xmax = 26;
dx = 0.25;
ymin = -3;
ymax = 2;
dy = 0.25;
```

```
23
24 Results =   OpenWrite[  "C:\\Users\\ogier\\Desktop\\DATA\\4182_SAXS_BOKU\\results.txt "];
25
26 l = {};
27
28 For [i = 1, i < imax + 1, i++,
29  Filename = Part [FileNameList, i];
30  Filenametrans = Part [FileNameListtrans, i];
31  in = Import[files[[i]], Path -> pathin];
32  intrans = Import[filestrans[[1]], Path -> pathin];
33  fulldata = in;
34  datprel = Drop [in , DropFront];
35  dat = Drop[datprel, -DropBack];
36  trans = intrans[[i, 1]];
37
38  l1 = {};
39  l2 = {};
40  For [k = Beamstopstart*2 - 360, k < Beamstopend*2 - 360, k = k + 25,
41   m = Mean[{dat[[k, 2]], dat[[k + 1, 2]], dat[[k + 3, 2]],
42       dat[[k + 4, 2]], dat[[k + 5, 2]], dat[[k + 6, 2]]}];
43   AppendTo[l1, m];
44   AppendTo[l2, dat[[k + 3, 1]]];
45   ];
46  Clear[j, k];
47  For[j = 0, j < 4, j++,
48   For[k = 0, k < 25, k++,
49    dat[[Beamstopstart*2 + 25*j + k, 2]] =
50      Mean[{dat[[Beamstopstart*2 + 25*j - 3, 2]],
51         dat[[Beamstopstart*2 + 25*j - 2, 2]],
52         dat[[Beamstopstart*2 + 25*j - 1,
53          2]]}] + (l1[[j + 2]] - l1[[j + 1]])/(l2[[j + 2]] -
54           l2[[j + 1]])*(dat[[Beamstopstart*2 + 25*j + k, 1]] -
55          dat[[Beamstopstart*2 + 25*j - 1, 1]]);]];
56
57  (* to not take the minimum in the beam stop shadow*)
58  backg = Min[ Drop[Part[dat[[All, 2]]], -170]];
59  valuepeak = Max[ Part[dat[[All, 2]]]];
60
61       If[valuepeak <= 0.005 || valuepeak >= 17,
62   z == WriteString[Results, Filename, " ; ",
63     " Not consistent value ", "\n"];
64   donnee = ListPlot[in[[All, {1, 2}]], PlotStyle -> RGBColor[1, 0, 0]];
65
66   Print["FileName: ", Filename,  " Value not consistent"]
67    Print[Show[donnee, PlotRange -> All]]
68    (* for the vector plot*)
69    (*Degree of orientation*)
70    Clear[degoforient, bfit];
71   degoforient = 0;
72   (*Direction of orientation*
73   1=90degree real space, 0=0degree real space, -1=90 degree realspace*)
74
75
76   bfit = 0;
```

```
l = AppendTo[
  l, {{degoforient*Cos[bfit], degoforient*Sin[bfit]}, trans}];
,
valueangle = Part[Pick[dat[[All, 1]], dat[[All, 2]], valuepeak], 1];
(*Test to know where might be the peak*)
If [valueangle <= 45,
 g = backg + a*E^-(((x - b)^2)/(2 c^2)) +
   a*E^-(((x - b - 180)^2)/(2 c^2)) +
   a*E^-(((x - b - 360)^2)/(2 c^2)),
 If[45 < valueangle <= 135,
  g = backg + a*E^-(((x - b)^2)/(2 c^2)) +
    a*E^-(((x - b - 180)^2)/(2 c^2)),
  If[135 < valueangle <= 225,
   g = backg + a*E^-(((x - b + 180)^2)/(2 c^2)) +
     a*E^-(((x - b - 180)^2)/(2 c^2)) + a*E^-(((x - b)^2)/(2 c^2)),
   If[225 < valueangle <= 315,
    g =
     backg + a*E^-(((x - b)^2)/(2 c^2)) +
      a*E^-(((x - b + 180)^2)/(2 c^2)),
    If[315 < valueangle <= 360,
     g = backg + a*E^-(((x - b)^2)/(2 c^2)) +
       a*E^-(((x - b + 180)^2)/(2 c^2)) +
       a*E^-(((x - b + 360)^2)/(2 c^2))]]]]];
Fitfunction[x_] = g;

nlm = NonlinearModelFit[dat[[All, {1, 2}]],
  Fitfunction[x], {{a, valuepeak}, {b, valueangle}, c}, x,
  VarianceEstimatorFunction -> (Mean[#^2] &)];
nlm["BestFitParameters"];
Rsq = nlm["RSquared"];
ARsq = nlm["AdjustedRSquared"];
AIC = nlm["AIC"];
AICc = nlm["AICc"];
BIC = nlm["BIC"];
cerr = nlm["ParameterErrors"];
afit = a /. nlm["BestFitParameters"];
bfit = b /. nlm["BestFitParameters"];
cfit = c /. nlm["BestFitParameters"];
dfit = backg /. nlm["BestFitParameters"];
(*ctriterium for isotropy*)
If[cerr[[3]] > 0.93,
 Print["FileName: ", Filename, " , Point is isotrope.", cerr[[3]] ];
 Clear[degoforient, bfit];
 (* for the vector plot*)
 (*Degree of orientation*)
 degoforient = 0;
 (*Direction of orientation*
 1=90degree real space, 0=0degree real space, -1=
 90 degree realspace*)
 bfit = 0;
 l = AppendTo[
   l, {{degoforient*Cos[bfit], degoforient*Sin[bfit]}, trans}];
 (*graph*)
 donnee =
```

```
131      ListPlot[in[[All, {1, 2}]], PlotStyle -> RGBColor[0.5, 1.5, 0]];
132     Print[Show[donnee, PlotRange -> All]]
133
134       z == WriteString[Results, Filename, "␣;␣isotrope␣", "\n"];
135     ,
136
137     (*Degree of orientation*)
138     degoforient = 1/cfit;
139     (*Direction of orientation*
140     1=90degree real space, 0=0degree real space, -1=
141     90 degree realspace*)
142     direction = Cos[bfit];
143     l = AppendTo[
144       l, {{degoforient*Cos[bfit], degoforient*Sin[bfit]}, trans}];
145     Print["OrientationVector"];
146     OrVec = {direction, degoforient};
147
148     Print["FileName:␣", Filename,  "␣,␣background:␣", backg,
149      "␣␣,␣peak␣height:␣", afit, "␣␣,␣peak␣position␣(deg):␣", bfit,
150      "␣␣,␣peak␣width:␣", cfit, "␣,␣standard␣deviation␣on␣{a,b,c}:␣",
151      cerr[[3]]];
152     (* " , Rsquared: ", Rsq,  "   , AdjRsquared: ", ARsq," , AIC: ",
153     AIC, " , AICc: ", AICc, " , BIC: ", BIC*)
154     (*graph*)
155     fittedcurve = Plot[nlm[x], {x, 0, 360}];
156     donnee = ListPlot[dat[[All, {1, 2}]]];
157     Print[Show[donnee, fittedcurve, PlotRange -> All]]
158       z ==
159      WriteString[Results, Filename, "␣;␣", afit, "␣;␣", bfit, "␣;␣",
160       cfit, "␣;␣", dfit, "␣;␣", degoforient, "␣;␣", direction, "␣;␣",
161       OrVec, "\n"];
162     ]  ] ]
163 (*creation of the array for the vector plot*)
164 liste = {};
165 Clear[k, j, x, y];
166
167 For[j = 0, j < 1 + (ymax - ymin)/dy , j++,
168  For[k = 0, k < 1 + (xmax - xmin)/dx, k++,
169   If[(-1)^j > 0,
170    liste =
171     AppendTo[liste, {{ymin + dy*j, xmin + dx*k}, Part[l, k + (1 + (xmax - xmin)/dx)*j +
            1]}],
172    liste =
173     AppendTo[liste, {{ymin + dy*j, xmax - dx*k}, Part[l, k + (1 + (xmax - xmin)/dx)*j +
            1]}]
174    ]  ] ]
175 ListVectorDensityPlot[liste,
176  VectorPoints -> {Floor[2 + (ymax - ymin)/dy],
177    Floor[2 + (xmax - xmin)/dx ]}, FrameLabel -> {y, x},
178  VectorStyle -> {Thick, Arrowheads[0]}, VectorScale -> Medium,
179  PlotRange -> Full]
180
181 Close[  "C:\\Users\\ogier\\Desktop\\DATA\\4182_SAXS_BOKU\\results.txt"];
182 ttotal = TimeUsed[] - t0
```

List of Tables

List of Figures

Bibliography

[1] Peter Fratzl and Richard Weinkamer. Nature's hierarchical materials. Progress in Materials Science, 52(8):1263–1334, 2007.

[2] S. Weiner, W. Traub, and H. D. Wagner. Lamellar bone structure–function relations. Journal of Structural Biology, 126:241–255, 1999.

[3] Jae-Young Rho, Liisa Kuhn-Spearing, and Peter Zioupos. Mechanical properties and the hierarchical structure of bone. Medical Engineering and Physics, 20:92–102, 1998.

[4] Lutz Moeller. Elefant femur, April 2007. http://lutzmoeller.net/Wild/Elefantenjagd/Elefantskull.php.

[5] Matthew J. Olszta, Xingguo Cheng, Sang Soo Jee, Rajendra Kumar, Yi-Yeoun Kim, Michael J. Kaufman, Elliot P. Douglas, and Laurie B. Gower. Bone structure and formation: A new perspective. Material Science and Engineering, 58(3-5):77–116, 2007.

[6] OpenStax College. Bone cells, April 2013. http://cnx.org/content/col11496/1.6/.

[7] S. C. Manolagas. Birth and death of bone cells: Basic regulatory mechanisms and implications for the pathogenesis and treatment of osteoporosis. Endocrine reviews, 21(2):115–137, 2000.

[8] Sebastian Bauer, Patrik Schmuki, Klaus von der Mark, and Young c Park. Engineering biocompatible implant surfaces. Progress in Materials Science, 58:261–326, 2013.

[9] Kolosso. Intramodullar rod, April 2006. http://upload.wikimedia.org/wikipedia/commons/8/89/K-Knie-z2.jpg.

[10] John D Enderle, Joseph D Bronzino, and Susan M. Blanchard. Introduction to biomedical engineering. second ed. amsterdam; boston. Elsevier Academic Press, 2005.

[11] Frank Witte. The history of biodegradable magnesium implants: A review. Acta Biomaterialia, 6(5):1680–1692, 2010.

[12] Mark P. Staiger, Alexis M. Pietak, Jerawala Huadmai, and George Dias. Magnesium and its alloys as orthopedic biomaterials: A review. Biomaterials, 27(9):1728–1734, 2006.

[13] F. Witte, V. Kaese, H. Haferkamp, E. Switzer, A. Meyer-Lindenberg, and C. J Wirth. In vivo corrosion of four magnesium alloys and the associated bone response. Biomaterials, 26:3557–3563, 2005.

[14] PA Revell, E Damien, XS Zhang, P Evans, and CR Howlett. The effect of magnesium ions on bone bonding to hydroxyapatite. Key to Engineering Materials, page 254–256:447–50, 2004.

[15] Stefan Franz Fischerauer. In vivo Mikro-CT Untersuchung von bioresorbierbaren Magnesiumimplantaten. PhD thesis, MEDIZINISCHEN UNIVERSITAET GRAZ, 2010.

[16] Anja C. Haenzi, Isabel Gerber, Michael Schinhammer, Jörg F. Löffler, and Peter J. Uggowitzer. On the in vitro and in vivo degradation performance and biological response of new biodegradable mg–y–zn alloys. Acta Biomaterialia, 6:1824–1833, 2010.

[17] Jens Als-Nielsen and Des McMorrow. Elements of Modern X-ray Physics. John Wiley & Sons, Ltd, 2011.

[18] Helga Lichtenegger. Scattering techniques in nanomaterials science, 2013. Lecture Number 892304 at University of Natural Resources and Life Sciences.

[19] Alain Guinier. Compte rendu hebdomadaires des séances de l académie des sciences paris. 204, 1937.

[20] O. Glatter and O. Kratky. Small Angle X-RAy Scattering. Academic Press, 1982.

[21] Peter Fratzl. Statistical model of the habit and arrangement of mineral crystals in the collagen of bone. Journal of Statistical Physics, 77(1-2):125–143, 94.

[22] Aurelien Gourrier, Chenghao Li, Stefan Siegel, Oskar Paris, Paul Roschger, Klaus Klaushofer, and Peter Fratzl. Scanning small-angle x-ray scattering analysis of the size and organization of the mineral nanoparticles in fluorotic bone using a stack of cards model. Journal of Applied Crystallography, 43(6):1385–1392, 2010.

[23] Boualem Hammouda. A new guinier–porod model. Journal of Applied Crystallography, 43(4): 716–719, 2010.

[24] Boualem Hammouda. Analysis of the beaucage model. Journal of Applied Crystallography, 43 (6):1474–1478, 2010.

[25] B. Beaucage. Approximations leading to a unified exponential/power-law approach to small-angle scattering. Journal of Applied Crystallography, 28:717–728, 1995.

[26] B. Beaucage. Small-angle scattering from polymeric mass fractals of arbitrary mass-fractal dimension. Journal of Applied Crystallography, 29:134–146, 1996.